Wetting of Structured Packing Elements - CFD and Experiment

Vom Fachbereich für Maschinenbau und Verfahrenstechnik
der Technischen Universität Kaiserslautern
zur Erlangung des akademischen Grades

Doktor – Ingenieur (Dr.-Ing.)

genehmigte Dissertation

Vorgelegt von

G. Dipl. B. Sc. Eng. Adel Ataki

aus Aleppo (Halab) - Syrien

Eingereicht am: **10. April 2006**

Mündliche Prüfung am: **16. August 2006**

Promotionskomission:

Vorsitzender: Prof. Dr.-Ing. habil. Werner Müller

Referenten: Prof. Dipl.-Ing. Dr. techn. habil. Hans-Jörg Bart

Prof. Dr.-Ing. Matthias Kraume

Dekan: Prof. Dr.-Ing. Jan Aurich

Kaiserslautern 2006

D 386

Wetting of Structured Packing Elements - CFD and Experiment

by

G. Dipl. B. Sc. Eng. Adel Ataki

From Aleppo (Halab) - Syria

Accepted Dissertation

Submitted to the Faculty of Mechanical and Process Engineering
Technical University of Kaiserslautern

For the fulfilment of the requirements of the Doctor of Philosophy degree

Doktor – Ingenieur (Dr.-Ing.)

Submitted on: **10. April 2006**

Oral Examination on: **16. August 2006**

Examination Committee:

Chairman: Prof. Dr.-Ing. habil. Werner Müller

Referees: Prof. Dipl.-Ing. Dr. techn. habil. Hans-Jörg Bart

Prof. Dr.-Ing. Matthias Kraume

Dean: Prof. Dr.-Ing. Jan Aurich

Kaiserslautern 2006

D 386

ACKNOWLEDGMENT

This work is performed during my stay as a Ph.D. student at the Technical University of Kaiserslautern, Germany at the Institute of Chemical Engineering chaired by Prof. Dipl.-Ing. Dr. techn. Hans-Jörg Bart.

At first I would like to thank my supervisor Prof. Hans-Jörg Bart for his permanent and extensive support as well as encouraging me to accomplish this hard work. I highly appreciate his trust and his excellent advice and guidance during all stages of this long term research, in particularly for his contributions to my publications. Second, I am very grateful to Prof. Dr.-Ing. M. Kraume for his serving as committee member and to Prof. Dr.-Ing. habil. W. Müller for taking the chairmanship of the examination Committee.

This work is supported by the precious scholarship of my home University, Aleppo University, and partially through the State Postgraduate Scholarship Programme of the TU Kaiserslautern and the German Academic Exchange Service (DAAD), as well as the financial support by and the initiative of the German Federal Ministry for Education and Research: Process Engineering and Technology Network of Competence - PRO3, and the chairman of the Institute of Chemical Engineering: Prof. Bart, to all those I gratefully acknowledge this support.

I am deeply indebted to all my colleges at the Institute of Chemical Engineering for the continuous and greatly help in facilitating my research and especially the technician Mr. L. Drumm. I also wish to thank the Secretaries of the Institute, Mrs I. Behrendt, Mrs. B. Schneider and Mrs E. Jeblick. I appreciate the company Kuhni in Switzerland for their cooperative work and supplying the samples for the experimental work in this research.

My special grateful is for my mother that she fight to let me and my brothers to continue our higher education. She has been suffering for her patient to see me getting my Ph.D. degree, to my uncle Omar Reda and my cosine Mohammed Assad Ataki, for their support to get the Syrian scholarship, to the whole members of my family who are waiting for my successful comeback.

Adel Ataki

Kaiserslautern, in August 2006

To the soul of my patient father, to my mother and my brothers

ABSTRACT

Wetting of Structured Packing Elements - CFD and Experiment

Wetting of a solid surface with liquids is an important parameter in the chemical engineering process such as distillation, absorption and desorption. The degree of wetting in packed columns mainly contributes in the generating of the effective interfacial area and then enhancing of the heat and mass transfer process. In this work the wetting of solid surfaces was studied in real experimental work and virtually through three dimensional CFD simulations using the multiphase flow VOF model implemented in the commercial software FLUENT. That can be used to simulate the stratified flows [1].

The liquid rivulet flow which is a special case of the film flow and mostly found in packed columns has been discussed. Wetting of a solid flat and wavy metal plate with rivulet liquid flow was simulated and experimentally validated. The local rivulet thickness was measured using an optically assisted mechanical sensor using a needle which is moved perpendicular to the plate surface with a step motor and in the other two directions using two micrometers.

The measured and simulated rivulet profiles were compared to some selected theoretical models founded in the literature such as Duffy & Muffatt [2], Towell & Rothfeld [3] and Al-Khalil et al. [4]. The velocity field in a cross section of a rivulet flow and the non-dimensional maximum and mean velocity values for the vertical flat plate was also compared with models from Al-Khalil et al. [4] and Allen & Biggin [5]. Few CFD simulations for the wavy plate case were compared to the experimental findings, and the Towel model for a flat plate [3].

In the second stage of this work 3-D CFD simulations and experimental study has been performed for wetting of a structured packing element and packing sheet consisting of three elements from the type Rombopak 4M, which is a product of the company Kuhni, Switzerland. The hydrodynamics parameters of a packed column, e. i. the degree of wetting, the interfacial area and liquid hold-up have been depicted from the CFD simulations for different liquid systems and liquid loads. Flow patterns on the degree of wetting have been compared to that of the experiments, where the experimental values for the degree of wetting were estimated from the snap shooting of the flow on the packing sheet in a test rig.

A new model to describe the hydrodynamics of packed columns equipped with Rombopak 4M was derived with help of the CFD–simulation results. The model predicts the degree of wetting, the specific or interfacial area and liquid hold-up at different flow conditions. This model was compared to Billet & Schultes [6], the SRP model Rocha et al. [7-9], to Shi & Mersmann [10] and others.

Since the pressure drop is one of the most important parameter in packed columns especially for vacuum operating columns, few CFD simulations were performed to estimate the dry pressure drop in a structured and flat packing element and were compared to the experimental results.

It was found a good agreement from one side, between the experimental and the CFD simulation results, and from the other side between the simulations and theoretical models for the rivulet flow on an inclined plate. The flow patterns and liquid spreading behaviour on the packing element agrees well with the experimental results.

The VOF (Volume of Fluid) was found very sensitive to different liquid properties and can be used in optimization of the packing geometries and revealing critical details of wetting and film flow. An extension of this work to perform CFD simulations for the flow inside a block of the packing to get a detailed picture about the interaction between the liquid and packing surfaces is recommended as further perspective.

Keywords

CFD Simulation; Fluent; Dry Pressure Drop; Multiphase Flow; Packed columns; Rombopak; Structured Packing; VOF Model; Wetting

KURZFASSUNG

Benetzung von strukturierten Packungselementen – CFD und Experiment

Benetzung einer festen Oberfläche mit Flüssigkeiten ist ein bedeutsames Thema bei z.B. Destillation, Absorption und Desorption. Der Benetzungsgrad in Packungskolonnen trägt hauptsächlich zur Bildung der Phasengrenzfläche bei, die dann den Wärme- und Stofftransport beeinflusst. In dieser Arbeit wurde die Benetzung von festen Oberflächen durch experimentelle Arbeit und durch dreidimensionale CFD - Simulationen mit dem VOF Mehrphasenströmungsmodell, das in dem kommerziellen Code FLUENT eingebunden ist, untersucht. Dieses Modell kann verwendet werden, um die Strömung mit freier Oberfläche zu simulieren [1].
Die hier untersuchte Flüssigkeitsrinnsalströmung ist ein spezieller Fall der Filmströmung, die in Packungskolonnen auftreten kann. Die Benetzung einer festen flachen und wellenförmigen Metallplatte mit Rinnsalströmung wurde mit dreidimensionalen CFD-Simulationen modelliert und experimentell validiert. Die lokale Rinnsalhöhe wurde mit einem optisch unterstützten mechanischen Sensor, der senkrecht zur Plattenoberfläche mit einem Schrittmotor und in den anderen zwei Richtungen mit zwei Mikrometern verschoben werden kann, gemessen.
Die gemessenen und simulierten Rinnsalprofile wurden mit einigen ausgewählten theoretischen Modellen, aus der Literatur wie Duffy u. Muffatt [2], Towell u. Rothfeld [3] und Al-Khalil et Al. [4] verglichen. Das Geschwindigkeitsfeld in einem Querschnitt der Rinnsalströmung und die dimensionslose maximale und mittlere Rinnsalsgeschwindigkeit für die vertikale flache Platte wurden auch mit den Modellen von Al-Khalil et Al. [4] und Allen u. Biggin [5] verglichen. CFD Simulationen für die wellenförmige Platte wurden mit dem experimentellen Ergebnissen und dem Towell u. Rothfeld Modell [3] für flache Platten verglichen, um den CFD Code an einfachen Fällen zu validieren.
Im zweiten Teil dieser Arbeit wurden 3-D CFD-Simulationen und experimentelle Untersuchungen für die Benetzung eines strukturierten Packungselements und Packungsblattes bestehend aus drei Elementen der Kühni Rombopak 4M durchgeführt. Die hydrodynamischen Parameter der Packungskolonne, das heißt der Benetzungsgrad, die Phasengrenzfläche und der Flüssigkeitshold-up wurden mit den CFD Simulationen für unterschiedliche Flüssigkeiten und Belastungen ermittelt. Aus den experimentell aufgenommenen Bildern der Strömungsmuster wurde den Benetzungsgrad berechnet.
Es wurde ein neues Modell zur Beschreibung der Packungskolonnen, die mit Rombopak 4M befüllt sind, mit Hilfe der CFD-Simulationen abgeleitet. Das Modell gibt den Benetzungsgrad, die spezifische Phasengrenzfläche und den Flüssigkeitshold-up für unterschiedliche Flüssigkeiten bei unterschiedlichen Flüssigkeitsbelastungen wieder. Dieses Modell wurde mit den Modellen von Billet u. Schultes [6], Rocha et Al. (SRP-Modell) [7-9], Shi & Mersmann [10] und anderen verglichen. Zum Druckabfall, einem der wichtigsten Parameter in Packungskolonnen, wurden CFD-Simulationen durchgeführt, um den trockenen Druckverlustes eines strukturierten und flachen Packungselements zu finden. Die Ergebnisse wurden mit den experimentellen Daten verglichen.
Es wurden gute Übereinstimmungen zwischen den experimentellen und CFD-Ergebnissen und zwischen den Simulationen und den theoretischen Modellen für die Rinnsalströmung auf einer geneigten Platte gefunden. Die Strömungsmuster und die Ausbreitung bzw. das Verhalten der Flüssigkeit auf dem Packungselement stimmt sehr gut mit den experimentellen Resultaten überein. Das VOF Modell ist sehr empfindlich für die unterschiedlichen Flüssigkeitseigenschaften und kann verwendet werden um kritische Details der Benetzung mit Filmströmung aufzudecken. Damit kann es zur Optimierung der Packungsgeometrie eingesetzt werden.
Eine Fortführung der Arbeit, um CFD - Simulationen für die Strömung innerhalb eines Blockes der Packung durchzuführen, um ausführliche Informationen über die Interaktion zwischen der Flüssigkeit und der Packungsoberfläche zu erhalten, wird empfohlen.

Stichwörter

Benetzung, CFD - Simulation; Fluent; Mehrphasenströmung; Packungskolonnen; Rombopak; Strukturierte Packung, VOF – Modell

Contents

List of Figures

List of Tables

Chapter 1

Overview

1.1 Introduction

There is an increasing trend towards separation processes that are operated in packed columns with stacked or random packing in the chemical and related industry. The use of structured column packing dates back to 1960s. The packings are generally manufactured from different materials such as ceramics, metal and plastics and divided according to their shape into: gauze packing, grid type packings, metal sheet and random packings (s. Fig. (1-1)). Random packings are the best choice for applications with very high liquid loads, whereas gauze packings for applications operate at very low pressures and liquid loads. Metal and grid type packing are suitable for a wide range of applications and are particularly suited for applications where the maximum allowable pressure drop and limitations in height are of importance [11]. Metal sheet packings have a specific surface micro (3-8 mm) or macro (1 to 5 cm) structure in the forms of corrugation, bunches and holes, and may have been treated mechanically or chemically to improve and stabilize their wetting performance [12]. This structure allows for liquid–vapour contact with low overall pressure drop and help to increase the stability of the liquid film by preventing break-up and dry-batches [12-14].

The wetting performance and spatial liquid distribution inside the packings has been recognized as one of the weak areas of knowledge and demands further experimental and theoretical work [12]. It also has a significant impact on the packed columns where a higher wetted area leads to an increase of the interfacial area and enhances heat and mass transfer rates. Liquid flow patterns inside the packed columns depend on the geometry of the channels formed by the arrangement and size of the packing in the bed, liquid properties and loading conditions. The most important parameters in the research connected to the hydrodynamics of packed columns are the pressure drop, the wetted area, the interfacial or effective area and liquid hold-up in addition to the mass transfer coefficient.

Understanding the mechanics of wetting and liquid spreading and the role of interfacial properties on the distribution of the liquid in packed beds will have important consequence in the design of gas-liquid contactors and will lead to a more efficient structured packing design [12]. Heat and mass transfer in a packed column is a function of the effective area resulting mainly from the wetted area of the packing surface, which is affected by the hydrodynamics of flow.

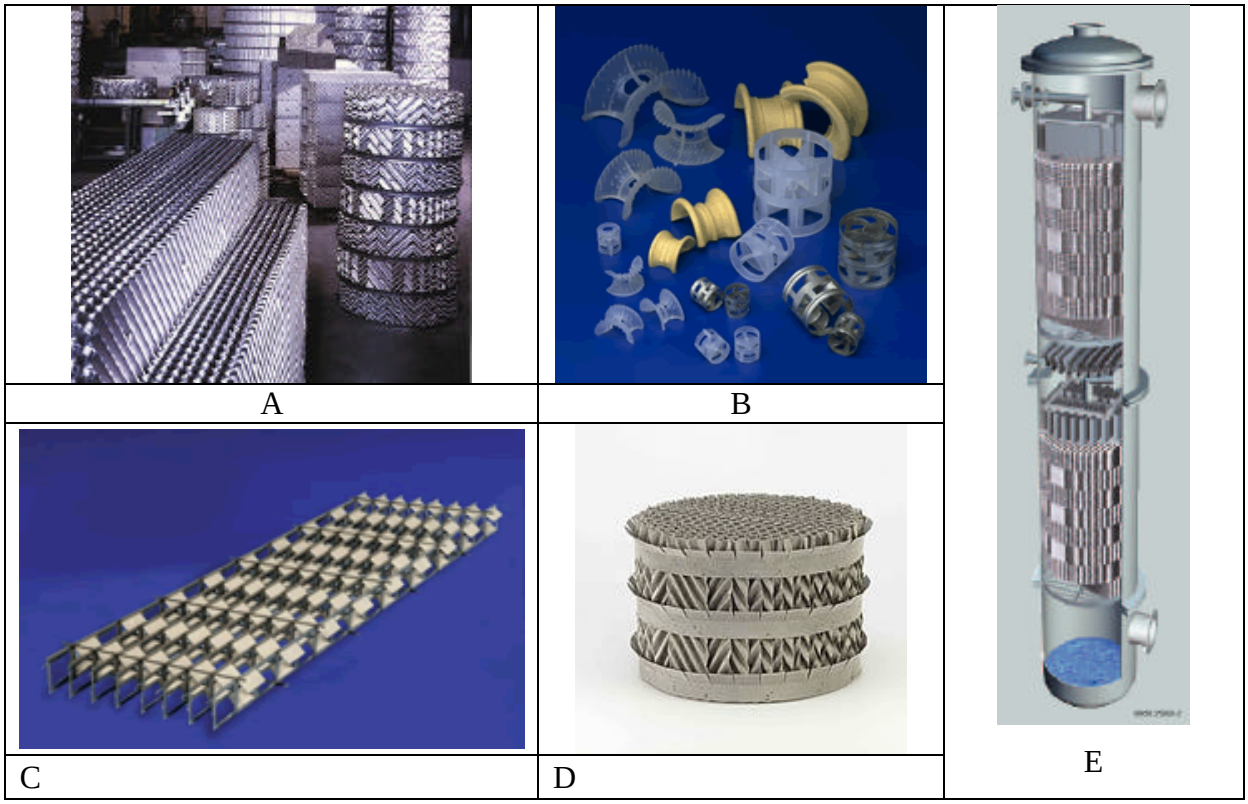

Figure (1-1): Some packing types, A: structured (ordered) packing, B: dumped packing, C: grid packing, D: gauze packing, E: packed column (Q. Sulzer)

1.2 Literature Review

The flow type on an inclined plate, which represents a basic element of the structured packing, depends on flow rate, liquid properties, liquid distributors and plate surface material. The liquid flows as a film, rivulet or dropwise. The rivulet flow is the flow pattern which takes place when the flow rate is reduced so that the film flow on a solid surface develops from a flat continuous liquid layer to a narrow liquid line. When the flow rate is further reduced, it converts to a dropwise flow. Wetting of a solid surface with rivulets is characterized through the contact angle at the three phase line and mostly found in the packing.

A discussion on the different patterns of rivulet liquid flow on a flat plate and the development of liquid flow from drops to a single laminar rivulet and then to a wavy and turbulent rivulet flow was presented by Kern [15-16]. Schmuki & Laso [17] discussed the stability of rivulet flow in their work and the existing regimes of different patterns exhibited by a liquid flowing down an inclined plate. They presented a model to predict the decay frequency of an oscillating or pendulum rivulet. They found that the viscosity and surface tension had the greatest influence on the stability of rivulet flow. Shi & Mersmann [10,18]

presented a correlation for the rivulet width, depending on their experimental measurements. The theoretical analysis of liquid rivulet flow has been performed by many other authors. Towell & Rothfeld [3] and Duffy & Muffatt [2] had presented analytical models to describe the laminar rivulet flow on an inclined plate. Bentwich et al. [19] presented an analytical solution for the velocity distribution of rectilinear rivulet flow down a vertical plate and polynomial one for the inclined plate case. Rivulet profile shapes for both cases were discussed in this work. Stein [20] presented a study about the wetting of solid surfaces with liquids in his work. He developed a new correlation for the Reynolds number at the wetting point for the rivulet and film flow on an inclined plate and for the liquid flow in packed columns making use of the measurements of other authors. Al-Khalil et al. [4] investigated the hydrodynamics and thermal characteristics of the laminar rivulet down a vertical surface. They determined the velocity distribution numerically by the use of a finite element method and presented the average Nusselt number for the two cases of constant wall temperature and constant heat flux. Donic [21] studied the rivulet flow on a vertical plate and presented a correlation for the maximum rivulet thickness.

Wetting of structured simple surfaces are connected to the packing, and the research on this field is very wide. Zhao & Cerro [14] have studied the film flow on different structured surfaces and estimated experimentally the interfacial shape at the free surface by measuring the spatial film thickness. They measured the film thickness profiles on solid surfaces with different micro- and macro-structures in addition to the streamlines patterns and free film velocity to characterize the liquid film flow. Shetty & Cerro [22] have discussed in their experimental work the spreading of liquid over a pre-wetted corrugated plate from a point source and have suggested a Gaussian distribution for the liquid rivulet flow. In another work [23] they studied the thin film flow over complex surfaces; a two dimensional streamline function was used to compute the component of velocity field and to reduce the equation of motion to a single nonlinear ordinary deferential equation for the film thickness. The film thickness profiles were measured in a direction normal to the solid surface, as opposed to the experimental film thickness measured in a direction normal to the axis of the solid surface.

Bontozoglou & Papapolymerou [24] theoretically performed a study on the laminar film flow down inclined sinusoidal corrugations.

In an initial study Ausner et al. [25] made an attempt to measure the velocity inside the rivulet by MPIV (Micro Particle Image Velocimetry) method. In a further work of Ausner et al. [26-27] initial results have been presented on a two immiscible liquids film flow (film, rivulet) flowing on inclined plates. Trivanov [28] studied experiment and theory of viscous film flow

down a vertical periodic surface. Shape of film free surface and stream lines functions were calculated. Stagnation zones were found and their transformation with increasing Reynolds number is obtained. Comparison with experimental data was carried out. There are many publications about wavy films. Adomeit & Renz [29] studied the velocity profiles within the wavy film, with typical film thickness of about 0.5 mm that was measured by the MPIV method.

Structured packing in the packed columns on the other hand was the subject of many scientific publications. Billet & Schultes [6,30] presented a model for the degree of wetting of ordered and dumped packing with the help of large experimental database of different kinds of packings. In addition to that, they correlated the wetted and interfacial areas, liquid hold-up and mass transfer coefficient in packed columns.

A model often used for predicting mass transfer and hydraulic performance of structured packing was developed several years ago within the Separation Research Program (SRP) at the University of Texas, Austin, as it was discussed elsewhere [7-9]. The basis for this model is a modified wetted-wall flow arrangement through channels of the packing. The author used the correlation suggested by Shi & Mersmann [18] for the specific wetted area prediction in packed columns after modification. An alternative model has been developed more recently at the Delft University of Technology. It assumes a complete wetting of the metal surface with liquid film flow down inclined corrugated plates and explicitly takes into account several macro geometrical parameters, which can affect the packing performance [31,32]. The liquid hold-up is determined from the packing area and the average film thickness. In a recently published work [33] a comprehensive total reflux distillation study of metal sheet structured packing was carried out using the two models. In this study a discussion was performed on the deviations of predictions from measurements for Montz packings that have a specific surface area between 244 and 382 m^2/m^3. The two models have given different predictions for the specific interfacial area and liquid hold-up. Delft's predictions for liquid hold-up were lower than that of SRP models. The predicted effective area from SRP increased strongly with F-factor and pressure, but Delft's model prediction of effective area increased slightly with F-factor. The authors concluded that an increase of the reliability and the overall accuracy of the two models demand an improved modelling of the effective area and recommended an empirical correlation [34], which was developed for dumped packing. It assumes that the wetted area on the packing is identical with the gas liquid interface. It is a function of different liquid properties and liquid load, and does not demand any packing-specific coefficients. In relatively new work an experimental investigation was carried out to examine

the specific wetted area and mass transfer behaviour for the flow on a set of corrugated plates in a square section [35].

In the recent years, there has been considerable academic and industrial interest in the use of the CFD methods to simulate the two phase flows found in the industrial applications. Wetting of a solid surface is considered an open or free surface liquid flow and this phenomenon can be solved macroscopically with the multiphase flow VOF method (Volume of Fluid). This model, which is described in the next chapters, is used to track the interface between two or more phases. Applications of this VOF approach developed by Hirt & Nichols [36] to simulate complex, separated phases have started recently [37]. Very few works can be found in the literature, which deal with the CFD simulations of multiphase flows with free surface. In the work of Casey et al. [38] some results are presented for the application of the VOF model to simulate the liquid flow on an inclined solid surface in 2-D mode. Simulation of the film flow over an inclined plate, for example, was a subject of the work published in [39] and the CFD simulation of the two-liquid phase film flow on a flat plate of the work presented in [26-27,40]. Few experimental and CFD simulation results on the film flow of inclined plate were presented by Ausner et al. in [26-27] using the CFD-code from the commercial Ansys-CFX.

Very few works can be found in the literature, which deal with the CFD simulations of one or multiphase flow in structured packing. Some of these CFD-simulation works have been performed to estimate the pressure drop in a basic packing element of the packing. Liquid hold-up was determined approximately through CFD simulations of a film flow over a plate similar to that of the packing [41]. The work presented by Raynal et al. [42] reports the CFD simulation for the pressure drop in a packing element in addition to 2D CFD-simulations with the VOF model to determine the liquid thickness on a wavy plate similar to the packing surface. These last results were used to derive the liquid hold-up on the packing. Another attempt was also presented by Valluri et al. [41] where 3D simulation for the film flow over a wavy plate was discussed.

1.3 Objectives and Significances

The thesis is dedicated to investigate the wetting of packing elements experimentally and using the CFD methods. These objectives are:

- CFD simulations of the rivulet flow on structured and flat inclined plate using the VOF (Volume of Fluid) multiphase flow model
- CFD simulations of the wetting patterns on the structured packing of Rombopak 4M using the VOF (Volume of Fluid) multiphase flow model

- Experimental validation of the CFD simulation results for the rivulet flow and the wetting flow patterns on the packing
- Revealing details on the flow structure, liquid-solid surface and liquid-gas interaction
- Comparing the results with the models from literature
- Developing correlations to describe the hydrodynamics of the structured packing Rombopak 4M
- Dry pressure drop CFD simulation in Rombopak 4M and 9M and comparing them with the experimental data at different gas loadings.

The study should be performed on one and multi-element packing sheet of the packing Rombopak 4M, which is a product of the Kühni company in Switzerland and is shown in Fig. (1-2) [43]. The smallest part of the packing is represented in the packing sheet (PS) consisting of four connected lamellas and shown in Fig. (1-2C). The hydrodynamic parameters of structured packing columns are the degree of wetting, the effective area and the liquid hold-up and the dry pressure drop.

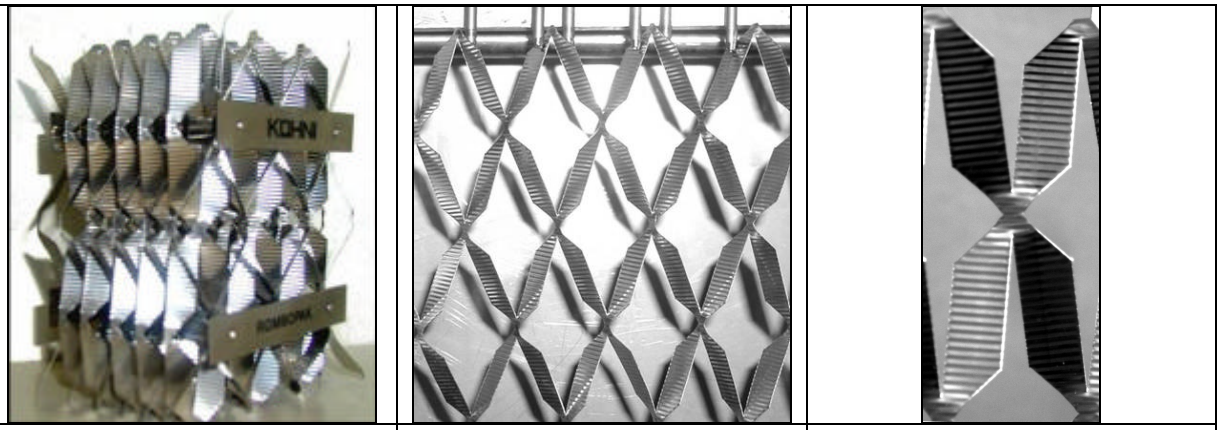

Figure (1-2): A- Structured packing Rombopak, B- Structured packing sheet C- Structured packing element

Chapter 2

Theoretical Basics

2.1 Wetting Phenomenon

Wettability denotes the ability of liquids to spread on surface; the phenomenon of wetting (hydrophilic) or non-wetting (hydrophobic) of a solid by a liquid is better understood by studying what is known as the contact angle. It is defined geometrically as the angle formed by a liquid at the three phase boundary where a liquid, gas and solid intersect as shown in Fig. (2-1), the better the wettability the lower is the contact angle; surfaces are called incompletely wettable in case of an occurring contact angle <90°. In other words good wetting liquids have small contact angle 90>?>0, whereas bad wetting liquids have high contact angle values >90° (s. Fig. (2-2)). A zero contact angle represents complete wetting. On a hydrophobic surface, the water remains more like a droplet, so there is a minimum contact area with the substrate and a maximum contact angle. On a hydrophilic surface a water droplet will easily spread out, making the contact surface between the water and the substrate maximum and the contact angle minimum. The drop of liquid forming an angle may be considered as resting in equilibrium by balancing the three forces involved. Namely, the interfacial tensions between solid and liquid s_{SL}, that between solid and vapour s_S and that between liquid and vapour s_L and given in Young equation [44]:

$$s_S = s_{SL} + s_L \cos q \qquad \textbf{(2-1)}$$

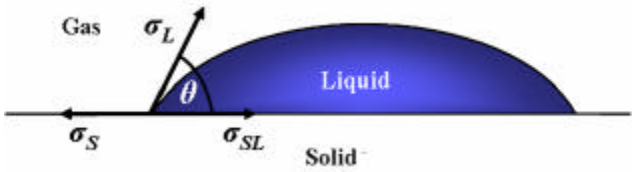

Figure (2-1): Single drop contact angle balance

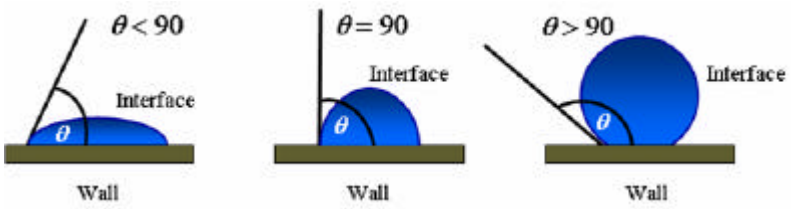

Figure (2-2): Single drop contact angle

The measurement of a single static contact angle to characterize the interaction is no longer thought to be adequate. For any given solid/ liquid interaction there exists a range of contact angles which may be found. The value´s of static contact angles are found to depend on the recent history of the interaction. When the drop has recently expanded the angle is said to represent the 'advanced' contact angle. When the drop has recently contracted the angle is said to represent the 'receded' contact angle. These angles fall within a range with advanced angles approaching a maximum value and receded angles approaching a minimum value.

If the three phase (liquid/solid/vapour) boundary is in actual motion the angles produced are called Dynamic Contact Angles and are referred to as 'advancing' and 'receding' angles. The difference between 'advanced' and 'advancing', 'receded' and 'receding' is that in the static case motion is incipient and in the dynamic case motion is actual. Dynamic contact angles may be assayed at various rates of speed. Dynamic contact angles measured at low velocities should be equal to properly measured static angles. The difference between the maximum advanced/advancing) and minimum (receded/receding) contact angle values is called the contact angle hysteresis [45]. A great deal of research has gone into analysis of the significance of hysteresis. It has been used to help to characterize surface heterogeneity, roughness and mobility [46-47]. The surface roughness affects the contact angle values [48]. It is important to be considered, when developing new materials for specific applications. This will not discussed here, hence we will perform our study only on one kind of metal packing.

Wetting of a solid surface is a complex phenomenon and it depends on many factors in the process, these factors are:

- Liquid properties such as viscosity, density, temperature etc.
- Solid-liquid interaction and surface kind: the contact angle at the three phase line gas-liquid-solid which, reflects also the surface roughness.
- Operating conditions: liquid load in a packed column.

2.1.1 Measuring Methods of Contact Angle on Solids

2.1.1.1 Sessile Drop Method (Goniometry)

Sessile drop method is an optical contact angle method. This method is used to estimate wetting properties of a localized region on a solid surface. The angle between the baseline of the drop and the tangent at the drop boundary is measured (s. Fig. (2-2)). It is ideal for curved samples or where one side of the sample has different properties than the other. Analysis of the shape of a drop of test liquid placed on a solid is the basis for goniometry. The basic elements of a goniometer include a light source, sample stage, lens and image capture.

Contact angle can be assessed directly by measuring the angle formed between the solid and the tangent to the drop surface.

The production of drops with advanced and receded edges involves one of two strategies. Drops can be made to have advanced edges by addition of liquid. Receded edges may be produced by allowing sufficient evaporation or by withdrawing liquid from the drop. Alternately, both advanced and receded edges are produced when the stage on which the solid is held tilted to the point of incipient motion. Using an instrument with high speed image capture capabilities shapes of drops in motion may be analyzed.

Limitations

The assignment of the tangent line which will define the contact angle is a factor which can limit the reproducibility of contact angle measurements. Conventional goniometry relies on the consistency of the operator in the assignment of the tangent line. This can lead to significant error, especially subjective error between multiple users. The conditions which produce advanced and receded angles are sometimes difficult to reproduce. Although drops in motion can produce data on dynamic contact angles but the velocity of motion cannot be controlled. It is also less suited, when compared to tensiometry, to analyse the effects of wetting on changes in contact angle.

2.1.1.2 Dynamic Wilhelmy Method (Tensiometry)

It is a method for calculating average advancing and receding contact angles on solids of uniform geometry. Both sides of the solid must have the same properties. Wetting force on the solid is measured as the solid is immersed in or withdrawn from a liquid of known surface tension. The tensiometric method for measuring contact angles measures the forces that are present when a sample of solid is brought into contact with a test liquid. If the forces of interaction, geometry of the solid and surface tension of the liquid are known the contact angle may be calculated. The user first makes a measurement of the surface tension of the liquid using either a Wilhelmy plate or DuNouy ring. The sample of the solid to be tested is then hung on the balance and tarred. The liquid is then raised to contact the solid. When the solid contacts the liquid the change in forces is detected and this elevation is registered as zero depth of immersion. As the solid is pushed into the liquid the forces on the balance are recorded.

The forces on the balance are:

$$F_{total} = \text{wetting force} + \text{weight of probe} - \text{buoyancy}$$

For a probe the weight of the probe is tarred and the effects of the buoyancy force are removed by extrapolating the graph back to zero depth of immersion. The remaining component force is the wetting force which is defined as:

$$\text{Wetting force} = s\,P\cos?$$

Where, s is the liquid surface tension, P is the perimeter of the probe. Thus at any depth data is received which can be used to calculate contact angle. This contact angle, which is obtained from data generated as the probe advances into the liquid, is the advancing contact angle. The sample is immersed to a set depth and the process is reversed. As the probe retreats from the liquid the force is measured and used to calculate the receding contact angle.

Advantages

The use of tensiometry for measurement of contact angle has several advantages over conventional goniometry. At any point of the immersion graph, all points along the perimeter of the solid at that depth contribute to the force measurement recorded. Thus the force used to calculate q at any given depth of immersion is already an averaged value. You may calculate an averaged value for the entire length of the sample or average any part of the immersion graph data to assay changes in contact angle along the length of the sample. This technique allows the user to analyze contact angles produced from wetting over an entire range of velocities from static to rapid wetting. Because the contact angles are determined from the forces measured by the instrument there is no possibility of subjective error. The graphs produced by this technique are very useful in studying hysteresis. Variations in both advancing and receding contact angles for the entire length of the sample tested are visualized on the same graph. In addition variations generated over multiple wetting/dewetting cycles can yield information on changes caused by wetting (such as absorption or surface reorientation).

Limitations

There are two major limitations for the application of this technique. Firstly the user must have enough of the liquid being tested available so that can immerse a portion of his solid in it. Secondly the solid in question must be available in samples which meet the following constraints. The sample must be formed or cut in a regular geometry such that it has a constant perimeter over a portion of its length. Rods, plates or fibers of known perimeter are ideal. The sample must have the same surface on all sides which contact the liquid. The sample must also be small enough so that it can be hung on the microbalance measuring apparatus. It is also more difficult to use this technique in systems which are measured at high

temperatures. Liquids at a temperature of 100 °c or below can be easily handled but for measurements above this range goniometry is recommended.

2.1.1.3 Single Fiber Wilhelmy Method

Dynamic Wilhelmy method can be applied to single fibers to measure advancing and receding contact angles.

2.1.1.4 Powder Contact Angle Method (Washburn Method)

This method enables measurement of average contact angle and sorption speed for powders and other porous materials. Change of weight as a function of time is measured. This method is chosen when the solid sample to be tested contains a porous architecture which leads to absorption of the wetting liquid. The solid is brought into contact with the testing liquid and the mass of liquid absorbed into the solid is measured as a function of time. The amount absorbed is a function of the viscosity, density and surface tension of the liquid, the material constant of the solid, and the contact angle of the interaction. If the viscosity, density and surface tension of the liquid are known the material constant and contact angle can be solved.

2.1.2 Characterization of the Solid Surface

Measurements of surface tension yield data which directly reflect thermodynamic characteristics of the liquid tested. Measurement of contact angles yields data which reflect the thermodynamics of a liquid/solid interaction. If one wishes to characterize the wetting behavior of a particular liquid/solid pair one only needs to report the contact angle. It is possible to characterize the wettability of your solid in a more general way. Various methods are used but the same basic principle applies for each. The solid is tested against a series of liquids and contact angles are measured. Calculations based on these measurements produce a parameter (critical surface tension, surface free energy, etc) which quantifies a characteristic of the solid which mediates wetting. Two basic approaches are covered here.

2.1.2.1 Critical Surface Tension (Zisman's method)

Fox & Zisman [49] showed that the cosines of the contact angles formed by drops of homologous liquids on a solid surface vary linearly with their surface tensions. The critical surface tension can then be found extrapolating the linear function to *cos?=1* as followed: Series of homologous liquids of different surface tensions are used; a graph of *cos?* vs. *s* is produced. It will be found where the data form a line which approaches *cos? =1* at a given value of *s*. This is the maximal surface tension of a liquid which may completely wet the solid

surface. This value, called the critical surface tension, can be used to characterize the solid surface.

2.1.2.2 Free Surface Energy

In addition to contact angles, wettability can be described in terms of the surface free energy. This concept allows a description of surface properties, which is independent of the test liquid. While the surface free energy of liquids can be obtained easily by measuring the work necessary to create one unit area of new surface. Most approaches start with the Young equation (Young, 1805) (Eq. (2-1)), which describes the energy balance of a water drop let on a solid surface. s_L, s_S, and s_{SL} are the surface free energy of the liquid (mJ/m^2), the surface free energy of the solid (mJ/m^2), and the interfacial free energy between the liquid and the solid (mJ/m^2), respectively. From Eq. (2-1) it follows that, perfect wetting occurs when *cos?*=1 and it is favoured by a high solid surface free energy, a low interfacial free energy and a low liquid surface free energy. Both of surface free energy of a liquid s_L, and the surface free energy of a solid s_S, can be expressed as the sum of two components of interaction; that is,

$$s_L = s_{Ld} + s_{Lp} \quad \textbf{(2-2)}$$

$$s_S = s_{Sd} + s_{Sp} \quad \textbf{(2-3)}$$

Where, s_{Ld} and s_{Lp} are the dispersion (Lifshitz-van der Waals) and polar (acid-base) components of the surface free energy of the liquid, and s_{Sd} and s_{Sp} are the corresponding dispersion components of the surface free energy of the solid. Owens & Wendt [50] successfully used concept to derive an expression for the contact angle of a liquid on a solid surface in terms of the dispersion and polar components that is:

$$1\text{-}\cos q = 2 s_{\mathrm{Sd}}^{1/2} (s_{\mathrm{Ld}}^{1/2} / s_{\mathrm{L}}) + 2 s_{\mathrm{Sp}}^{1/2} (s_{\mathrm{Lp}}^{1/2} / s_L) \quad \textbf{(2-4)}$$

By use of Eq. (2-4), it is possible to quantify the surface free energy of the solid from the contact angle values of different test liquids with known dispersion and polar components of surface free energy. In practice the surface free energy of the solid can be obtained by transforming Eq. (2-4) into a linear equation of the type $y = mx + b$; and depicting y vs. x for different test liquids. The squared slope is the polar component and the squared intercept is the dispersion component of the solid surface free energy. The total free surface energy is merely the sum of its two component forces as Eq. (2-3).

2.1.3 Typical Contact Angles

On extremely hydrophilic surfaces, a water droplet will completely spread (an effective contact angle of 0°). This occurs for surfaces that have a large affinity for water (including materials that absorb water). On many hydrophilic surfaces, water droplets will exhibit

contact angles of 10° to 30°. On highly hydrophobic surfaces, which are incompatible with water, one observes a large contact angle (70° to 90°). Some surfaces have water contact angles as high as 150° or even 180°. On these surfaces, water droplets simple rest on the surface, without actually wetting to any significant extent. The contact angle thus directly provides information on the interaction energy between the surface and the liquid. In our experiments the sessile drop method was used to determine the static contact angle for different liquid systems as it will be seen in chapter 3.

2.1.4 Pressure Jump across a Curved Surface

If viscous forces are absent, the pressure jump across a curved surface is given by the Young-Laplace equation, which relates pressure inside a liquid with the pressure outside it, the surface tension and the geometry of the surface.

$$\Delta p = s\,\frac{dA}{dV} \qquad \textbf{(2-5)}$$

This equation can be applied to any surface:

For a flat surface $\frac{dA}{dV} = 0$ so the pressure inside is the same as the pressure outside.

For a spherical surface with radius R:

$$p_I = p_O + \frac{2s}{R} \qquad \textbf{(2-6)}$$

For curved surface measured by two radii in orthogonal directions, R_1, and R_2:

$$p_1 - p_2 = s\,(\frac{1}{R_1} + \frac{1}{R_2}) \qquad \textbf{(2-7)}$$

2.2 Rivulet Flow Models

2.2.1 Rivulet Flow on a Flat Plate

The rivulet flow is the flow pattern which takes place when the flow rate is reduced so that the film flow on a solid surface develops from a flat continuous liquid layer to a narrow liquid line. When the flow rate is further reduced, it converts to a dropwise flow. The specific rivulet profile is shown in Fig. (2-3), where w_r is the rivulet width and d_r is the maximal rivulet thickness at a certain inclination of the plate b. Here $u_{r,mean}$ is the mean velocity of the rivulet and q the contact angle.

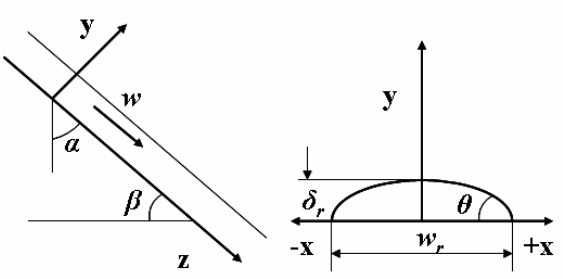

Figure (2-3): Rivulet flow parameters

In this work we restrict our research to laminar rivulet flow, whereby the Navier-Stokes equations given by Eqs. (2-8) to (2-10) are simplified for a flat plate case using the following assumptions: The flow is one dimensional and parallel to plate edge in *z*-direction. The flow is incompressible, is at steady state and fully developed and there is no change in the width and thickness. The shear stress at the gas-liquid interface is neglected.

Moreover the pressure is considered constant along the *x*-axis (Eq. (2-8)) and the hydrostatic pressure gradient along the y axis is given with Eq. (2-9). The velocity distribution and the rivulet profile are given by Eq. (2-10), which balances viscous and gravitational forces.

$$\frac{\partial p}{\partial x} = 0 \qquad \textbf{(2-8)}$$

$$\frac{\partial p}{\partial y} = -r\,g\sin a \qquad \textbf{(2-9)}$$

$$\frac{\partial^2 w}{\partial x^2} + \frac{\partial^2 w}{\partial y^2} = -\frac{g\cos a}{n} \qquad \textbf{(2-10)}$$

2.2.1.1 Model of Towell and Rothfeld

The model presented by Towell & Rothfeld [3] deals with the solution of Eqs. (2-8) to (2-10) for the three cases: small, flat and the general rivulet flow. In the general case, this includes all these cases, their solution starts with the differential form of the expression for curved interfaces. It is given in non-dimensional form by Eq. (2-11) where the pressure at the interface is set equal to the normal stress and the z stress component in flow direction equal to zero.

$$\frac{Y''}{(1+Y'^2)^{3/2}} = \frac{a_c}{R} + Y \qquad \textbf{(2-11)}$$

Where

$a_c = \sqrt{s\,/\,r_L g\sin a}$ is the capillary constant, $Y = (h_0 - h)/a_c$, where $h=h(x)$ is the rivulet profile function, the maximum rivulet thickness $h=h_0$ is at $X=0$, $Y=Y(X)$, $X=x/a_c$, and R is the radius of the interface curvature at $Y=0$. In this model Eq. (2-11) represents a family of curves with $a_c/R=d$ as a parameter and only one of them at a definite value of d describes the

interface for a given stream width (or flow rate) and contact angle. To find the interface profile for a given flow rate, Eq. (2-11) must be solved together with a flow rate equation (Eq. (2-12) which needs velocity and interface profiles according to Eq. (2-13). This problem has to be solved by iteration using an approximated velocity profile given by Eq. (2-13) resulting from an approximated non-dimensional form of Eq. (2-10), with $\frac{\partial w}{\partial x} << \frac{\partial w}{\partial y}$ as a starting point of the solution.

$$Q_r = \int_{-l/2}^{l/2} \int_{0}^{h} w(x,y)dxdy \quad \textbf{(2-12)}$$

$$w = (Y_0 - Y)x - \frac{1}{2}x^2 \quad \textbf{(2-13)}$$

where $x=y/a_c$.

The general solutions of Eq. (2-11) are given implicitly by eqs. (2-14,2-15) with respect to the parameter f. This parameter changes from $\pi/2$ at X=0 to a minimum value at f_{min} at the other outer edge of the rivulet and can be estimated from the contact angle q using Eq.(2-16).

$$X = \frac{2-k^2}{k}\left[K - F(k,f)\right] - \frac{2}{k}\left[E - E(k,f)\right] \quad \textbf{(2-14)}$$

$$Z = \frac{2}{k}\sqrt{1-k^2\sin^2 f} \quad \textbf{(2-15)}$$

$$\sin(f_{\min}) = \cos(q/2) \quad \textbf{(2-16)}$$

where

$$Z = Y + d \quad \textbf{(2-17)}$$

$$k = \frac{2}{\sqrt{4+d^2}} \quad \textbf{(2-18)}$$

and $E(k, f)$, $F(k,f)$ are elliptical integrals and $E=E(k, fmin)$, $F=F(k,fmin)$ [3].

2.2.1.2 Model of Duffy and Moffatt

Duffy & Muffatt [2] presented an approximate solution for rivulet flow. They solved a similar form of the Navier-Stokes Eqs. (2-8) to (2-10) depending on the thin film theory and using the same expression for the curved interface given by Eq. (2-11), but in a dimensional form:

$$p(h) = p_g - \frac{s\,h''}{(1+h'^2)^{3/2}} \quad \textbf{(2-19)}$$

where $h=y(x)$ is the rivulet profile and h', h'' are the first and second derivatives with respect to x. Here the velocity profile is only a function of y, since $\frac{\partial w}{\partial x} << \frac{\partial w}{\partial y}$ and $h'^2 << 1$. According to these assumptions, these authors presented an explicit solution for the rivulet profile across the whole range of inclination angles, when $a<\pi/2$, the rivulet profile is given explicitly by:

$$h(x) = \left(\frac{s}{r_L g \left|\sin a\right|}\right)^{1/2} \tan q \, \frac{\cosh B - \cosh z\, B}{\sinh B} \qquad \textbf{(2-20)}$$

Where B is Bond number defined as:

$$B = w_r \left(\frac{r_L g \left|\cos a\right|}{m_L}\right) \qquad \textbf{(2-21)}$$

And the maximum rivulet height at the symmetry where x=0 is given by the equation:

$$d_r = \left(\frac{s}{r_L g \left|\sin a\right|}\right)^{1/2} \tan q \, \tanh \frac{1}{2} B \qquad \textbf{(2-22)}$$

The film thickness and width from this model can be simply calculated at any liquid flow rate and physical properties.

2.2.1.3 Al-Khalil and Kern Models

For vertical plate Kern [15-16] has presented a model for prediction the maximum rivulet thickness for a laminar rivulet flow as a function of Reynolds number in the following correlation:

$$\frac{d_r}{((\mu_L / r_L)/g)^{1/3}} = 1.645 \mathrm{Re}_r^{1/3} \qquad \textbf{(2-23)}$$

Similar correlation for the turbulent rivulet flow was given by Kern [15], where the critical Reynolds number has a value $\mathrm{Re}_{r,cr}$=220 and this was proved only for water. It has the form:

$$\frac{d_r}{((\mu_L / r_L)/g)^{1/3}} = 0.815 \mathrm{Re}_r^{7/15} \qquad \textbf{(2-24)}$$

Re is defined as: $\mathrm{Re}_r = \dfrac{r_L u_{r,mean} d_r}{m_L}$

Later Al-Khalil et al. [4] rederived Eq. (2-23) analytically by determining the velocity distribution numerically using the FEM (Finite Element Method) with 1.643 as a constant instead of 1.645.

In addition to that a dimensionless mean and maximum velocity was defined by the two authors according to Eq. (2-25 and 26).

$$V_{r,mean} = \frac{u_{r,mean} m_L}{r_L g d_r^{\,2}} \qquad \textbf{(2-25)}$$

$$V_{r,\max} = \frac{u_{r,\max} m_L}{r_L g d_r^{\,2}} \qquad \textbf{(2-26)}$$

In the case of vertical plate and small contact angles: The laminar film flow, the dimensionless mean and maximum velocities have values of 1/3 [19] and 0.5 [16]

consequetly. The laminar rivulet flow $V_{r,mean}$ has a value of 0.225 [4,16] and $V_{r,max}$ is less than 0.5 [16].

2.2.1.4 Bentwich Model

Bentwich et al. [19] presented an analytical solution for the velocity distribution of rivulet flow down a vertical plate. He also used a generalized Ritz-Galerkin method to obtain a polynomial solution for the case of inclined plate. The cross section was also presented as elliptical integration for contact angels up to 150°. He presented an approaching for the rivulet profile shapes on vertical and inclined plates as they shown in Fig. (2-4). On inclined plate, end effects of the rivulet profile become negligible, and the flow cross section tends to fill the bounding rectangular of finite height.

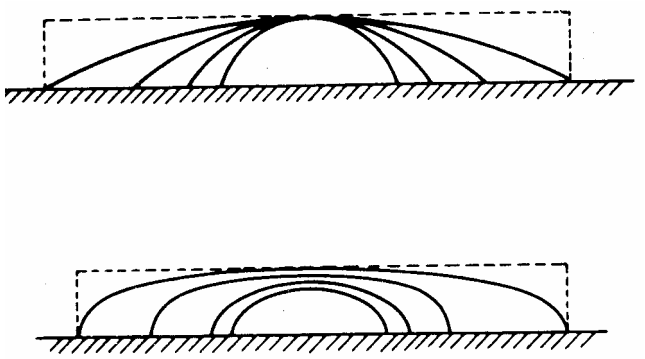

Figure (2-4): Bentwich predictions for the rivulet profile shapes on vertical (top) and inclined (bottom) flat plate

2.2.1.5 Shi and Mersmann Model

Shi & Mersmann [10,18] investigated the rivulet flow and determined the relation between the surface tension and contact angle for different substrates. They correlated the rivulet width, which was used later by Rocha et al. [8-9] in modelling the degree of wetting in packed column.

$$w_r = 3.49 Q_r \left(\frac{m_L}{r_L}\right)^{0.2} \left(\frac{r_L}{s\,g}\right)^{0.15} (1 - 0.93\cos q)^{-1} \qquad \textbf{(2-27)}$$

There are many other theoretical studies about the rivulet flow on a solid surface. A brief survey is given in the work of Stein [20]. Film flow and the evolution of interfacial waves were discussed in a lot of works and it will not be discussed in this research [51-54].

2.2.2 Rivulet Flow on a Wavy Plate

Rivulet flow on a wavy plate is less discussed in the literature. Shetty & Cerro [22] have studied in their experimental work, the spreading of liquid over a pre-wetted corrugated plate

from a point source and have suggested a Gaussian distribution for the liquid rivulet flow. The studied corrugated plate had a macro structure; where the rivulet maximum thickness is smaller than the corrugation.

Film flow over different structured surfaces was discussed by Zhao & Cerro [13-14] and he has estimated experimentally the interfacial shape at the free surface by measuring the spatial film thickness.

2.3 Packed Columns

For intensivation the contact between the counter-current two phase flow of gas and liquid and consequently a good heat and mass transfer, different internals are used in the columns, which are called packings. An objective of the packing development is the creation of a large wettable and effective volume-specific packing surface area *a* as possible and at the same time high availability of the cavities of the packing for the gas and liquid flow. The liquid trickles downward over the surface of the packing in the form of rivulets or films.

2.3.1 Porosity and Specific Area and Diameter

Column calculations are carried out by representing the different packings with simple geometric models, which are usually parallel tubes or beds of spheres. The model structure is chosen so that it has the same ratio of surface area to volume (*a*) and the same porosity *e* as the actual packing. If a bed-of-spheres model is assumed,

$$a = \frac{A}{V} = \frac{Nd^2p}{V} \qquad \textbf{(2-28)}$$

where *A* is the surface area of the packing, *V* the bed volume, *N* the number of "model" spheres, and d their diameter. Furthermore,

$$e = \frac{V - Vsp}{V} = 1 - \frac{N}{V}\frac{d^3p}{6} \qquad \textbf{(2-29)}$$

where, V_{sp} is the volume occupied by the spheres. *e* is defined as the porosity of the packing and will be provided by the manufacuter for every packing kind in addition to the specific packing area *a*.

By eliminating the number of spheres z, the following equation is obtained:

$$d = \frac{6(1-e)}{a} \qquad \textbf{(2-30)}$$

Because the surface area relative to the volume *a* and the porosity *e* is known for the actual model, the diameter of the model sphere can be determined by using Eq. (2-30). The

porosities of modern packings are so large that the spheres in the model structure do not touch each other.

2.3.2 Wetting of a Packed Column

Wetting of packed columns is very important in the distillation, absorption and desorption processes, which affect directly the interfacial area, where heat and mass transfer occur. In contrast to plate columns, packed columns require a minimum liquid load to ensure sufficient mass transfer. Below this minimum value, only a very small part of the column is wetted, and liquid and vapour are no longer in intimate contact. This results in a considerable drop in separating efficiency. The minimum liquid load $L_{L,min}$, can be calculated from:

$$L_{L,\min} = 7.7\times10^{-6}\left(\frac{r_L s^3}{m_L g}\right)^{2/9}\left(\frac{g}{a}\right)^{1/2} \quad \textbf{(2-31)}$$

In practice, minimum liquid loads for dumped packings are 10 (m^3/ m^2h) for aqueous systems and 5 (m^3/ m^2h) for organic systems. Columns with structured packings can be operated in an organic medium with liquid amounts as small as 0.2 (m^3/ m^2h) [46].

2.3.3 Liquid Hold-up and the Pressure Drop

The liquid hold-up in a wetted packed column consists of two parts: the static and the dynamic hold-up $h_L=h_{L,stat}+h_{L,dyn}$ [46,55].

The static liquid hold-up $h_{L,stat}$ is bound by capillary and adhesion forces and remains in the packing after irrigation is stopped. It describes the liquid prevailing in the pores and gaps of the packing. The static liquid hold-up is a function of the physical properties of the liquid flow (density $?_L$, dynamic viscosity μ_L, and surface tension s), the characteristic packing properties (void fraction e, and specific packing surface a), the liquid load u_L, and the acceleration of gravity g. On the contrary, dynamic hold-up is the amount of liquid participating active in the liquid flow, thus raising the liquid velocity. An increase of the dynamic hold-up results in a better mass transfer.

Altogether, the increase of the liquid hold-up leads to following phenomena:

- The free cross-sectional area reduces.
- The pressure drop, the vapour velocity, the liquid rivulet width and wetted packing area increases.
- The phase interface becomes more turbulent which leads to more intensive mass transfer.

The total liquid hold-up can be calculated by:

$$h_L = \frac{V_L}{V} \quad \textbf{(2-32)}$$

where V_L is the liquid volume and V the bed volume. There are many published models for the prediction of the liquid hold-up. Some of them will be discussed below.

Typical experimental curves for the hold-up h_L in a Bialecki ring packing at various gas and liquid loads are shown in Fig. (2-5). Two regions can be distinguished:

- A low vapour load region in which the hold-up h_L depends solely on the liquid load, the linear part of the curves in Fig. (2-5).
- A high vapor-load region in which h depends on both the liquid load and the vapor loads (*h* in the figure), the curvy part of curves in Fig. (2-5).

The transition between these two regions occurs at the loading point [46].

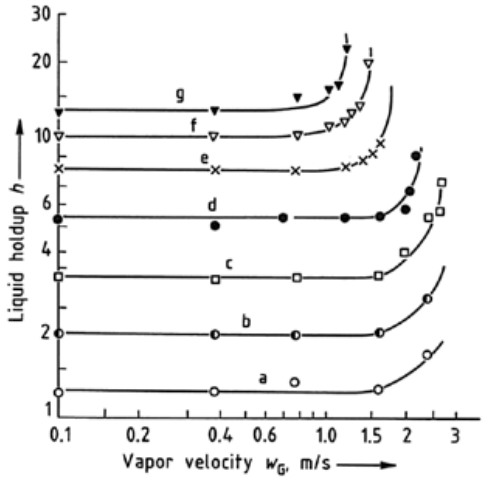

Figure (2-5): Liquid hold-up *h* in a dumped packing composed of 25-mm Bialecki rings, as a function of vapour and liquid loads

Liquid velocity u_L (m/h): a) 2.8; b) 5; c) 10; d) 20; e) 40; f) 60; g) 80. Measurements were made using air – water at 20 °C and 0.1 MPa in a column with a packing height of 1.5 m and a diameter of 0.15 m

Pressure drop in packed columns is an important parameter especially in vacuum columns, when the separated liquid is sensitive to the temperature. The dry pressure drop is measured in packed column in absence of the liquid flow. It is always lower than the wet pressure drop measured with liquid flow, because of the liquid flowing through the column changes the bed structure due to liquid hold-up. There are a many works to model the pressure drop in packed columns, for examples in [6,8].

2.3.4 Liquid and Gas Load

The gas or liquid load can be expressed in what is known as superfacial velocity of gas or liquid. It is defined as the fluid flow rate divided by the free cross sectional area of the packed

column. They are used in modelling of the hydrodynamics of packed columns. The liquid superfacial velocity u_L and the gas superfacial velocity u_g are given in the following expressions:

$$u_L = \frac{L_L}{A_{sec}} \quad \textbf{(2-33)}$$

$$u_g = \frac{L_g}{A_{sec}} \quad \textbf{(2-34)}$$

The gas or vapour load in a packed column is usually expressed by the F-factor, which is given by

$$F'\text{-}factor = u_g \sqrt{\frac{r_g}{r_L - r_g}} \quad \textbf{(2-35)}$$

At low and moderate pressures, $?_g$ is small compared to $?_L$ and can be neglected [30]. Hence, F-factor, which is often resorted in practice as a measure of the dynamic load on the column, is the product of the superfacial velocity u_g and the square root of the vapour density, i. e.

$$F\text{-}factor = u_g \sqrt{r_g} \quad \textbf{(2-36)}$$

2.3.5 Flooding in Packed Columns

The flooding point is an important parameter in column dimensioning (s. Fig. (2-6). It represents the column load at which the liquid can no longer flow counter currently to the rising vapour. Liquid flow is obstructed by the high vapour load to such an extent that it collects in the bed. The flooding point is clearly indicated by a very steep increase in the pressure drop. Empirical correlations are available for determining the flooding point in form of diagrams [46].

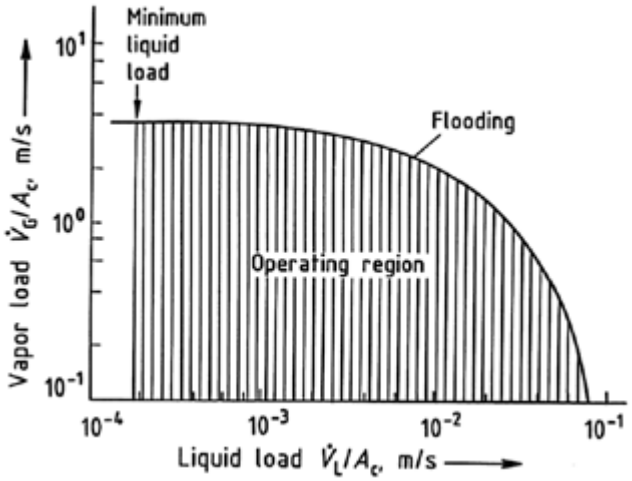

Figure (2-6): Operating region of a packed column

2.3.6 Structured Packing Models

The structured packing models in the literature describe from one side the hydrodynamics of packed columns, this includes pressure drop, flooding and liquid hold-up. From the other side they predict the mass transfer efficiency through prediction the interfacial area as a function of the surface type, packing geometry, phase flow conditions, and fluid properties. Some models can predict the degree of wetting and correlate it to the specific interfacial area. In the following section we will discuss different models found in the literature.

The liquid generally moves in rivulets over the surface of the bed, but complete wetting of the packing usually does not occur. Hence, the mass-transfer area is generally smaller than the surface area of the packing.

2.3.6.1 Billet & Schultes Model

Billet & Schultes [6] have presented a calculation method for the mass transfer for dumped and structured packings. In their work, they have also presented a correlation for the hydrodynamic surface area a_h at two ranges of Reynolds numbers given in Eqs. ((2-37) and (2-38). The hydrodynamic surface area increases less in the range of low Reynolds number, compared to that for large Reynolds number, if the liquid load becomes higher:

$Re_L < 5$

$$\frac{a_h}{a} = C_h \,\mathrm{Re}_L^{\,0.15}\, Fr_L^{0.1} \qquad \textbf{(2-37)}$$

$Re_L = 5$

$$\frac{a_h}{a} = C_h 0.85\,\mathrm{Re}_L^{\,0.25}\, Fr_L^{0.1} \qquad \textbf{(2-38)}$$

The liquid hold-up in packed columns is given by the correlations suggested by Billet & Schultes [6] in Eq. (2-39) as a function of the degree of wetting. As discussed above the wetting correlation of Billet & Schultes [6] for ordered packing does not include the parameters surface tension and contact angle. The same can be said about the liquid hold-up correlation, which does not change at different values of the surface tension and contact angle.

$$h_L = (12\frac{1}{g}\frac{m_L}{r_L}u_L a^2)^{1/3}(\frac{a_h}{a})^{2/3} \qquad \textbf{(2-39)}$$

2.3.6.2 Onda Model

An alternative correlation was suggested by Onda et al. [34] for dumped packing with a nominal size less than 15 mm and low liquid loads with help of experimental results and given in Eq. (2-40) as a function of different liquid properties and contact angle, represented by the critical surface tension of the packing material. In this correlation Onda et al. [34] assumed that the wetted area is identical with the interfacial area.

$$\frac{a_h}{a} = 1 - \exp\left(-1.45 \left(\frac{s_{cr}}{s} \right)^{0.75} \mathrm{Re}_L^{\,0.1} Fr_L^{-0.05} We_L^{0.2} \right) \quad \textbf{(2-40)}$$

2.3.6.3 Shi & Mersmann Model

The correlation derived by Shi & Mersmann [10-18] and given in Eq. (2-41) was derived from the rivulet width correlation given in Eq. (2-27).

$$\frac{a_h}{a} = 0.76 \frac{(Fr_L We_L)^{0.15}}{(\mathrm{Re}_L)^{0.2} (1 - 0.93\cos q) e^{0.6}} \quad \textbf{(2-41)}$$

2.3.6.4 SRP Model

The SRP model (Separation Research Program, at the University of Texas, Austin) which was publiched in [7-9] has given correlation for the effective area and given in Eg. (2-42). Here F_{SE} is the surface enhancement factor of the packing. It has a value of 0.35 for the metal sheet packing Flexipac, for example [7].

$$\frac{a_{ph}}{a} = F_{SE} F_t = F_{SE} \frac{29.12 (We_L Fr_L)^{0.15} S^{0.359}}{\mathrm{Re}_L^{\,0.2} e^{0.6} (1 - 0.93\cos q)(\sin y)^{0.3}} \quad \textbf{(2-42)}$$

The contact angle considers the wetting behaviour of the liquids on the packing surface. For metallic packing:

cos*?=0.9* for s <0.055 N/m

cos*?=5.211e*$^{-16.835s}$ for s >0.055 N/m

For liquid hold-up the following correlation was given in the SRP model in Eq. (2-43).

$$h_L = (4 \frac{F_t}{S})^{2/3} (\frac{3 m_L u_L}{r_L (\sin q) e g_{eff}})^{1/3} \quad \textbf{(2-43)}$$

Chapter 3

Introduction to the CFD Method

3.1 Introduction

Computational Fluid Dynamics (CFD) is a numerically based tool for the prediction of flow field, concentration and temperature distribution. Its main parts are mathematical modelling, discretization, numerical solution of the discretized equations and the interpretation of numerical results.

Basic equations in all mathematical models for CFD are balances for momentum and total mass determining velocity, pressure and density field. Depending on the case considered, they are supplemented by mass balances for single species and a heat balance. Additional models are required to describe, e.g. turbulence, multiphase flows, chemically reactive systems and other special cases.

Basis for the discretization of the balance equation is the discretization of a space or the grid generation. Most codes can handle unstructured grids. Nevertheless, certain requirements concerning grid structure have to be fulfilled to get stable convergence and an accurate solution. Traditionally, most CFD codes use finite volume discretization for the balance equations, even if finite element algorithms are of increasing relevance for simulations with adaptively moving grids and for coupling CFD with structural dynamics simulations. A new approach for simulations with high resolution in space and time is the lattice-Boltzmann method.

Finally, the numerical results have to be graphically presented and interpreted. Because of the huge amount of numerical data provided by each simulation this cannot be done with a general method. It must always be analyzed in reference to a certain research question. Errors caused by the model formulation and by the numerical scheme have to be analyzed in order to judge the accuracy of a simulation. Quantitative estimates are required for an adequate interpretation of the results [46].

Fig. (3-1) declares the necessary steps to go on with a CFD problem for direct numerical solution or in the commercial softwares:

- Pre-processing: Grid generation and definition of the boundary conditions.
- Solver: Selection of the software parameters such as descretisation schemes, physical models and numerical solution methods of the balance equations.
- Post-processing: Visualisation of the results, derivation of different parameters from the solution, analysis and reveal more details about the studied problem.

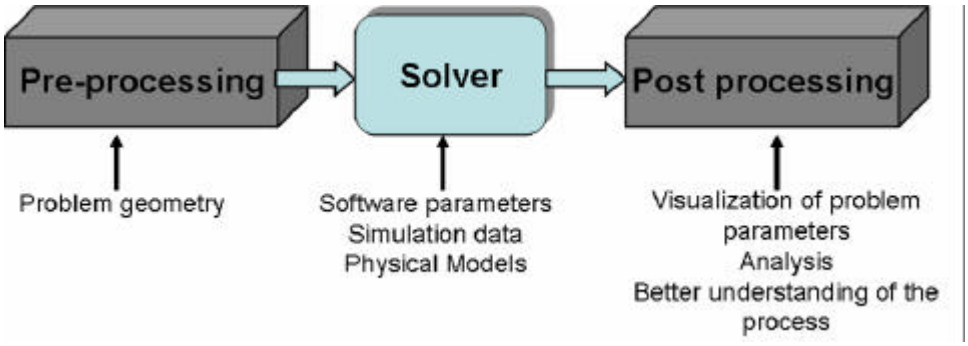

Figure (3-1): Solution steps of a CFD-problem

3.2 Multiphase Flow

In multiphase flow, a phase can be defined as an identifiable class of material that has a particular inertial response to and interaction with the flow and the potential field in which it is immersed. Multiphase flow can be classified by the following regimes, grouped into four categories:

3.2.1 Gas-Liquid or Liquid-Liquid Flows

- Bubbly flow: Discrete gaseous or fluid bubbles in a continuous fluid. Examples: absorbers, aeration, air lift pumps, cavitations, evaporators, flotation and scrubbers.
- Droplet flow: Discrete fluid droplets in a continuous gas. Examples: absorbers, atomizers, combustors, cryogenic pumping, dryers, evaporation, gas cooling, and scrubbers.
- Slug flow: large bubbles in a continuous fluid. Examples: large bubble motion in pipes or tanks.
- Stratified/free-surface flow: immiscible fluids separated by a clearly-defined interface. Examples: sloshing in offshore separator devices, boiling and condensation in nuclear reactors.

3.2.2 Gas-Solid Flows

- Particle-laden flow: discrete solid particles in a continuous gas. Examples: cyclone separators, air classifiers, dust collectors, and dust-laden environmental flows.
- Pneumatic transport: flow pattern depends on factors such as solid loading, Reynolds numbers, and particle properties. Typical patterns are dune flow, slug flow, packed beds, and homogeneous flow. Examples: transport of cement, grains, and metal powders.

- Fluidized beds: consist of a vertical cylinder containing particles where gas is introduced through a distributor. The gas rising through the bed suspends the particles. Depending on the gas flow rate, bubbles appear and rise through the bed, intensifying the mixing within the bed. Examples: fluidized bed reactors, circulating fluidized beds.

3.2.3 Liquid-Solid Flows

- Slurry flow: transport of particles in liquids. The fundamental behaviour of liquid-solid flows varies with the properties of the solid particles relative to those of the liquid. In slurry flows, the Stokes number is normally less than 1. When the Stokes number is larger than 1, the characteristic of the flow is liquid-solid fluidization. Examples: slurry transport, mineral processing.
- Hydro transport: densely-distributed solid particles in a continuous liquid. Examples: mineral processing, biomedical and physiochemical fluid systems.
- Sedimentation: tall column initially containing a uniform dispersed mixture of particles. At the bottom, the particles will slow down and form a sludge layer. At the top, a clear interface will appear, and in the middle a constant settling zone will exist. Examples: mineral processing.

3.2.4 Three-Phase Flows

Combinations of the others listed above.

Describing such flow regimes is a big scientific challenge because of the complex phenomena involving in such flows, for example a flow with reaction or droplet flow with breakage or coalescence. Many attempts are done to simplify the analytical analysis of such flows in order to implement them in the CFD codes.

3.3 Multiphase Flow Models

Advances in computational fluid mechanics have provided the basis for further insight into the dynamics of multiphase flows. Currently, there are several approaches for the numerical calculation of multiphase flows: the Euler-Lagrange, the Lagrange-Lagrange, and the Euler-Euler approach.

3.3.1 The Euler-Lagrange Approach

The Lagrangian discrete phase model follows the Euler-Lagrange approach. The fluid phase is treated as a continuum by solving the time-averaged Navier-Stokes equations, while the dispersed phase is solved by tracking a large number of particles, bubbles, or droplets through

the calculated flow field. The dispersed phase can exchange momentum, mass, and energy with the fluid phase. A fundamental assumption made in this model is that the dispersed second phase occupies a low volume fraction, even though high mass loading $\dot{m}_{particles} \geq \dot{m}_{fluids}$ is acceptable. The particle or droplet trajectories are computed individually at specified intervals during the fluid phase calculation. This makes the model appropriate for the modelling of spray dryers, coal and liquid fuel combustion, and some particle-laden flows, but inappropriate for the modelling of liquid-liquid mixtures, fluidized beds, or any application with a high volume fraction of the dispersed phase.

3.3.2 The Euler-Euler Approach

In the Euler-Euler approach, the different phases are treated mathematically as interpenetrating continua. Since the volume of a phase cannot be occupied by the other phases, the concept of phasic volume fraction is introduced. These volume fractions are assumed to be continuous functions of space and time and their sum is equal to one. Conservation equations for each phase are derived to obtain a set of equations, which have similar structure for all phases. These equations are closed by providing constitutive relations that are obtained from empirical information, or, in the case of granular flows, by application of kinetic theory. In FLUENT, three different Euler-Euler multiphase models are available: the volume of fluid (VOF) model, the mixture model, and the Eulerian model.

3.3.2.1 The VOF Model

The VOF model is a surface-tracking technique applied to a fixed Eulerian mesh. It is designed for two or more immiscible fluids where the position of the interface between the fluids is of interest. In the VOF model, a single set of momentum equations is shared by the fluids, and the volume fraction of each of the fluids in each computational cell is tracked throughout the domain. Applications of the VOF model include stratified flows, free-surface flows, filling, sloshing, the motion of large bubbles in a liquid, the motion of liquid after a dam break, the prediction of jet break-up (surface tension), and the steady or transient tracking of any liquid-gas interface. More details about this model are given below.

3.3.2.2 The Mixture Model

The mixture model is designed for two or more phases (fluid or particulate). As in the Eulerian model, the phases are treated as interpenetrating continua. The mixture model solves the mixture momentum equation and prescribes relative velocities to describe the dispersed phases. Applications of the mixture model include particle-laden flows with low loading,

bubbly flows, sedimentation, and cyclone separators. The mixture model can also be used without relative velocities for the dispersed phases to model homogeneous multiphase flow.

3.3.2.3 The Eulerian Model

The Eulerian model is the most complex of the multiphase models in FLUENT. It solves a set of momentum and continuity equations for each phase. Coupling is achieved through the pressure and interphase exchange coefficients. The manner in which this coupling is handled depends upon the type of phases involved; granular (fluid-solid) flows are handled differently than non-granular (fluid-fluid) flows. For granular flows, the properties are obtained from application of kinetic theory. Momentum exchange between the phases is also dependent upon the type of mixture being modelled. FLUENT's user-defined functions allow customizing the calculation of the momentum exchange. Applications of the Eulerian multiphase model include bubble columns, risers, particle suspension, and fluidized beds.

The models discussed above are not complete, the reader is recommended to refer to the literature for a complete list of multiphase flow models [1,37].

3.3.3 The Lagrange-Lagrange Approach

A Lagrangian mesh free approach for incompressible flow simulations which is called Finite Pointset Method (FPM) is a new CFD tool, developed during the last few years at the Fraunhofer Institute for Industrial Mathematics, Kaiserslautern, Germany [56]. This tool is mainly designed to overcome several drawbacks of classical CFD methods (Finite Element Method (FEM) and Finite Volume Method (FVM)). The main drawback of the classical methods (FEM, FVM) is the relatively expansive geometrical meshgrid required to carry out all numerical computations. The computational cost to establish and maintain these grids becomes more dominant as the considered geometry becomes complex or moves in time. For several applications, the effort for grid maintenance is beyond acceptance, the computations take too long or fail completely. The presented FPM, however, works completely without complex geometrical meshing of the flow geometry. FPM is a Lagrangian particle method, where the ?uid domain is represented by a ?nite number of arbitrarily distributed particles (pointset).

Thus the flow domain is represented by a cloud of numerical points. Each point carries all necessary local flow information. The FPM points move exactly with fluid velocity and change all carried flow information as they move along their track. Thus, they show the characteristic flow behaviour of the local fluid particles. The collection of the dynamics of all FPM points, then provides a complete picture of the dynamics of the considered flow

problem. In order to provide a physically correct dynamical behaviour, the FPM points have to communicate with one another inside of a certain neighbourhood relationship in the same fashion, as real fluid particles would interact as well. This interaction is a key point of FPM and is a mathematical application of the conservations laws (mass, momentum, energy) to the structure of the point cloud [57]. The equations to be solved by FPM are the Navier-Stokes-equations, completed by the mass and energy conservation. These equations are approximated in a direct sense.

3.4 The VOF Model (Volume of Fluid)

The first step in solving any multiphase problem is to determine which of the regimes described before best represents of the flow discussed. From the brief description above the Eulerian VOF model has been found the best choice to describe the wetting of a solid surface with liquids. In the next section, this model will be outlined. For simulating the wetting of solid surface which represents separated two phase flow, the Volume of Fluid (VOF) model implemented in FLUENT has been found appropriate [1].

This model was developed by Hirt & Nichols [36] for tracking the interface between two or more non-interpenetrated phases. It is a fixed grid technique to track the interface between two or more immiscible liquids. VOF solves a single set of momentum equations given in Eq. (3-1) throughout the domain, where the resulting velocity field is shared among the phases. The accumulation and convective momentum terms in every control volume (cell) in the left hand side of this equation balance the pressure forces, shear forces, gravitational body forces and additional forces $\vec{F}$, which may be added depending on the problem.

$$\frac{\partial}{\partial t}(r\vec{v}) + \nabla.(r\vec{v}\vec{v}) = -\nabla p + \nabla.[m(\nabla\vec{v} + \nabla\vec{v}^{T})] + r\vec{g} + \vec{F} \qquad \textbf{(3-1)}$$

The momentum equation is dependent on the volume fractions of all phases through the mean properties like density *?* and viscosity μ. In each control volume, the volume fractions a_q of all phases sum to unity.

$$\sum_{q=1}^{n} a_q = 1 \qquad \textbf{(3-2)}$$

The tracking of the interface(s) between the phases is accomplished by the solution of a continuity equation for the volume fraction of one (two phase flow) or more of the phases. For the q^{th} phase, this equation has the following form:

$$\frac{1}{r_q}\left[\frac{\partial}{\partial t}(a_q r_q) + \nabla.(a_q r_q \vec{v_q}) = S_{a_q} + \sum_{p=1}^{n}(\dot{m}_{pq} - \dot{m}_{qp})\right] \qquad \textbf{(3-3)}$$

where $\dot{m}_{qp}$ is the mass transfer from phase q to phase p and $\dot{m}_{pq}$ is the mass transfer from phase p to phase q. By default, the source term S_{a_q} on the right-hand side of Eq. (3-3) is zero, but it can be specified as a constant or user-defined mass source for each phase [1]. The mass transfer terms between the phases are also considered zero in this study, where no mass transfer occurs. The fields for all variables and properties are shared by the phases and represent volume-averaged values, as long as the volume fraction of each of the phases is known at each location. Thus the variables and properties in any given cell either represent one or a mixture of the phases, depending upon the volume fraction values. For $0<a_q<1$ the cell contains the interface between the qth fluid and one or more other fluids. Otherwise the cell is empty ($a_q=0$) or full ($a_q=1$).

Based on the local value of a_q, the appropriate properties and variables will be assigned to each control volume within the domain. The primary-phase volume fraction will be computed based on Eq. (3-2). The properties appearing in the transport equations, for example the density and viscosity, are determined as mean values of the phases properties according to Eq. (3-4) in a two phase system. All other properties (e.g. viscosity) are computed in the same manner.

$$r = a_2 r_2 + (1 - a_2) r_1 \qquad \textbf{(3-4)}$$

The additional forces appearing in the momentum equation represent in our study the volumetric forces at the interface resulting from surface tension effect along the interface between each pair of phases. The surface tension can be specified as a constant, as a function of temperature or through a user defined function and arises as a result of attractive forces between molecules in a fluid. The surface tension is a force acting only at the surface required to maintain equilibrium in such instances. It acts to balance the radially inward inter-molecular attractive force with the radially outward pressure gradient force across the surface. In regions where two fluids are separated the surface tension acts to minimize free energy by decreasing the area of the interface.

The surface tension model in FLUENT is the continuum surface force (CSF) model proposed by Brackbill et al. [58]. With this model, the addition of surface tension to the VOF calculation results in a source term in the momentum equation. To understand the origin of the source term, consider the special case where the surface tension is constant along the surface, and where only the forces normal to the interface are considered. It can be shown that the pressure drop across the surface depends upon the surface tension coefficient, s, and the surface curvature as measured by two radii in orthogonal directions, R_1, and R_2:

$$p_1 - p_2 = s\,(\frac{1}{R_1} + \frac{1}{R_2}) \quad \textbf{(3-5)}$$

where p_1, p_2 is the pressure in fluids across the interface. In FLUENT, a formulation of the CSF model is used, where the surface curvature is computed from local gradients in the surface normal at the interface as following: Let n be the surface normal, defined as the gradient of a_q, the volume fraction of the q^{th} phase

$$n = \nabla a_q \quad \textbf{(3-6)}$$

The curvature, k, is defined in terms of the divergence of the unit normal $\vec{n}$ [58]:

$$k = \nabla.\vec{n} \quad \textbf{(3-7)}$$

where,

$$\vec{n} = \frac{n}{|n|} \quad \textbf{(3-8)}$$

The surface tension can be written in terms of the pressure jump across the surface. The force at the surface can be expressed as a volume force using the divergence theorem. It is the added volume force to the momentum equation as a source term. It has the following form:

$$F_{vol} = \sum_{pairs\ ij, i<j} s_{ij} \frac{a_i r_i k_j \nabla a_j + a_j r_j k_i \nabla a_i}{\frac{1}{2}(r_i + r_j)} \quad \textbf{(3-9)}$$

This expression allows for a smooth superposition of forces near cells where more than two phases are present. If only two phases are present in a cell, then k_j=-k_i and Eq. (3-9) simplifies to:

$$F_{vol} = s_{ij} \frac{r k_i \nabla a_i}{\frac{1}{2}(r_i + r_j)} \quad \textbf{(3-10)}$$

where r is the volume-averaged density computed using Eq. (3-4) and Eq. (3-10). Eq. (3-10) shows that the surface tension source term for a cell is proportional to the average density in the cell. An option to specify a wall adhesion angle in conjunction with the surface tension model is also available in the VOF model. The model is taken from work done by Brackbill et al. [58]. Rather than impose this boundary condition at the wall itself, the contact angle that the fluid is assumed to have with the wall is used to adjust the surface normal in cells near the wall. This so-called dynamic boundary condition results in the adjustment of the curvature of the surface near the wall.

If *?* is the contact angle at the wall, then the surface normal at the considered cell next to the wall is:

$$\vec{n} = \vec{n}_w \cos q + \vec{t}_w \sin q \quad \textbf{(3-11)}$$

where *?* is the contact angle at the wall, $\vec{n}_w$ and $\vec{t}_w$ are the unit vectors normal and tangential to the wall, respectively. The combination of this contact angle with the calculated surface

normal one cell away from the wall determines the local curvature of the surface. This curvature is used to adjust the body force term in the surface tension calculation. The contact angle is the angle between the wall and the tangent to the interface at the wall, measured inside the first phase of the pair listed in the wall panel, as shown in Fig. (3-2).

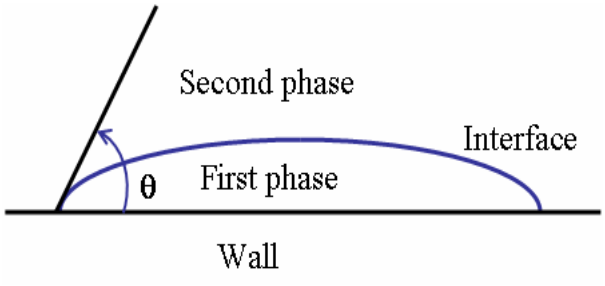

Figure (3-2): Contact angle at a solid boundary

Chapter 4

Experimental Work

In this chapter we will discuss the experimental part in this research, which includes the liquid rivulet flow on an inclined flat and wavy plate and the liquid flow on a structured metal packing sheet from the type Rombopak 4M. The main purpose of the experiments is to validate the CFD simulation results and to find the basic features of the liquid spreading and behaviour and the flow patterns on the geometries discussed. Liquid film thickness and wetted area measuring methods are discussed. All the experiments were done under room conditions.

4.1 Liquid Systems

Different glycerine water mixtures at different concentrations and 50% chlorbenzene-ethylbenzene have been used in the experiments. The physical properties, surface tension, density and viscosity in addition to the contact angles of the liquids are listed in Tab. (4-1).

Table (4-1): Liquid mixtures used in the experiments

Liquid system		surface tension	contact angle	density	viscosity
		mN/m	°	kg/m^3	mPas
1	distilled water	69.6	69.5	996.2	1
2	glycerine-water 15 wt.	66.5	67.8	1039.2	1.5
3	glycerine-water 50% wt.	63.9	67.3	1147	4.5
4	glycerine-water 50% wt. with surfactant	29.6	24.8	1147	4.5
5	glycerine-water 86.5 wt.	60	60	1200	7.54
6	chlorbenzene – ethylbenzene 50%	22.5	16	985	0.3

4.2 Experimental Set-up

4.2.1 Inclined Plate

Rivulet flow on inclined flat and wavy plate was studied experimentally using the experimental set-up shown in Fig. (4-1B). To get a rivulet flow with constant flow rate, the liquid is pumped (1) directly from the reservoir (2) to a small tube or capillary (3) on the top of a 0.1 mm thickness, 20 mm width and 300 mm long metal sheet (4) inclined with an angle of a= 68.5 degrees to the horizon. The liquid flows down afterwards under the gravity forces on the plate surface and it is directed form the sump tank (5) back to the reservoir. The flow rate is adjusted by changing the rotating speed by a control panel (6) of the gear pump (1). In

these experiments a flat and wavy stainless steel metal sheet, from which the structured packing is produced.

A

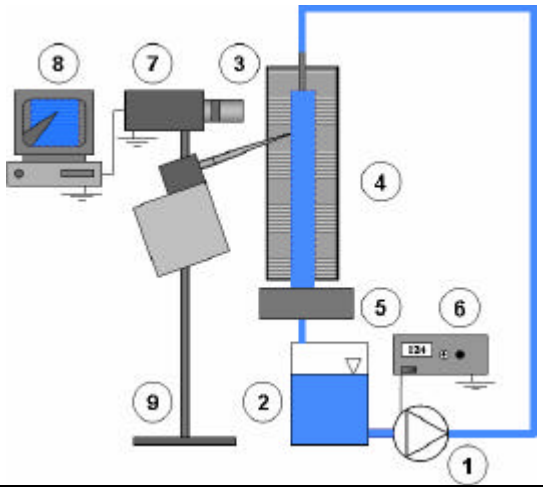

B

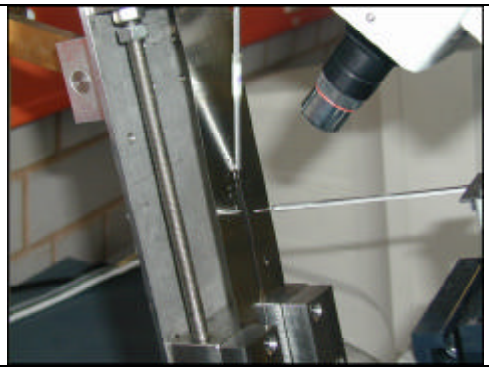

C

D

Figure (4-1): Experimental set-up for rivulet flow, A: Experimental set-up for rivulet flow, B: Schematic of the experiment, C: Rivulet flow on a flat plate, D: Rivulet flow on a wavy plate

4.2.2 Wetting of Structured Packing Element

Wetting experiments of the packing as shown in Fig. (4-2) have similar set-up as in Fig. (4-1). Here the liquid is pumped directly through pipe by gear pump (2) to a liquid distributor (4), which is welded to 6 capillaries (5) as liquid outlet at the top metal structured sheet of the packing (6). The liquid flows back from the sump (7) to the reservoir (1). Liquid flow rates can be adjusted by the rotating speed of the pump (2) and the valve (3). The liquid systems 3, 4 and 6 were used in these experiments. The difficulty in these experiments is to get an equal liquid flow distribution. This was proved and a deviation in the flow rate at different capillaries was less than 10%. The purpose of these experiments is to reveal the flow behaviour on the packing sheet and to use these results as a basis to compare the CFD simulation discussed in the next chapters.

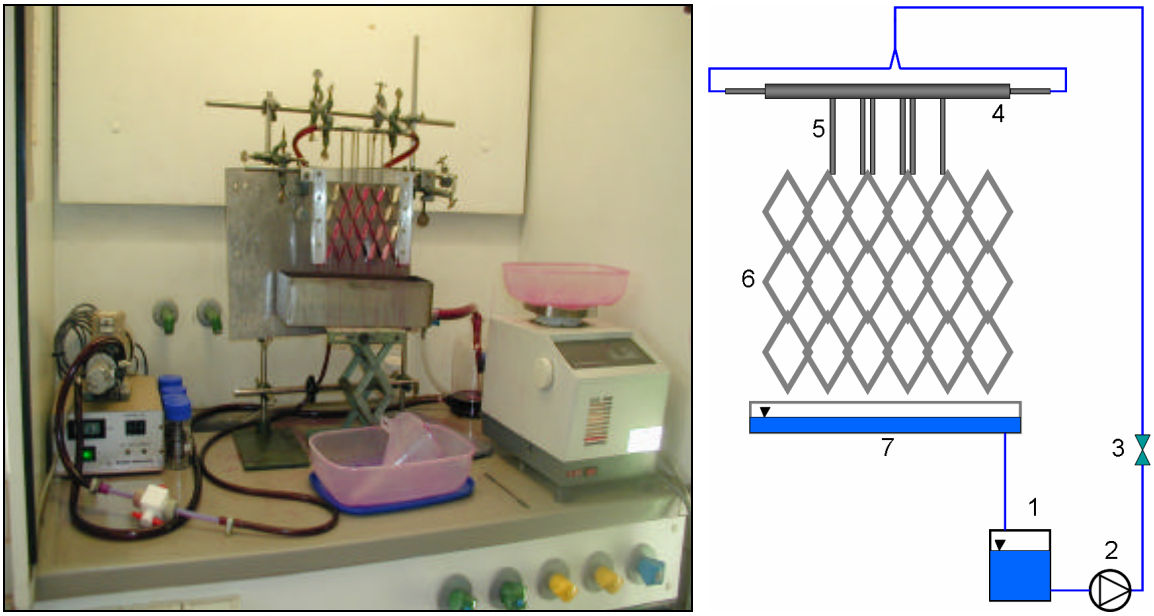

Figure (4-2): Experimental set-up for wetting of structured packing element

4.3 Measuring Methods

4.3.1 Rivulet Profile

Precise measuring methods of the rivulet thickness that are discussed in the literature need calibration when reflecting a fluorescence signal on a black background [59-60] or transmitting signals through glass [61-62] and can thus not be directly used with an inclined metal plate. For this reason the local rivulet thickness was measured using an optically assisted mechanical sensor having a needle which is moved perpendicular to the plate surface by a step motor and in the other two directions using two micrometers as it is shown in Fig. (4-3). Two key measurement points are the position where the needle head touches the plate surface and the position where the needle touches the liquid surface [63]. The thickness can then be determined as follows: before the start of measurement the needle tip head position is adjusted to be in an equal distance from the plate along x and z direction using the three micrometers (s. Fig. (4-3)). First the needle is positioned on a calibrated height $n_1 S$ and then the rivulet flows, the needle is positioned to $n_2 S$, thus the local rivulet height is:

$$y(x) = (n_1 - n_2)S$$

This process is repeated for other locations along the rivulet width from x=0 to w_r. The measuring error using this method is about 10 µm or 2 micrometer steps. To measure the film thickness in another location the third micrometer can be used to shift the needle to the new location along z axis.

Since the movement of the needle is very small, it was followed on a monitor (8) (s. Fig. (4-1B)) using a CCD camera (7) supplied with an objective (3) with a zoom factor of 40 and a

frame grabber card. The measurements were done only after the flow reaches a steady state case; a visual indication to the steady state is the absence of waves or drops.

In the case of the rivulet flow on a wavy plate, measurements were performed using the same above method. The plate in this case was wavy with the same macrostructure of the packing Rombopak 4 M. The corrugated plate had triangular notches with amplitude of 0.05 mm and a wavelength of 1.6 mm. In our study an inclination of ß =68.5° with respect to the horizon was selected in all experiments. Fig. (4-1C and D) show the real rivulet liquid on the flat and wavy plate alternatively.

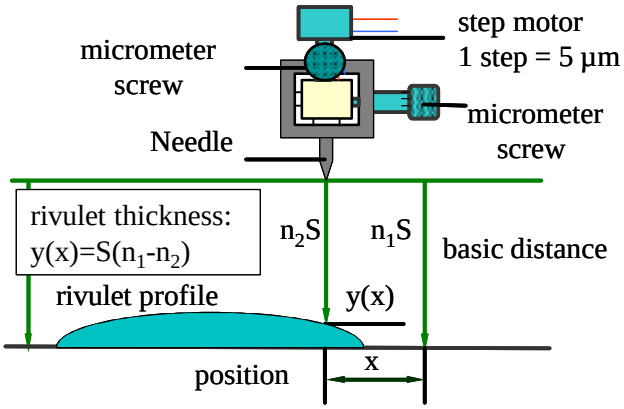

Figure (4-3): Rivulet thickness measuring method

Fig. (4-4) shows a two snap shootings of the needle in a distance to the surface of one step (ca. 5 µm), where the attraction of the liquid to the needle edge was exploited to perform this measuring method. The location of measurement was chosen where the rivulet is uniform and its edges were straight and parallel to each other and to the plate edge. Few measurements were performed for the liquid rivulet flow at the crest of the wavy surface.

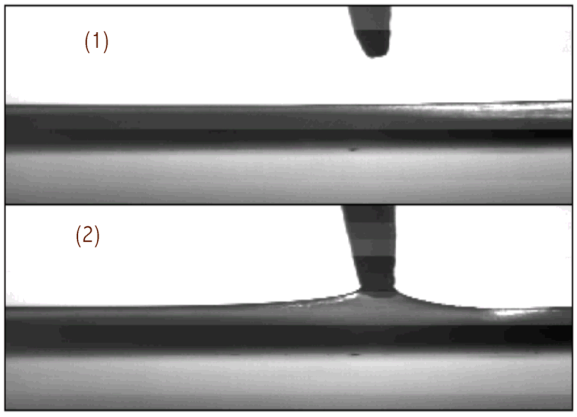

Figure (4-4): Liquid attraction to the needle due adhesion forces
(max. resolution of the height is 5 µm)

4.3.1.1 Contact Angle

The contact angle was measured by analyzing photographic images of a sessile drop on a plate surface similar to that of the packing. Details about this method were discussed in chapter 2.

4.3.1.2 Wetted Area of the Packing

Liquid flow patterns on the structured packing element for different liquid systems and flow rates were obtained by snap shootings with a CCD camera for every case. To get better and clear pictures for the liquid flow patterns on the packing sheet two dyes were used. For aqueous liquid systems 3 and 4 (glycerine-water mixtures) toluidine blue O from Merck was used and for the non-aqueous liquid system 6 (chlorobenzene-ethylbenzene mixture) fat red bluish from Fulka was used. Liquid flow rates were measured by weighting the liquid amount within a specific time. Every image was analyzed by dividing the wetted area into simple geometries and summing their areas to get the total wetted area one more packing elements.

4.3.1.3 Dry Pressure Drop

Few measurements of dry pressure drop have been performed by the Kühni Company and were available for comparison. Rombopak 4M and 9M are discussed at different gas load represented by the F-factor defined in chapter 2.

4.4 Experimental Results

4.4.1 Rivulet Flow

In a set of measurements four capillaries with different interior diameters varying from 0.8 to 2.6 mm were used to study the inlet conditions effect on the rivulet profile. In order to avoid errors due to pre-wetting and flow hysteresis, an attempt was made to minimize these effects by drying the used plates after cleaning them carefully with acetone and distilled water prior to re-use. Fig. (4-5) shows an example of such hysteresis through the rivulet profiles on the flat plate for glycerine-water mixture at different flow rates. In this case the re-wetting of the plate surface forced the rivulet to follow the same bath line creating semi-width rivulet profiles in spite of increasing the flow rates.

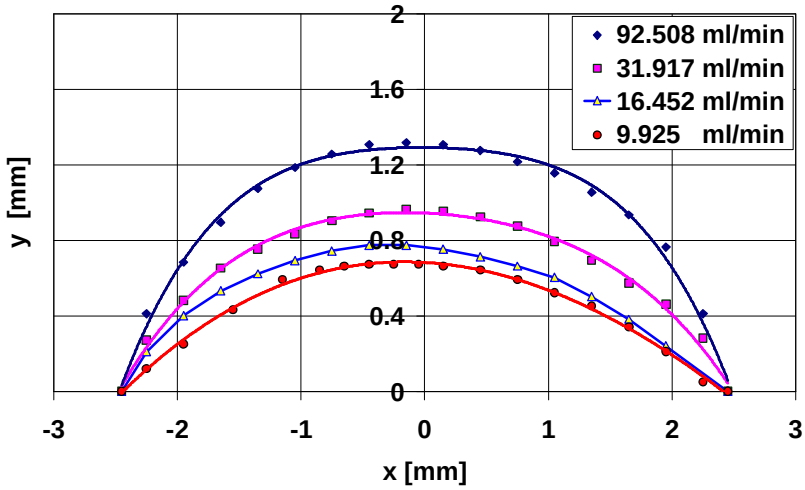

Figure (4-5): Hysteresis effect (re-wetting) on the rivulet profiles

Fig. (4-6) shows the rivulet profiles liquid system 2 at different liquid flow rates without hysteresis effect. The rivulet width and maximum height increases with the flow rate. Additional rivulet profiles for different liquid systems are shown in Appendix A.

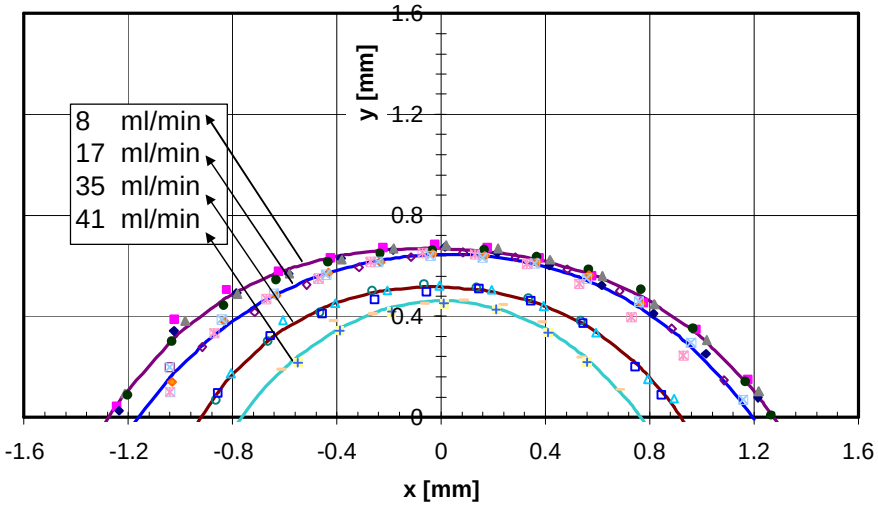

Figure (4-6): Liquid rivulet profiles on a flat plate at different flow rates

Fig. (4-7) presented the trend lines of the liquid inlet velocity when using four capillaries with different diameters. As it is shown, the two main rivulet profile parameters, width and the maximum thickness, were found insensitive due to the change in inlet velocity. This result is important in respect of the design of liquid distributors in the packed columns. It was difficult to get experimental measurements for the velocity in the rivulet section because of the very small liquid height in order of 1 mm. Recently an experiment to measure the liquid film velocity profile using the PIV method was reported [25,64].

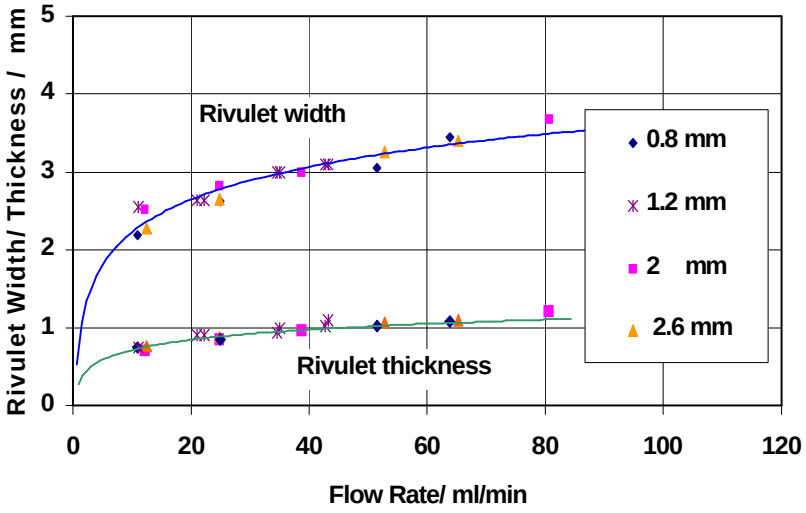

Figure (4-7): Rivulet width and maximum height function of inlet area and flow rates

Figs. (4-8) and (4-9) summarized the measured rivulet profiles for different flow rates and liquid systems. Higher liquid viscosity results in a higher rivulet cross section at the same flow rate.

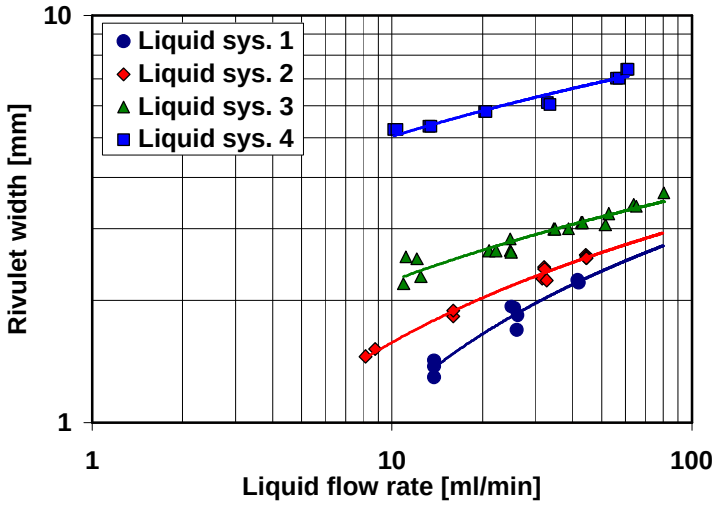

Figure (4-8): Experimental measurements of the rivulet width for different flow rates and liquid systems

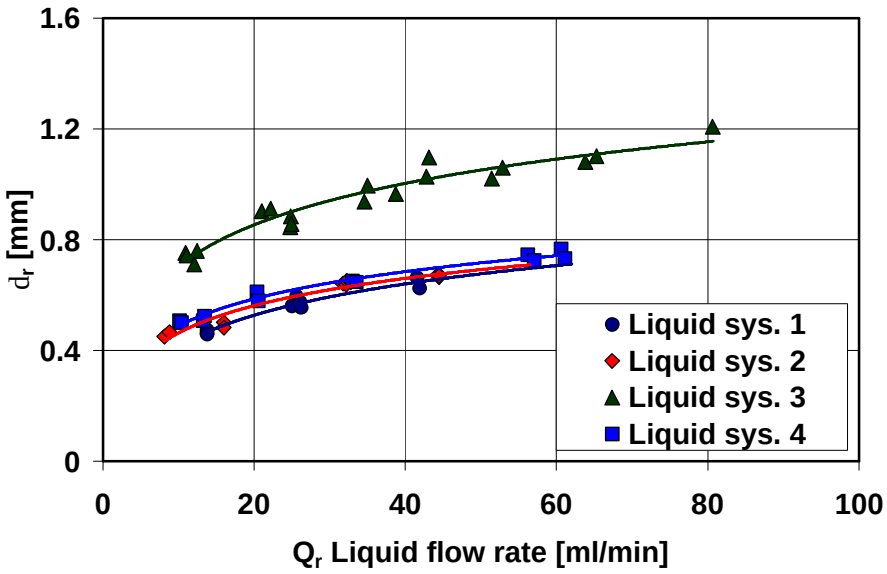

Figure (4-9): Experimental measurements of the rivulet's maximum width for different flow rates and liquid systems

Fig. (4-10) shows rivulet profiles for the liquid system 5 at different flow rates for the wavy plate case. The profiles were measured at the crest of the wavy plate and they are very similar to that of the flat plate case.

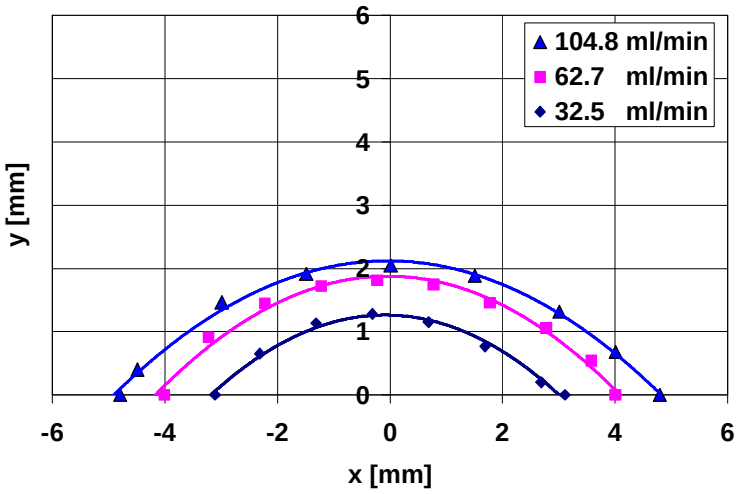

Figure (4-10): Rivulet profiles on a wavy plate at different flow rates, liquid system 5

Fig. (4-11) shows two rivulet sections snap shoots one for the flat plate A and one for the wavy plate B. The difference between the two rivulets is in the interface and three phase line at the rivulet edges. For the flat plate the rivulet boarders are linear, for the wavy one the liquid extends at the bottom of the crest and constricts at the top of the trough of the wavy wall. As a result of the shrinkage and expansion the liquid flows more slowly on a wavy plate

than on a flat one. This behaviour was also observed by Shetty & Cerro [22] in their work on a macro structured sinusoidal plate, where the liquid thickness was small compared to the wave amplitude of the solid surface.

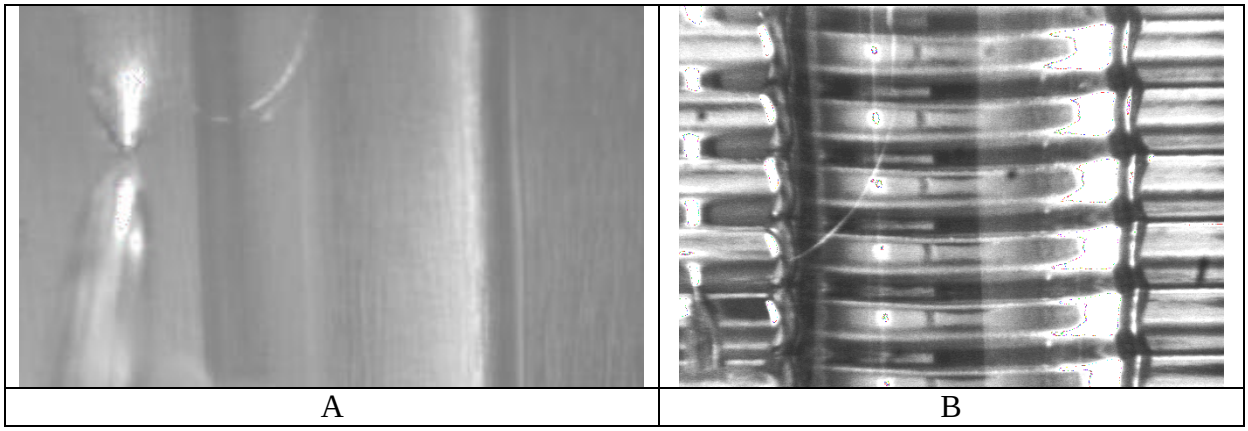

Figure (4-11): Liquid rivulet section on a flat A, and wavy plate B

4.4.2 Wetting Patterns of Packing Element

Liquid flow patterns for different liquid systems and flow rates were obtained by snap shootings with a CCD camera for every case. Samples of these patterns on the packing sheet (left) and on the top element (right) are shown in Fig. (4-12). Fig. (4-12A) represents the liquid flow pattern for liquid system 2 (glycerine-water mixture 50% wt.) at flow rate of 20.5 ml/min per plate. This liquid has high contact angle, viscosity and surface tension. The liquid flows in this case from the capillary on the top right plate of the top element as a rivulet similar to that of the wavy plate towards the element first node, where it further flows down to the bottom left plate of the element and then to the next node. This is repeated in the next element surfaces in similar manner. Increasing the flow rate leads to wider rivulet as in Fig. (4-12B). For the liquid system 3, which has moderate values for the contact angle, viscosity and surface tension, the liquid flows towards the node where it accumulates there with that part coming from the back side of the element. It flows afterwards under the node after bifurcation into two rivulets flowing on bottom two plates on the front and back sides as it is shown in Fig. (4-12C). Small liquid bridge can be seen under the node in this case. For liquid system 6, which has relatively low contact angle, surface tension and viscosity, the flow pattern is similar to that of the last one, but in this case the rivulets are very thin (s. Fig. 4-12D). The fully developed liquid flow pattern in all these cases locates under the first node away from the liquid inlet zone. In all these cases the capillaries touch the top lamella surface of the packing element avoiding drops building at the inlet zone and liquid flow disturbances.

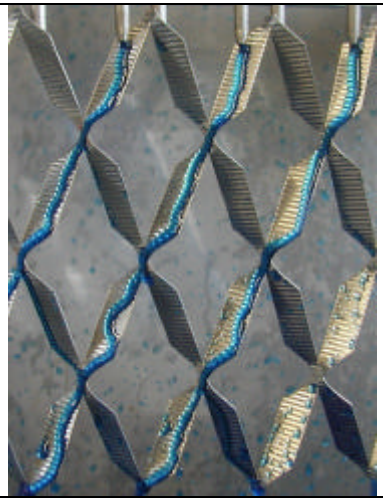
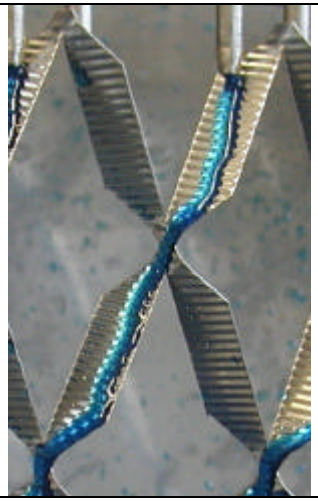

A, Glycerine-water 50%,
20.5 ml/min.plate

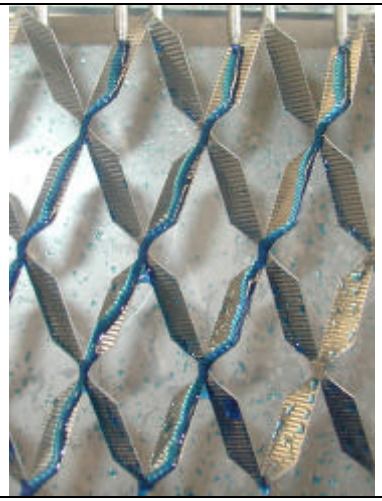
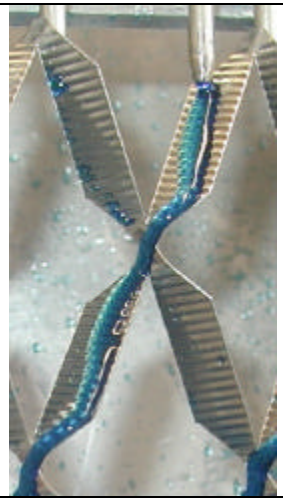

B, Glycerine-water 50%,
53.8 ml/min.plate

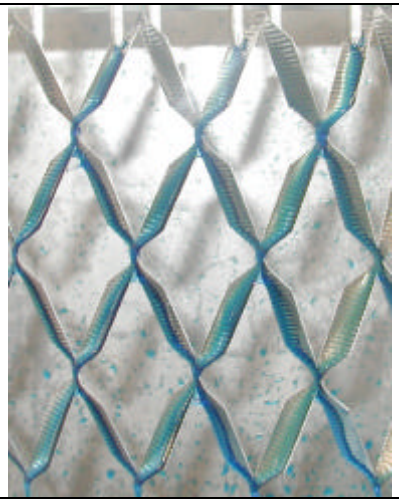


C, Glycerine-water 50% with surfactant,
53.9 ml/min.plate

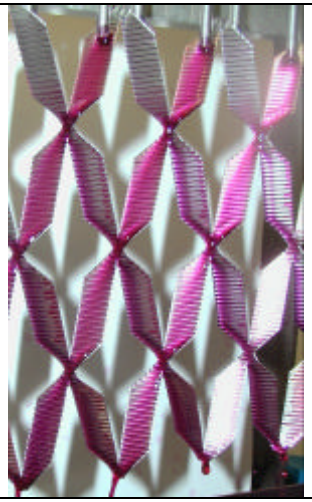
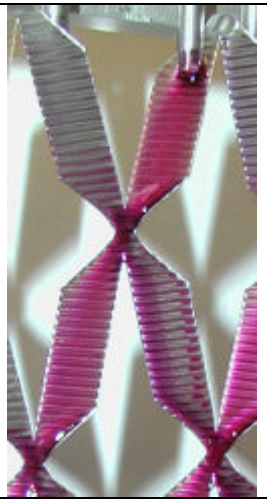

D, chlorbenzene – ethylbenzene 50%,
16.9 ml/min.plate

Figure (4-12): Liquid flow patterns for different liquid systems (right) top element

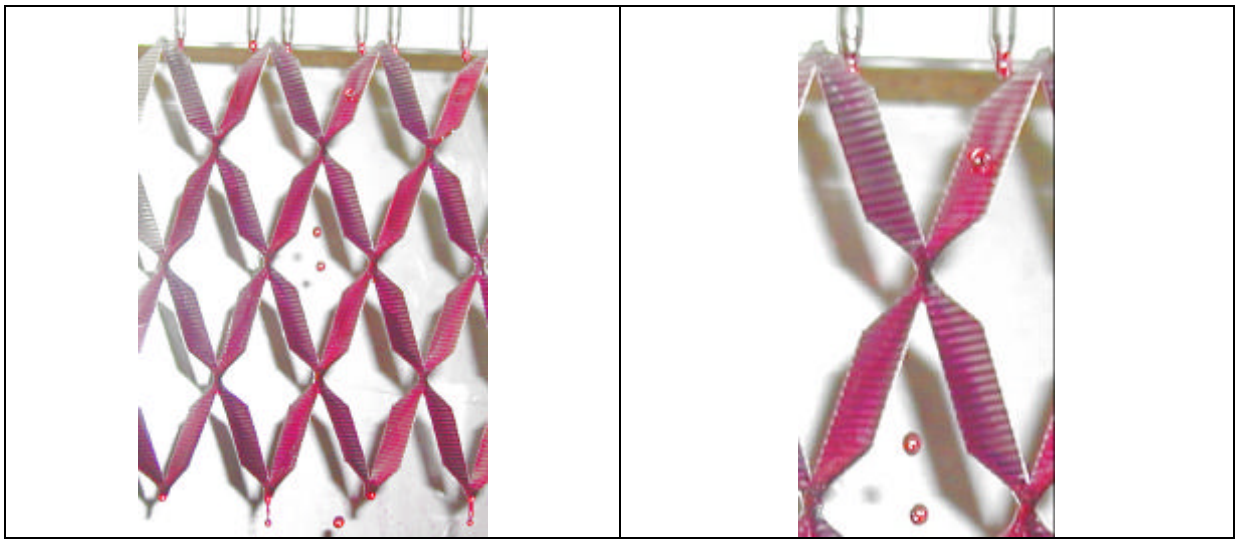

Figure (4-13): Liquid flow pattern for chlorbenzene – ethylbenzene 50% (16.9 ml/min.plate) with capillaries locate about 10 mm distance apart from the plates surfaces

An example can be shown in Fig. (4-13), where the capillaries are positioned at a distance of 10 mm away from the top lamellas surfaces. This set-up leads to dropwise flow, in which the liquid impacts the element surfaces and builds rivulet flows and at the same time creating drops that separate from it and flow in the surface free zone. Additional experimental results on the packing element are shown in Appendix A.

4.4.3 Pressure Drop

Pressure drop experimental results were available from Kühni in a packed column supplied with the packing Rombopak 4M and 9M. The results are discussed with the CFD simulation in chapter 7.

Chapter 5

Inclined Plate: CFD Simulations and Experiment

At the start stage of this research, it was vital to get representative results for the wetting study of solid surfaces with liquids. The rivulet flow on solid flat and wavy plates, which is the most common flow type that can found in the packed columns, was chosen. Measurements of the rivulet profiles for some liquid systems were discussed in chapter 4. In this chapter three dimensional CFD simulations for this kind of flow using the VOF model were performed. A discussion on the CFD simulations for the laminar rivulet flow on a flat and wavy plate for different liquid systems, flow rates and plate inclinations is presented. The experimental and CFD simulations findings on the gas-liquid interface of the rivulet are discussed with analytical solutions from the literature. CFD velocity contours in the rivulet cross section and its mean values for some cases were firstly discussed.

5.1 CFD-Domains

For the rivulet liquid flow CFD simulations on a wavy or flat plate, two dimensional CFD simulations are not relevant and three dimensional grids were needed. Fig. (5-1) shows the grids used for the flat plate (Grid 1, 2 and 3) and that for the wavy one (Grid 4). Grids specifications are summarized in Tab. (5-1). The grid in this case is a box. Its basic surface represents the flat or wavy surface with a similar structure of the packing (s. Fig. (5-1 Grid 2, and Grid 4)). To minimize the simulation time in the CFD calculations a symmetry plane was defined at the middle perpendicular to the plate length. Every grid represents 12 mm (20 mm for Grid 3) width plate. A rectangular channel with a liquid velocity inlet was connected at the midpoint of the top plate edge. The liquid flows from the velocity inlet through this channel to form a rivulet flowing on the plate surface. Hexahedral cells and unsteady state calculations were selected for these simulations. At the end and over the plate, a static pressure was set to zero value as outlet condition. Since the liquid inlet section area has no effect on the rivulet profile, as it was shown in chapter 4, Fig. (4-7), the rectangular channel chosen in the grid has an inlet area equal for some cases and different for others to the capillary cross sectional area used in the related experiments. A velocity inlet boundary condition was defined with a constant velocity value perpendicular to the inlet that supplies the required liquid flow rate. The channel has different lengths above the plate. As in the experiments the rivulet profiles were taken at a position in the fully developed liquid flow zone away from the top plate edge.

The steady state criterion for the simulation is the continuity of the flow on the plate. The simulated rivulet cases are summarized in Tab. (5-2).

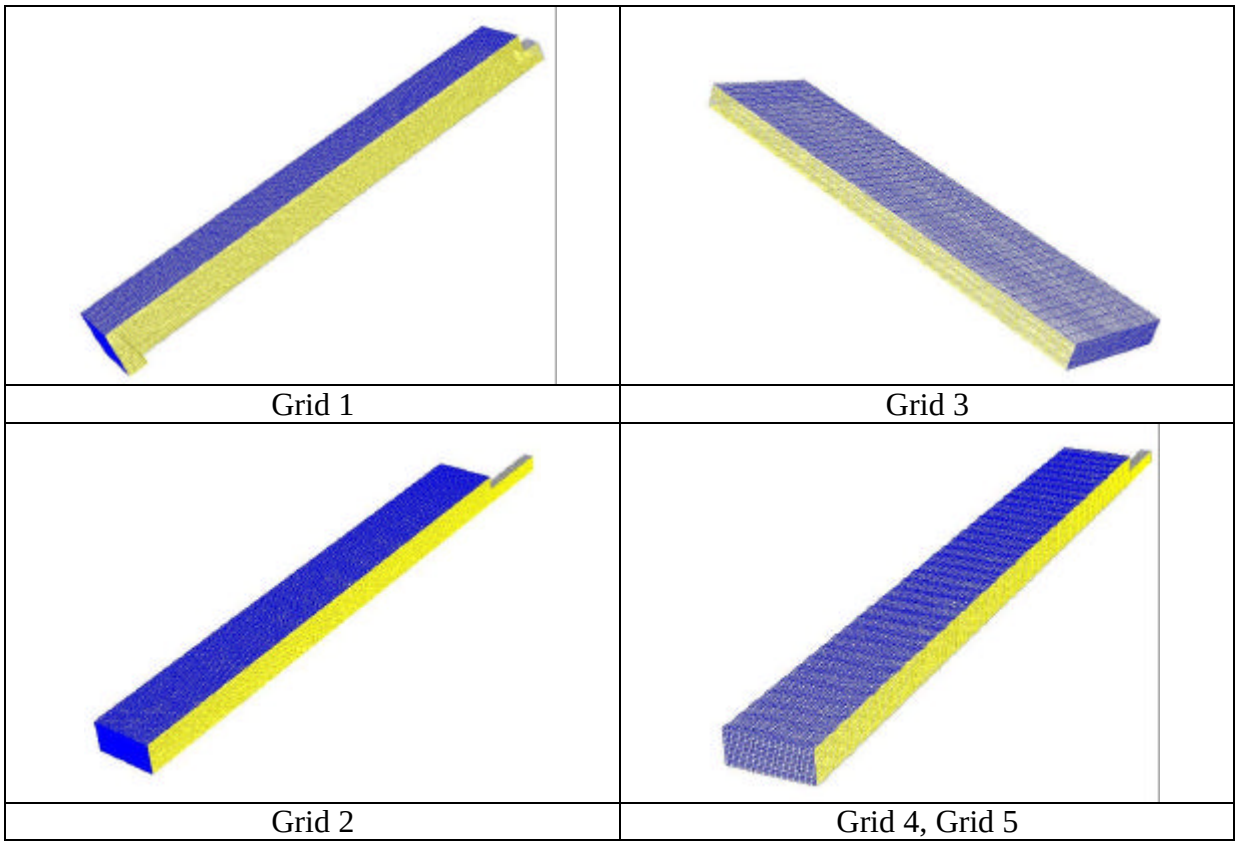

Figure (5-1): CFD domains for rivulet flow simulations

Table (5-1): CFD domains specifications for rivulet flow

		Grid 1	Grid 2	Grid 3	Grid 4	Grid 5
? x	mm	6	6	10	6	6[d]
? y	mm	4	3	2	3	2.5
? z	mm	51	50	40	50	53
d[e]	mm	4	3	2	3	2.5
grid size	cell	155500	306600	19680	337500	95790
cell size		constant	constant	constant	constant	constant
inlet, section ? x, ? y, Length	mm	4x2x2	2x1.5x8	2x0.5x0	2x1.5x9	2x1x6

[e] Grid thickness, distance from the plate surface

Table (5-2): Liquid properties for the different simulated rivulet flow on flat plate

	Q_r	μ_L	s	?	ß	$?_L$	d_r	w_r	A_r	$u_{r,mean}$	$V_{r,mean}$	$u_{r,max}$	$V_{r,max}$	Re_r
	ml/min	mPas	mN/m	°	°	kg/m^3	mm	mm	m2	m/s	-	m/s	-	-
R1	44.99	4.5	29	24.5	90	1147	0.665	5.808	2.87E-06	0.282	0.255	0.516	0.467	47.9
R2	44.99	4.5	29	10	90	1147	0.586	8.203	3.73E-06	0.207	0.241	0.409	0.476	30.9
R3	44.99	4.5	29	67	90	1147	0.936	2.717	1.88E-06	0.415	0.189	0.677	0.309	99.0
R4	44.99	4.5	10	24.5	90	1147	0.685	5.771	2.85E-06	0.278	0.237	0.507	0.432	48.5
R5	44.99	4.5	64	24.5	90	1147	0.657	6.16	3.01E-06	0.264	0.245	0.513	0.476	44.2
R6	44.99	1	29	24.5	90	1147	0.516	3.971	1.49E-06	0.515	0.172	0.772	0.258	304.6
R7	22.49	4.5	29	24.5	90	1147	0.571	4.341	1.83E-06	0.211	0.258	0.382	0.468	30.7
R8	89.97	4.5	29	24.5	90	1147	0.802	7.534	4.53E-06	0.347	0.216	0.616	0.384	71.0
R9	44.99	10	29	24.5	90	1147	0.8	7.059	4.21E-06	0.186	0.258	0.406	0.563	17.0
R10	44.99	4.5	29	24.5	68.5	1147	0.602	6.941	3.35E-06	0.238	-	0.427	-	-
R11	44.99	4.5	29	24.5	45	1147	0.601	8.265	4.13E-06	0.194	-	0.324	-	-
R12	44.99	4.5	29	24.5	30	1147	0.521	12	6.20E-06	0.127	-	0.183	-	-
R13	22.49	4.5	29	24.5	68.5	1147	0.562	4.849	2.01E-06	0.190	-	0.351	-	-
R14	89.97	4.5	29	24.5	68.5	1147	0.556	12	6.36E-06	0.253	-	0.397	-	-
R15	44.99	4.5	10	67	68.5	1147	0.867	3.054	1.99E-06	0.394	-	0.658	-	-
R16	44.99	4.5	29	67	68.5	1147	0.936	2.826	1.95E-06	0.385	-	0.667	-	-
R17	45.12	4.5	29	24.5	68.5	800	0.726	6.972	3.71E-06	0.213	-	0.392	-	-

5.2 Cell Size and Liquid Inlet Effect

It is important to prove the cell size non-dependency of the results. That was proved by taking two grids Grid 1 and 2, which have different cell sizes, dimensions and inlet areas (s. Fig. (5-1) and Tab. (5-1)). The CFD simulations for some rivulets (R1 to R4, R5, R7, R9, R11 and R13 to R16) using those two grids have given very similar profiles with a mean deviation of about 4% in the rivulet width (Fig. (5-2)) and 6% in the maximum rivulet thickness (Fig. (5-3)). The Maximum mean deviation for both was about 11%. These deviations are relatively small and can be neglected. As we have seen from the experiments that, the inlet section area had no effect on the fully developed rivulet profiles shown in Fig. (4-7). Here again an agreement to those results is proved by using the two grids having different inlet section areas. In the following discussion CFD results of grid 2 are discussed.

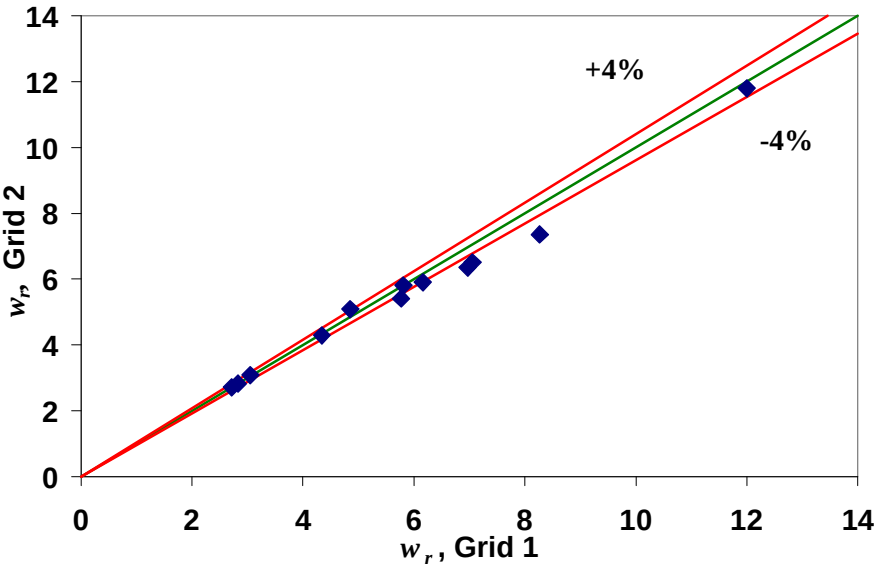

Figure (5-2): CFD results comparison of rivulet width using two different grids

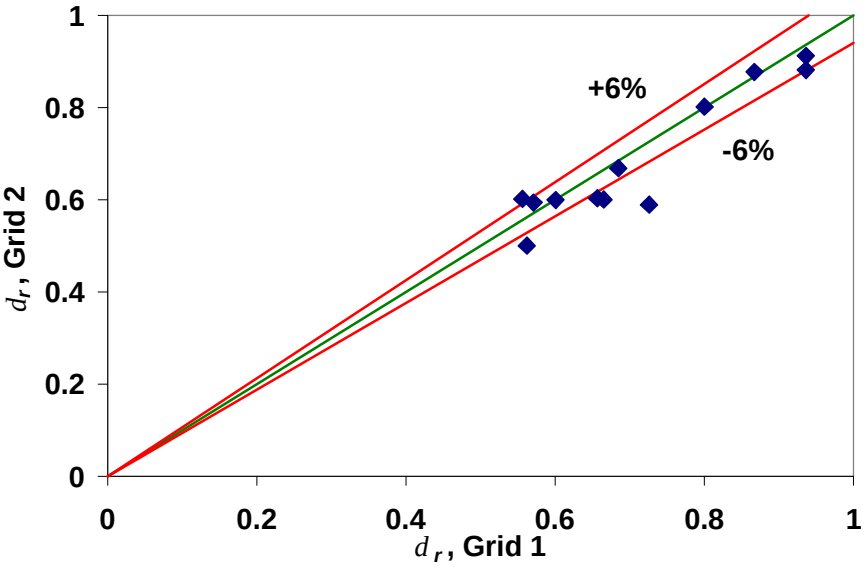

Figure (5-3): CFD results comparison of rivulet maximum thickness using two different grids

5.3 Parameter Effect on the Rivulet Profile

5.3.1 Flow Rate and Viscosity

Increasing the viscosity and flow rate leads to the conclusion that viscosity is a liquid stabilizing parameter. Increasing the viscosity has a positive effect on the wetting of liquids, it leads to higher and wider rivulet as it is shown in Fig. (5-4) and (5-6) for the vertical plate case and in Fig. (5-5) for the inclined plate. For the last case a complete wetting was obtained for a flow rate of 90 ml/min (R14). Increasing of the rivulet thickness produces higher

interfacial area but also higher resistance to heat and mass transfer processes. This is especially important in packed columns. The mean rivulet velocity $u_{r,mean}$ at the rivulet cross sectional area is proportional to the flow rate and inversely to the liquid viscosity, as it can be seen from Tab. (5-2).

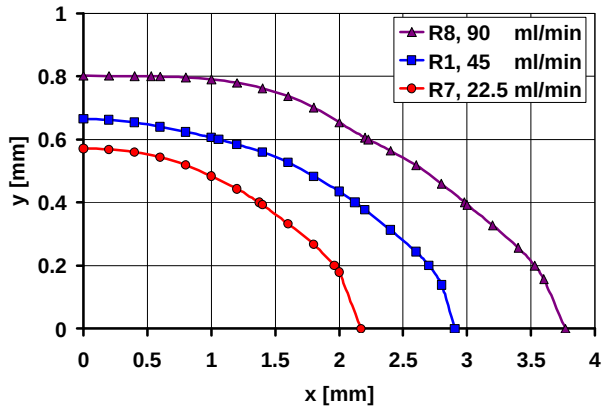

Figure (5-4): Rivulet profiles at different flow rates, vertical plate. s=29 mN/m, μ=4.5 mPas, ?=24.5°, ß=90°.

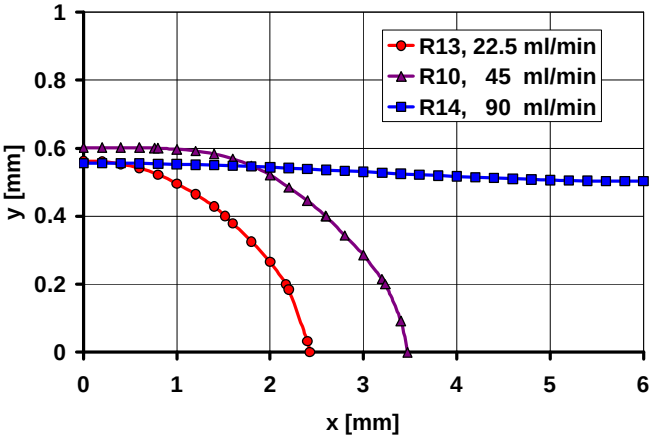

Figure (5-5): Rivulet profiles at different flow rates, inclined plate. s=29 mN/m, μ=4.5 mPas, ?=24.5°, ß= 68.5°

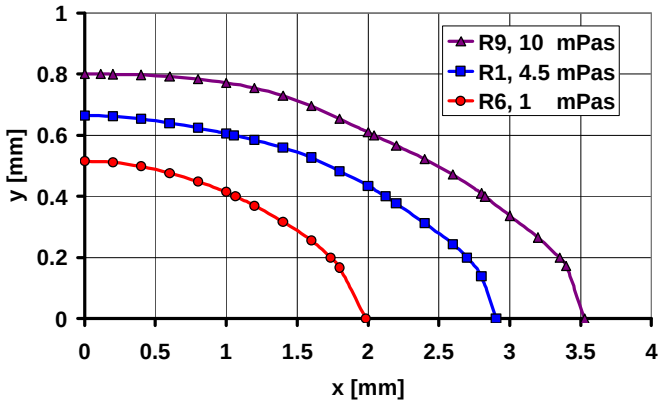

Figure (5-6): Rivulet profiles at different viscosity, ß=90°, Q_r=45 ml/min, s=29 mN/m, ?=24.5°

5.3.2 Contact Angle and Surface Tension

Lower contact angle leads to a more flatter rivulet and the rivulet cross sectional area increases but the velocity decreases. This is again an effective parameter for the heat and mass transfer processes. Lower film thickness means lower resistance. Fig. (5-7) shows the effect of the contact angle on the rivulet profile. Surface tension has small effect on the rivulet profile, as it is obvious from Fig. (5-8).

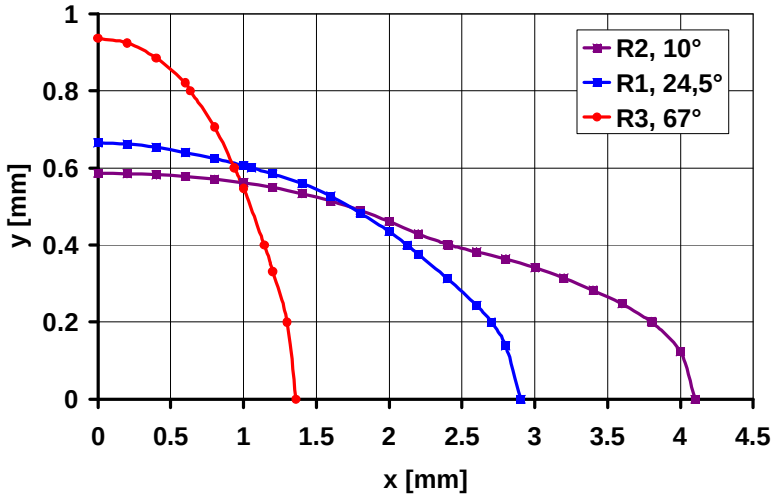

Figure (5-7): Rivulet flow at different contact angles, flow rate: Q_r=45 ml/min, s=29 mN/m, μ=4.5 mPas, ß=90° (vertical plate)

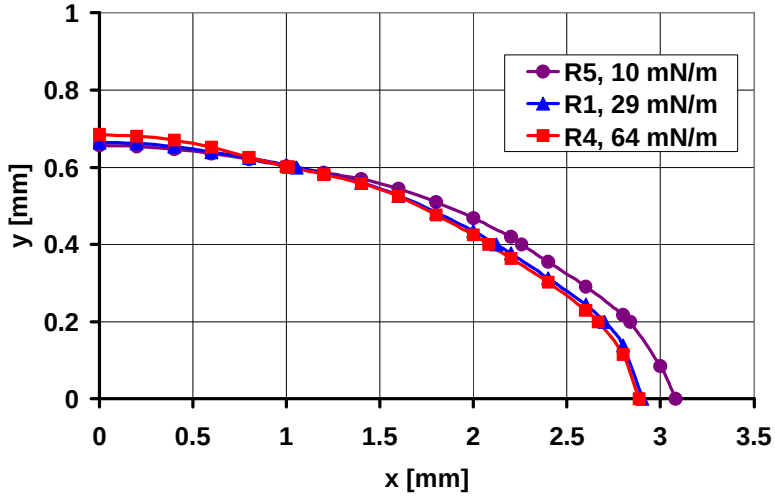

Figure (5-8): Rivulet profiles for different surface tensions, Q_r=45 ml/min, μ=4.5 mPas, ?=24.5°, ß=90°.

5.3.3 Plate Inclination

Rivulet profiles at different inclinations are shown in Fig. (5-9). From this figure, we can see that the rivulet width increases with decreasing the plate inclination and the maximum rivulet thickness stays approximately constant. Comparing of the rivulet profile on a flat vertical plate R1 or R2 to that on an inclined plate R10 or R11 shows the difference in the tendency of surface wetting. The profiles on vertical plate are circular and on inclined plates they have an oval shape, as it is shown in Fig. (5-10). This behaviour agrees qualitatively with the analytical rivulet profile predictions of Bentwich et al. [19] shown in Fig. (2-4).

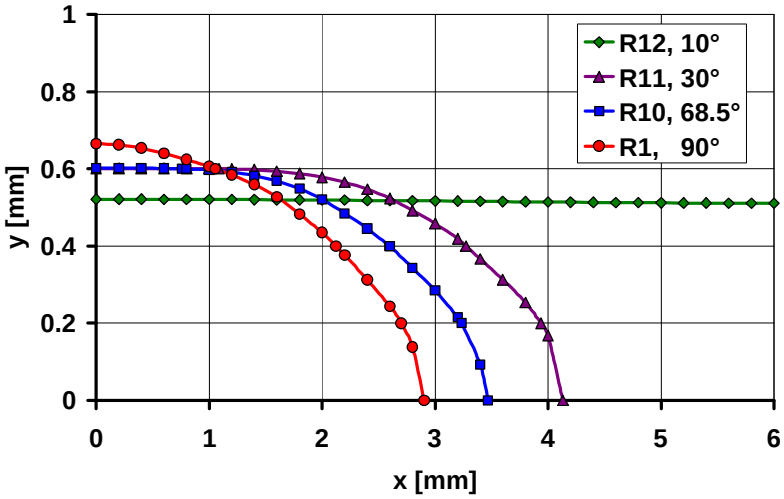

Figure (5-9): Rivulet profiles at different plate inclinations, Q_r=45 ml/min, s=29 mN/m, μ=4.5 mPas ?=24.5°

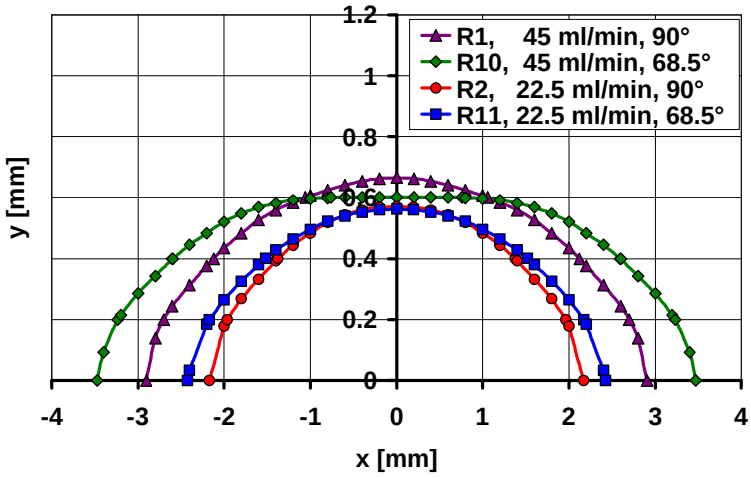

Figure (5-10): CFD results for rivulet profiles for flat vertical and inclined flat plates (ß=90°or 68.5°), Q_r=45 ml/min, s=29 mN/m, μ=4.5 mPas, ?=24.5°

5.3.4 Vertical Plate Models

Some CFD simulations on the vertical plate were compared to the model developed by Kern [15] for laminar and turbulent rivulet flow and to the Al-Khalil et al. model [4] for laminar case. The dimensionless maximum $V_{r,max}$ and mean $V_{r,mean}$ rivulet velocities defined in Eq. (2-25) and (2-26) were estimated from the CFD simulations and listed in Tab. (5-2). $V_{r,mean}$ has values of about 0.225. $V_{r,max}$ has values less than 0.5 and only for high viscous liquids (case R8, 10 mPas), its value higher than 0.5. The agreement between the VOF model results and the two mentioned models is very good, as it is shown in Fig. (5-11).

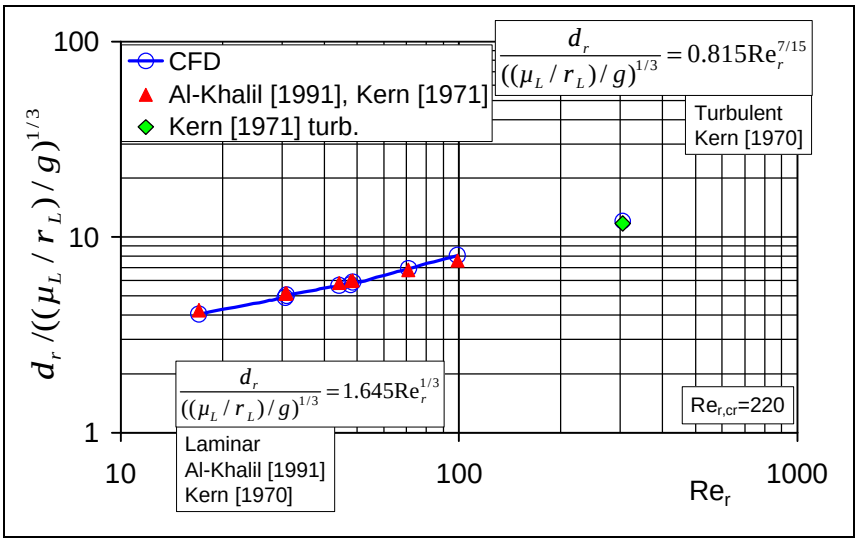

Figure (5-11): Rivulet flow on vertical plate: CFD simulation and models.

5.4 Summary

The CFD simulation results can be summarized in Fig. (5-12) for the rivulet maximum thickness and in Fig. (5-13) for its width as a function of different parameters. Some remarks can be deduced from these figures. Rivulet width increases more quickly when reducing the inclination in the range of angles less than 45°. The thickness seems to stay constant in the range between 65° and 45°. Decrease of the contact angle produces wider and thinner rivulets. Rivulet width and thickness are proportional to the viscosity. The surface tension has very small effect on the rivulet profile.

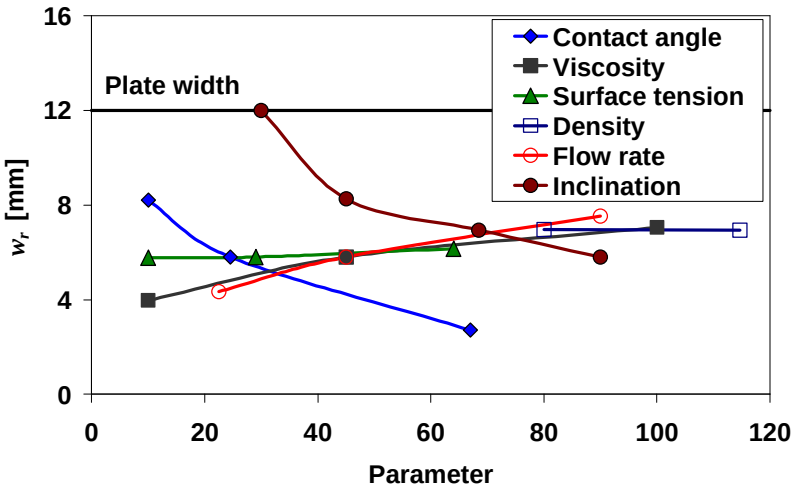

Figure (5-12): Rivulet width as a function of different parameters, units: contact angle (°/10), viscosity (mPasX10), surface tension (mN/m), density (kg/m^3/10) and flow rate (ml/min)

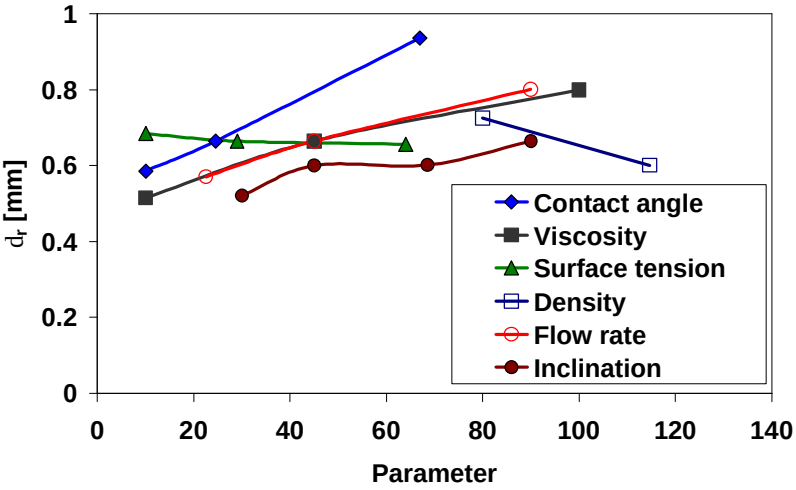

Figure (5-13): Rivulet width as a function of different parameters, units: contact angle (°/10), viscosity (mPasX10), surface tension (mN/m), density (kg/m^3/10) and flow rate (ml/min)

5.5 Velocity Profiles

Measurement of the velocity profile in the rivulet cross section is very difficult. The MPIV method (Micro Particle Image Velocimetry) has the potential to capture these measurements. Already several velocity measurements were performed by Ausner et al. [25]. In the work of Hoffman et al. [39], the break up of liquid film flow on inclined plate in rivulets was studied experimentally and simulated with CFX of ANSYS Inc. In this work, the velocity at the interface was measured with PTV (Particle Tracer Velocimetry) method. In this research, qualitative comparison can be performed between the CFD simulations and the solutions of

Al-Khalil et al. [4] and Allen & Biggin [5]. Fig. (5-14) shows good similarity between velocity profiles shape depicted from the CFD and the solutions published in [4-5]. The values of mean and maximum dimensionless rivulet velocity on a vertical plate were also almost similar to the values given by Al-Khalil et al. [4].

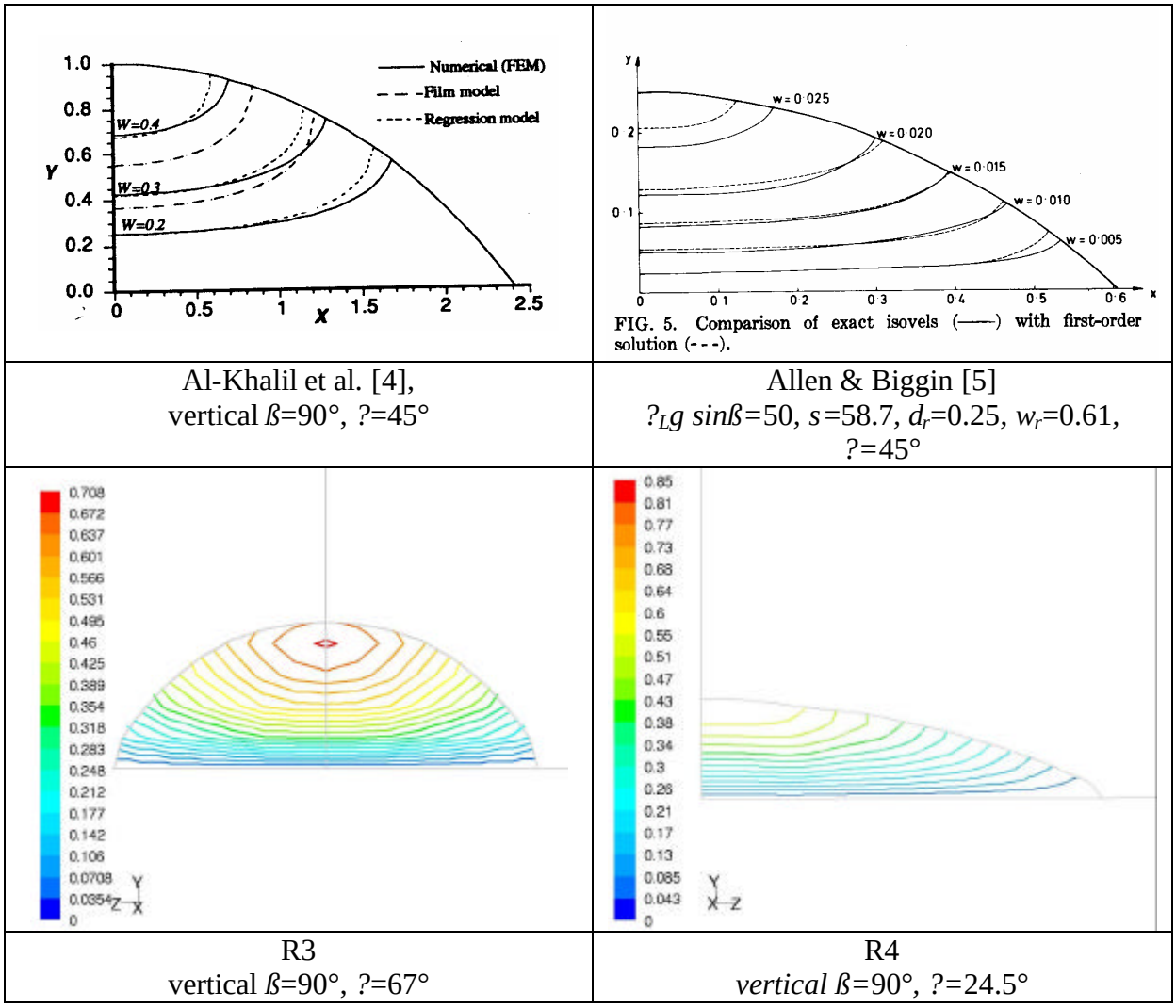

Al-Khalil et al. [4], vertical ß=90°, ?=45°	Allen & Biggin [5] $?_{LG}$ *sin*ß=50, s=58.7, d_r=0.25, w_r=0.61, ?=45°
R3 vertical ß=90°, ?=67°	R4 *vertical* ß=90°, ?=24.5°

Figure (5-14): CFD vs. solutions from the literature for the velocity contours at the rivulet section (m/s)

5.6 CFD-Simulations vs. Experiment

In this section the measurements of rivulet width w_r and maximum thickness d_r derived from the measured profiles for different liquid systems that given in Tab. (4-1) are compared to the CFD simulations. These simulations were performed at the initial stages of this research using grid 3.

Fig. (5-15) shows a typical result for the rivulet profile on an inclined plate estimated from the CFD simulation and from the two models of Duffy & Muffatt [2] and Towell & Rothfeld [3]. From this, the Duffy & Muffatt model [2] predicts a narrower and higher profile. However,

the Towell & Rothfeld model [3] can better describe the flow. The CFD simulation results are satisfactory. In Fig. (5-16) and (5-17) the rivulet main parameters, rivulet width and its maximum thickness, are presented as a function of the flow rate for liquid system 2.

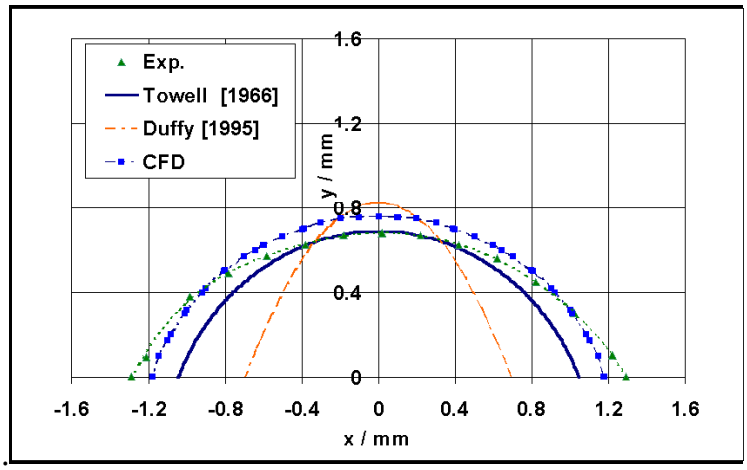

Figure (5-15): Typical rivulet profiles VOF, Duffy & Muffatt and Towell & Rothfeld models

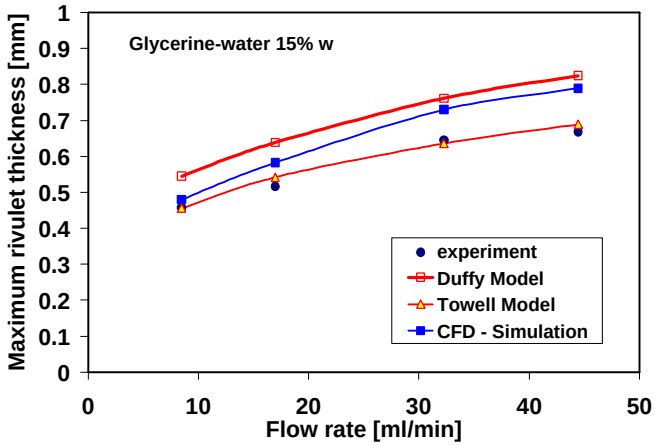

Figure (5-16): Rivulet maximum thickness on a flat inclined plate. Experimental data, CFD and literature models at different flow rates

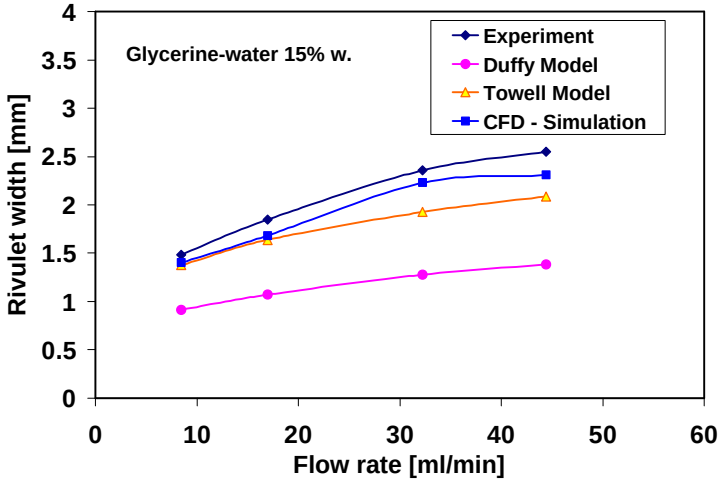

Figure (5-17): Rivulet width on a flat plate. Experimental data, CFD and literature models.

The agreement between the CFD results and the experimental measurements are also very satisfactory. An agreement between the rivulet profiles resulted from the experiment and that estimated from the CFD simulations means also an agreement between the mean rivulet velocity in the flow direction $u_{r,mean}$ derived from the CFD and that of the experiments. Additional diagrams are shown in the Appendix B.

5.7 Wavy Plate

The most popular micro/macro structure of the surface applied for structured packing is a corrugated form. In the following section the CFD simulation results of the rivulet flow on a wavy plate at different liquid properties and flow rates are discussed. Some CFD simulations have been done using grid 4 and 5. Table (5-3) summarizes the CFD simulation results for several cases. Additional CFD simulations were performed for liquid system 5 (s. Tab. (4-1) and compared to the experimental measurements.

Table (5-3): Liquid properties for the different simulated rivulets on wavy plate

	Q_r	μ_L	s	?	ß	$?_L$	d_r	w_r	$u_{r,mean}$ [a]	$u_{r,max}$
	ml/min	mPas	mN/m	°	°	kg/m^3	mm	mm	m/s	m/s
W1	**89.97**	**4.5**	**29**	**24.5**	**90**	**1147**	**0.929**	**6.55**	**0.366**	**0.619**
W2	**22.50**	**4.5**	**29**	**24.5**	**90**	**1147**	**0.634**	**4.31**	**0.210**	**0.368**
W3	**45.00**	**4.5**	**29**	**24.5**	**68.5**	**1147**	**0.753**	**5.69**	**0.260**	**0.455**
W4	**89.97**	**4.5**	**29**	**24.5**	**68.5**	**1147**	**0.910**	**7.34**	**0.336**	**0.563**
W5	**180.00**	**4.5**	**29**	**24.5**	**68.5**	**1147**	**0.912**	**11.11**	**0.401**	**0.618**
W6	**10.98**	**4.5**	**29**	**24.5**	**68.5**	**1147**	**0.516**	**3.70**	**0.141**	**0.258**
W7	**45.08**	**0.3**	**2.55**	**16**	**68.5**	**985**	**0.196**	**12.00**	**0.301**	**0.400**
W8	**44.99**	**4.5**	**64**	**24.5**	**68.5**	**1147**	**0.648**	**8.23**	**0.193**	**0.317**
W9	**10.98**	**1**	**29**	**24.5**	**68.5**	**1147**	**0.369**	**3.37**	**0.219**	**0.340**
W10	**45.00**	**4.5**	**29**	**67**	**68.5**	**1147**	**0.926**	**3.23**	**0.350**	**0.572**

[a] Values were taken at the dell

To give an example, some CFD simulations of rivulet flow on wavy plate were compared to that for the flat plate case. VOF contours examples are shown in Fig. (5-18) at different flow rates. The evaluation of the rivulets width and maximum thickness was taken at a save distance from the inlet and outlet, where the rivulet is fully developed and no changes were observed.

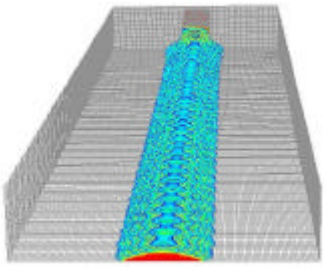	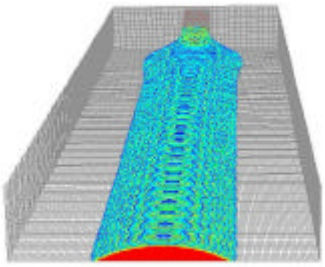	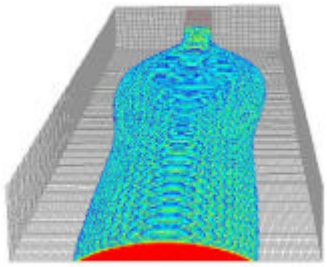
W6	W3	W4
11 ml/min	45 ml/min	90 ml/min

Figure (5-18): VOF contours (0.5-1) of the rivulet flow on a wavy plate at different flow rates, b=68.5 °

The rivulet profiles (at the crest) were estimated and found similar to that of the flat plate case as it is shown in Fig. (5-19). The last figure shows again that the rivulet maximum thickness has reached its maximum value and the profile shapes are similar to that for flat plate shown in Fig. (5-9) according to Bentwich et al. [19] shown in Fig. (2-4).

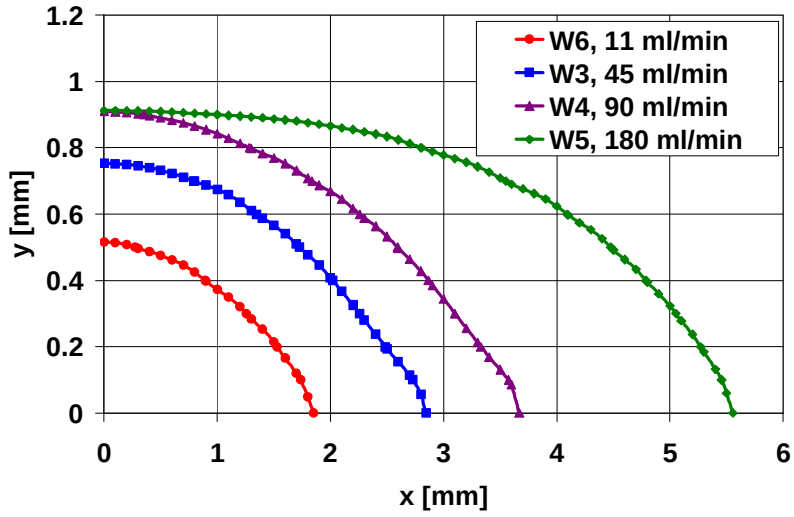

Figure (5-19): Rivulet profiles on a wavy plate at different flow rates

From the CFD simulations and experimental results, it was also found that the rivulet has no linear borderlines. At the crest it constricts and the liquid velocity increases and in the dell it extends but the liquid velocity decreases to fulfil the continuity (s. Fig. (5-20)). For the case W1 the mean rivulet velocity was estimated from the CFD simulation, and it has a value of 0.366 m/s (A_r=2.106x10^{-06} m^2) at the crest and 0.332 m/s (A_r=2.271x10^{-06} m^2) at the dell. In addition to that the interface was found to be also wavy. Fig. (5-21) shows the locations of the interface at the symmetry (x=0), where the rivulet has its maximum value and at a distance x=1 mm from the symmetry axis for the case W10 (w_r=3.23 mm). The interface is slightly wavy with similar wave length of the corrugation but lower amplitude. This amplitude increases until it reaches that on the plate surface at the rivulet boarders. This means that the

wavy plate structure causes wavy rivulet boarders and consequently a wavy interface to satisfy the flow continuity.

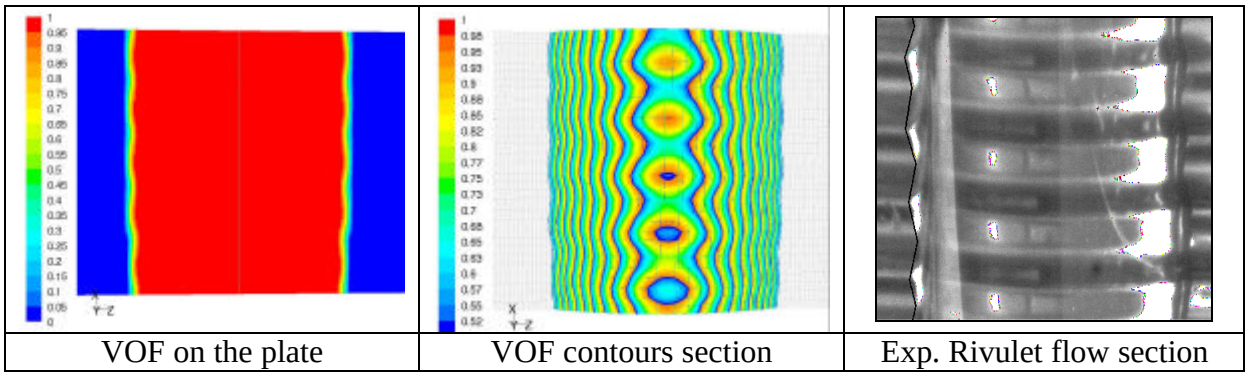

VOF on the plate	VOF contours section	Exp. Rivulet flow section

Figure (5-20): Rivulet edges from: CFD vs. experiment on a wavy plate

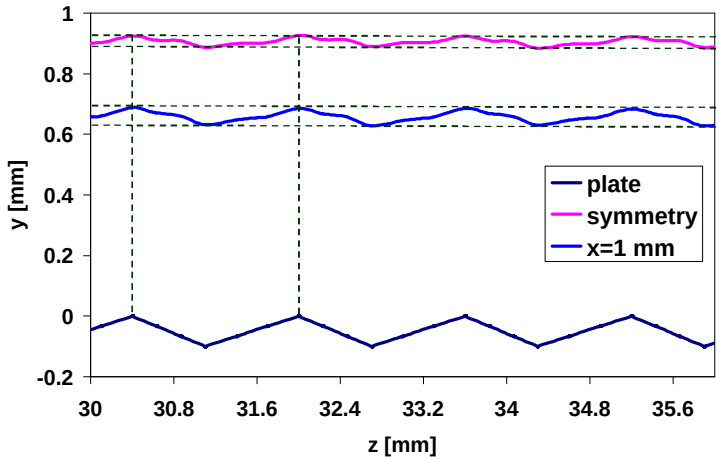

Figure (5-21): Interface profiles at the symmetry and a distance 1 mm from the symmetry for case W10

Measurements of the liquid rivulet profile for the liquid system 5 (s. Tab. (4-1) were presented in Fig. (5-22) and compared to CFD simulations using the grid 5. The measurements and CFD results are almost similar. However, there are some deviations when using simplified models derived for flat plates [3].

A virtual parametric study using the CFD method on the rivulet flow for the wavy plate has given similar behaviour to that of flat one. Appendix B shows further VOF-contours and experimental results.

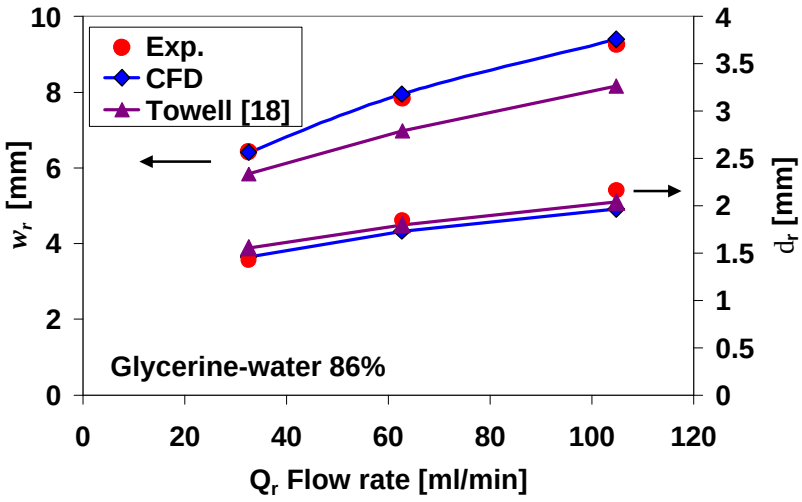

Figure (5-22): Comparison between the VOF results and experiments for glycerine-water 86.5% wt. on flat inclined plate.

5.8 Flat vs. Wavy Plate

Surface wetting behaviour of a flat plate is different from the wavy one. As discussed above the interface rivulet on a structured plate has the imprinted structure of the plate surface. This wavy structure gives a higher gas liquid interface which is positive in respect to the heat and mass transfer process.

Table (5-4): Rivulet flow for wavy plate W, vs. flat plate, R

	Q_r	μ_L	s	?	ß	$?_L$	d_r	w_r	$u_{r,mean}$	$u_{r,max}$
	ml/min	mPas	mN/m	°	°	kg/m^3	mm	mm	m/s	m/s
W1	90.0	4.5	29	24.5	90	1147	0.929	6.554	0.366	0.619
R8	90.0	4.5	29	24.5	90	1147	0.802	7.534	0.347	0.616
W2	22.5	4.5	29	24.5	90	1147	0.634	4.307	0.210	0.368
R7	22.5	4.5	29	24.5	90	1147	0.571	4.341	0.211	0.382
W3	45.0	4.5	29	24.5	68.5	1147	0.753	5.688	0.260	0.455
R10	45.0	4.5	29	24.5	68.5	1147	0.602	6.941	0.238	0.427
W10	45.0	4.5	29	67	68.5	1147	0.926	3.235	0.350	0.572
R16	45.0	4.5	29	67	68.5	1147	0.881	2.825	0.385	0.667

All results are within Grids 2 and 4.

From Tab. (5-4) and Fig. (5-23) and at a low contact angle (24.5°), the mean and maximum rivulet velocity for a wavy plate is higher than that of the flat plate, but the rivulet width is smaller and maximum thickness is higher. That means that the rivulet accelerate causing the flow to be higher and at the same time preventing it to spread out. For higher contact angle (67°, W10 vs. R16), the velocity of the wavy rivulet becomes smaller, its width is higher and its maximum thickness stays about the same. This case represents a narrow and small rivulet, where the width is about 3 times of the thickness and that may explain this behaviour.

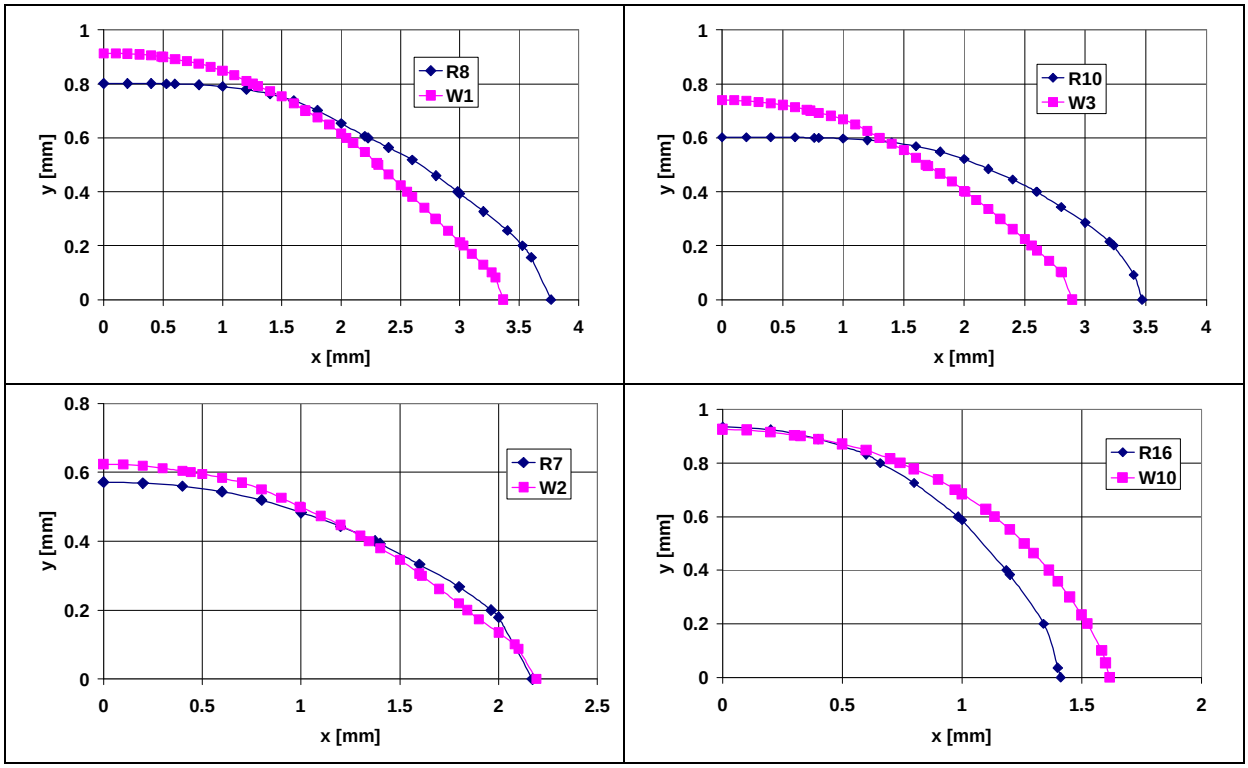

Figure (5-23): Rivulets on wavy plateW, and flat plate, R, at similar conditions

Chapter 6

Structured Packing: CFD Simulations and Experiment

6.1 Structured Packing Element

Multiphase flow modelling in packed beds is a challenging task because of the difficulty incorporating the complex geometry (e.g. tortuous interstices) into the flow equations, and the difficulty in accounting of the gas-liquid (fluid-fluid) interactions in the presence of a complex fluid-solid surface contacting (e.g., partial wetting). Moreover, until recently, the lack of non-invasive experimental techniques suitable for validating the numerical results was also a detrimental factor in numerical model development [65].

The three dimensional CFD simulation of the two phase liquid-gas flow in packed columns is very difficult and the simulation of the flow in a packing block needs very long time. However, it is possible to simulate the liquid flow in a packing element which represents the packing at some section of the packed column within reasonable CPU time consuming.

The lack of works in the literature on VOF applications in structured packing makes the task more difficult [41-42]. Under these conditions an attempt was carried out to simulate the wetting of single and multi-element packing sheet (SPE, PS) which is shown in Fig. (1-2). The multiphase flow model VOF described in chapter 2 was used. CFD-simulation results of a single packing element (SPE) were exploited to build up correlations, which describe the hydrodynamics performance of this packing.

6.1.1 CFD-Domains and the VOF-Model Discretization

Wetting of the packing element is a complex phenomenon and it is difficult to solve it analytically, but it can be solved via CFD methods with the VOF model. The domains used in the simulations were created using the GAMBIT tool. A big effort has been spent to represent the fine surface structure of this corrugated element in the CFD domain and starting from the surfaces of a flat element (compare Fig. (6-1A) with Fig. (1-2C)). After getting the surfaces of one element, volumes were generated around all surface sides and meshed with structured hexahedral elements as shown in Fig. (6-1A). Two rectangular channels with a cross section area equal to that of the capillary section area used in the experiments were added at the top of the two top lamellas of the SPE for the liquid inlets as shown in Fig. (6-1). At each channel a velocity inlet was defined. Varying the velocity values leads to get different flow rates or liquid loads. The element surfaces were defined as walls with an adhesion condition

represented by a constant static contact angle. Fig. (6-2A and C) shows the domain for the SPE and PS consequently. Different grids were used and their specifications are summarized it Tab. (6-1). The domain height apart from the element surfaces was selected to be higher than the expected maximum liquid film thickness (s. Tab. (6-1)).

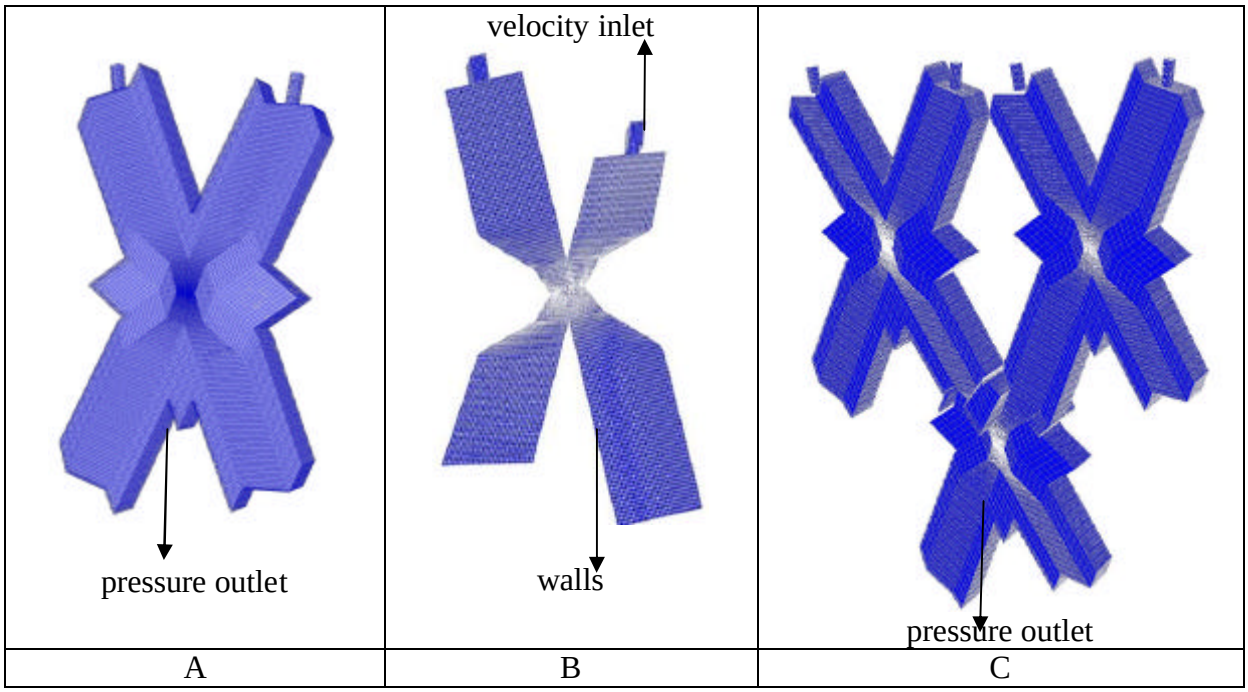

Figure(6-1): A: CFD domain for a single element (SPE), B: CFD domain for a multi-element sheet (PS).

Table (6-1): CFD domains for the single (SPE) and multi-element packing sheet (PS)

		Grid 1 [a]	Grid 2 [a]	Grid 3 [a]	Grid 4 [a]	Grid 5 [b]	Grid 6 [b]
?x	**mm**	**55**	**55**	**55**	**55**	**90**	**90**
?y	**mm**	**35**	**35**	**35**	**26**	**58**	**51**
?z	**mm**	**23**	**23**	**23**	**21**	**45**	**45**
D[c]	**mm**	**3**	**3**	**3**	**1.8**	**3**	**3**
grid size	**cell**	**35330**	**68660**	**268112**	**396744**	**299209**	**730276**
cell size	**mm^3**	**0.0365 0.5898**	**0.0158 0.426**	**0.00443 0.0833**	**$2.09x10^{-4}$ $2.01x10^{-3}$**	**0.3067 0.006994**	**0.061490 0.004241**

[a] SPE, [b] PS [c] Distance from the wall surface

In all of our simulations the Geo-reconstruction was used for the VOF estimation [1]. Transient simulations were carried out with a fixed time step between 10^{-5} and 5.10^{-5} seconds. The implicit first order upwind scheme using a Courant number of 0.25 and zero initial values was used for all variables. The body forces weighted discretization scheme was selected for the pressure and the first order upwind schema for the momentum [1]. The Courant number is

a dimensionless number that compares the time step in a calculation to the characteristic time of transit of a fluid element across a control volume:

$$\frac{\Delta t}{\Delta x_{cell} / v_{fluid}}$$

The FLUENT code release 6.2.16 in three dimensional, double precision and segregated solver was used for the CFD calculations. The following assumptions were adopted in the solution: laminar flow condition, constant static contact angle and no gas flow at this stage of the work. The second assumption is reasonable at a steady state without mass transfer. The gas phase was considered to be stagnant with zero velocity and does not affect the liquid flow. This assumption is valid for low gas loading, where the experimental results have shown no influence of the gas velocity on the hold-up for low gas loading, as it is shown in Fig. (2-5) [30]. The iso-surface, where VOF equals 0.5 represents the interface between the gas and liquid phase. The four element sides (plates) have an inclination of 68.5 degree.

6.2 CFD Simulation Results

In Tab. (6-2) the values of the degree of wetting, interfacial area and liquid hold-up calculated for the lower half lamella using the grid with small cell size (cases F1-F7) or fine cell size (cases F8÷F10) are listed.

6.2.1 Grid Size

In this paragraph the dependency of the CFD simulation results on the grid size is discussed. This is extremely important, since the grid consists from different cell sizes in comparison to the plate case, where the cells have the same size (s. Tab. (6-1) and (5-1)) and especially when corrugations are embedded in the grid. Fluid properties of the studied cases are shown in Tab. (6-2). Different grid sizes were used in these verifications with 35330, 68660 and 268112 cells, consequently. The small cell volumes range between 0.004425 and 0.0833mm^3, and every corrugation edge was linked with two elements. The smallest cells locate at the node of the element, where the flow situation is critical and bifurcation occurs. The mean cell sizes range between 0.0158 and 0.426 mm^3. Every corrugation here represents one element edge. The big cell sizes have values between 0.0365 and 0.5898 mm^3. The difference between the two last meshes is the number of elements along the plate width. For fluids with low viscosity (s. Tab. (6-2), F8÷F10)) finer cell size was needed because of the very low resulting liquid film thickness (under 0.5 mm), which was not clearly resolved using a coarse mesh. This was done through modification of the domain thickness from 6 to 3 mm and meshing the grid with smaller cells. The grid size in this case gives 396744 cells with cell sizes ranging between

$2.09x10^{-4}$ and $2.01x10^{-3}$ mm^3. To get an imagination about the cell size differences, Fig. (6-2) shows a part of the grids at the inlet regions.

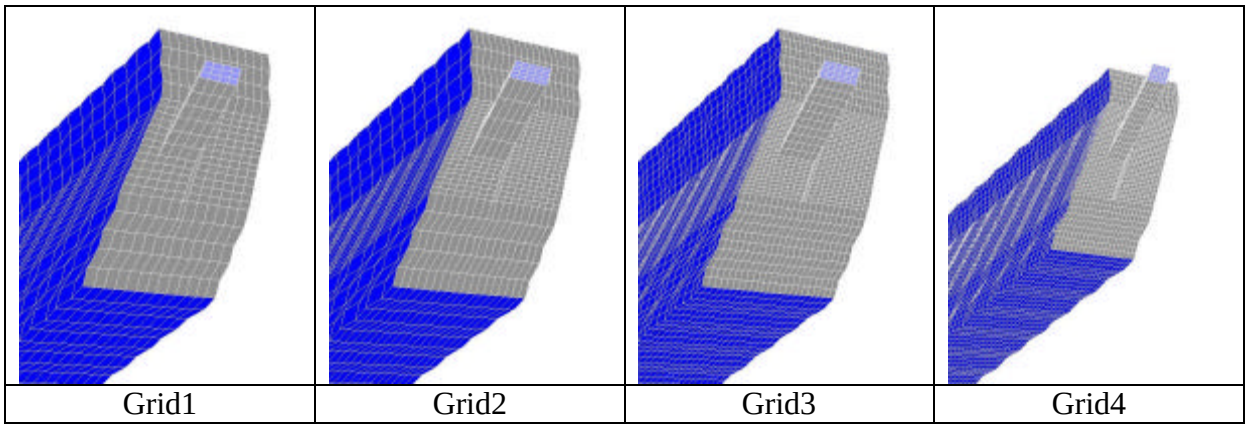

Figure (6-2): Grids used in the CFD simulations at the inlet region

Fig. (6-3) shows the VOF contours (VOF=0.5÷1) for some selected cases. In a rough comparison, it is obvious that the flow patterns for cases F4 and F6 (s. Tab. (6-2)) are almost identical. The liquid in case F4 flows as a rivulet, wetting one side of the top two plates and builds liquid bridges at the bottom and the sides when passing the element node. Afterwards, the liquid bifurcates into two rivulets in the front and back plates. F2 shows similar behaviour but the mean grid size (Fig. (6-3), F2-grid2) was not able to resolve the rivulet flow and some drops are shown on the element surface, which disappeared for the other grid sizes. Fluid F6, which has high viscosity and contact angle, creates only one rivulet for every liquid inlet. For low viscous liquid (F9, F10) also similar behaviour of the case F4 discussed above, is shown. For the case F9, the flow pattern using small grid size includes some liquid drops on the element surface, which disappear again when using the grid with fine cell sizes. That means care must be taken for extreme liquid properties to eliminate the dependency on the cell size. The difference comes from the fact that the liquid interface location for the VOF-model is not in a definite position of the domain, but in a location inside the cells having VOF-values between 0 and 1. It is more sensitive for a small liquid film thickness (case F9). All cells at the element surfaces having VOF values less than 0.5 will not be represented in the CFD flow pattern. Such comparison is very important to get and maintain reasonable and trustable results.

For a quantitative comparison, the four rivulet profiles in case F4 on the plane x=15 mm at all sides (front and back) of the element surfaces (s. Fig. (6-4)) were depicted from the simulations. At VOF=0.5, they are presented in Fig. (6-5) and the locations of VOF=0.5 for

all cases are almost identical. The first cell at the element surface (z=0) has caused the highest deviation between the results.

A qualitative comparison in estimating these parameters with different grids were given in Tab. (6-3), where the results using the small or fine grid size was taken as a reference. Systems with low viscosity, contact angle and surface tension (F8 to F10) are critical and have produced the highest deviations, so they need more computational effort. With a finer mesh, the lowest deviations in all comparisons were found in the liquid hold-up values. These deviations rely on the approximation in tracing the interface location in the VOF model. A maximum deviation of about 10% was accepted using a coarser grid with the benefit of shorter CPU time.

Table (6-2): Liquid properties and CFD simulation results of the wetting of the SPE

								Bottom half element				CFD	CFD	CFD
	Q	u_L	L_L	$?_L$	μ_L	s	$?$	Re_L	Fr_L	We_L	$cos\ ?$	a_h/a	a_{ph}/a	h_L
	ml/min.plate	m/s	m^3/m^2h	kg/m^3	mPas	mN/m	°	$u_L?_L/\mu_L.a$	u_L^2a/g	$u_L^2?_L/s\,a$	-	-	-	m^3/m^3
F1[1]	20.89	3.55E-03	12.79	1147	4.5	29	24.5	5.49	2.12E-04	3.03E-03	0.910	0.400	0.595	0.0263
F2[1]	41.78	7.10E-03	25.58	1147	4.5	29	24.5	10.98	8.49E-04	1.21E-02	0.910	0.499	0.758	0.0395
F3[1]	83.56	1.42E-02	51.16	1147	4.5	29	24.5	21.95	3.40E-03	4.84E-02	0.910	0.670	1.007	0.0640
F4[4]	41.78	7.10E-03	25.58	1147	10	29	24.5	4.94	8.49E-04	1.21E-02	0.910	0.552	0.903	0.0550
F5[4]	41.78	7.10E-03	25.58	1147	4.5	29	10	10.98	8.49E-04	1.21E-02	0.985	0.590	0.881	0.0453
F6[2]	41.78	7.10E-03	25.58	1147	4.5	64	67	10.98	8.49E-04	5.48E-03	0.391	0.195	0.384	0.0244
F7[4]	41.78	7.10E-03	25.58	1147	4.5	64	45	10.98	8.49E-04	5.48E-03	0.707	0.258	0.520	0.0300
F8[4]	41.78	7.27E-03	26.16	1147	1	64	24.5	50.52	8.88E-04	5.74E-03	0.910	0.411	0.661	0.0283
F9[4]	41.78	7.27E-03	26.16	1147	1	29	24.5	50.52	8.88E-04	1.27E-02	0.910	0.409	0.592	0.0255
F10[3]	41.78	7.11E-03	25.59	985	0.3	22.5	16	141.42	8.50E-04	1.34E-02	0.961	0.521	0.657	0.0207
F11[4]	41.78	7.10E-03	25.58	1147	4.5	64	20	10.98	8.49E-04	5.48E-03	0.940	0.565	0.846	0.0454
F12[4]	41.78	7.10E-03	25.58	1147	4.5	45	24.5	10.98	8.49E-04	7.80E-03	0.910	0.511	0.798	0.0436
F13[4]	41.78	7.10E-03	25.58	950	4.5	29	10	9.09	8.49E-04	1.00E-02	0.985	0.613	0.922	0.0499

[1] F1 to F3: glycerine water mixture 50% wt. with surfactant 1.8% Triton X100

[2] F6: glycerine water mixture 50% wt.

[3] F10: chlorobenzene-ethylbenzene 50% wt.

[4] F4 and F5 and F7 to F9, F11 to F13 arbitrary selected liquid properties

Table (6-3): Percentual deviations of the simulation results using different grid sizes

	Grid2	Grid2	Grid2	Grid1	Grid1	Grid1	Grid1	Grid1	Grid1
	Grid3	Grid3	Grid3	Grid3	Grid3	Grid3	Grid2	Grid2	Grid2
	a_h	a_{ph}	h_L	a_h	a_{ph}	h_L	a_h	a_{ph}	h_L
F1	**-4.22**	**-0.05**	**-1.09**	**5.72**	**16.68**	**4.95**	**9.54**	**16.72**	**5.98**
F2	**8.06**	**8.32**	**2.10**	**12.79**	**21.01**	**19.41**	**5.15**	**13.84**	**17.69**
F3	**9.72**	**2.21**	**6.16**	**14.95**	**8.52**	**18.30**	**5.80**	**6.45**	**12.94**
F4	**4.83**	**6.15**	**1.66**	**10.41**	**11.76**	**6.46**	**5.86**	**5.98**	**4.88**
F5	**2.22**	**6.55**	**-1.54**	**1.72**	**12.94**	**10.89**	**-0.51**	**6.83**	**12.24**
F6	**-1.32**	**-2.04**	**-2.39**	**10.01**	**3.67**	**9.97**	**11.18**	**5.59**	**12.07**
F7	**0.18**	**10.21**	**1.90**	**0.18**	**10.21**	**1.90**	**-**	**-**	**-**
F8	**-48.53**	**-34.59**	**-86.38**	**-**	**-**	**-**	**-**	**-**	**-**
F9	**-9.25**	**0.95**	**9.63**	**-9.25**	**0.95**	**9.63**	**-**	**-**	**-**
F10	**33.22**	**26.00**	**12.93**				***D***	***D***	***D***
F11	**3.91**	**6.27**	**1.10**			**F84**	**9.60**	**0.43**	**-2.24**
F12	**5.04**	**8.31**	**4.63**			**F94**	**-5.68**	**-12.58**	**-25.61**
F13	**3.04**	**8.17**	**1.39**			**F103**	**1.68**	**1.63**	**4.17**

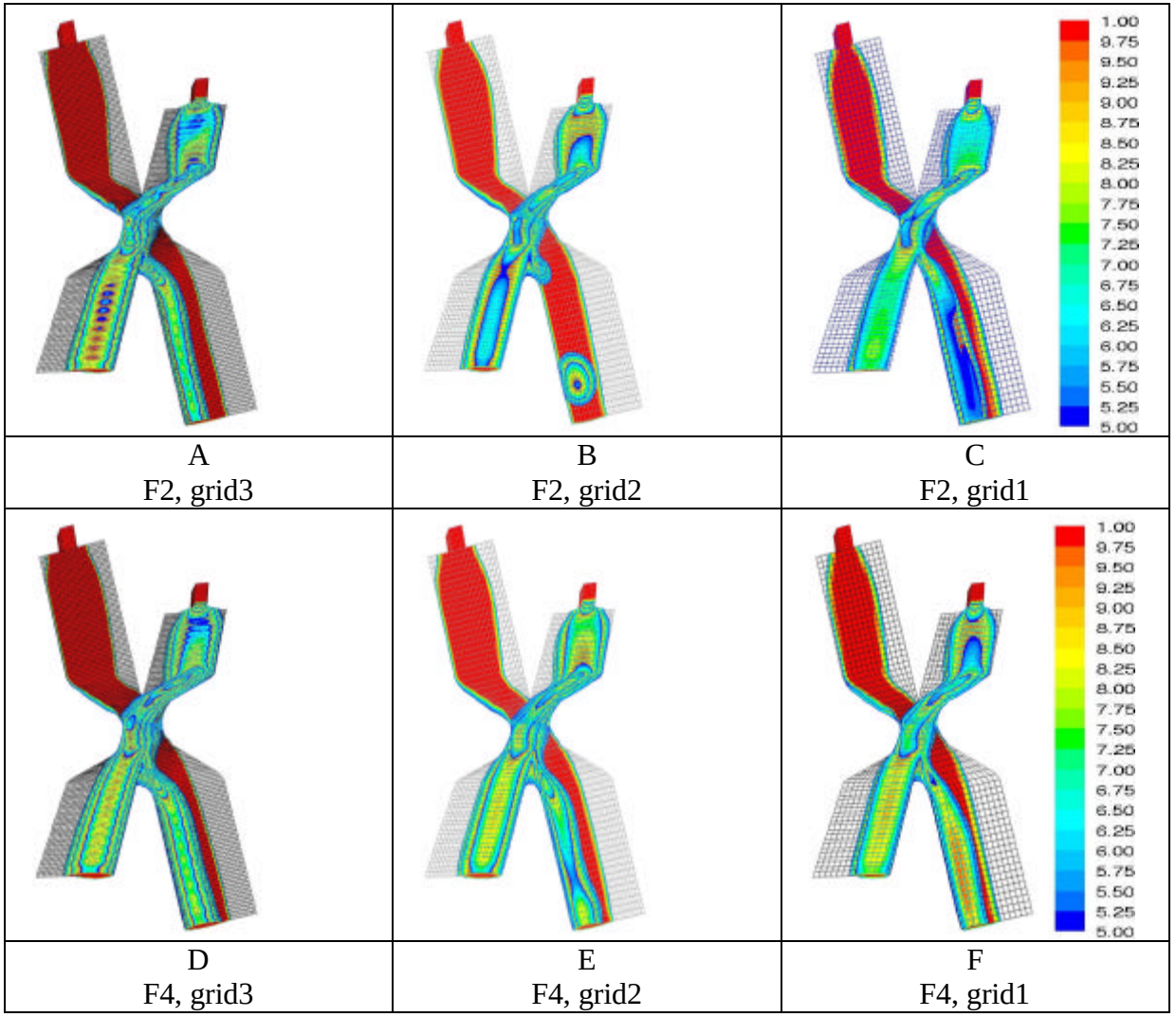

Figure (6-3): VOF-contours VOF=0.5 to 1 for some selected CFD -simulations at different grid sizes

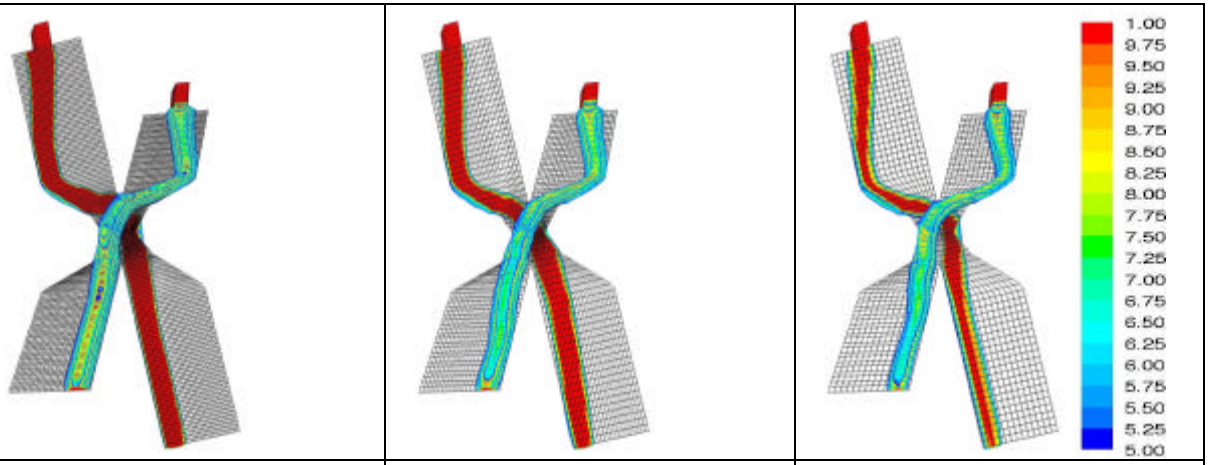

G	H	I
F6, grid3	F6, grid2	F6, grid1

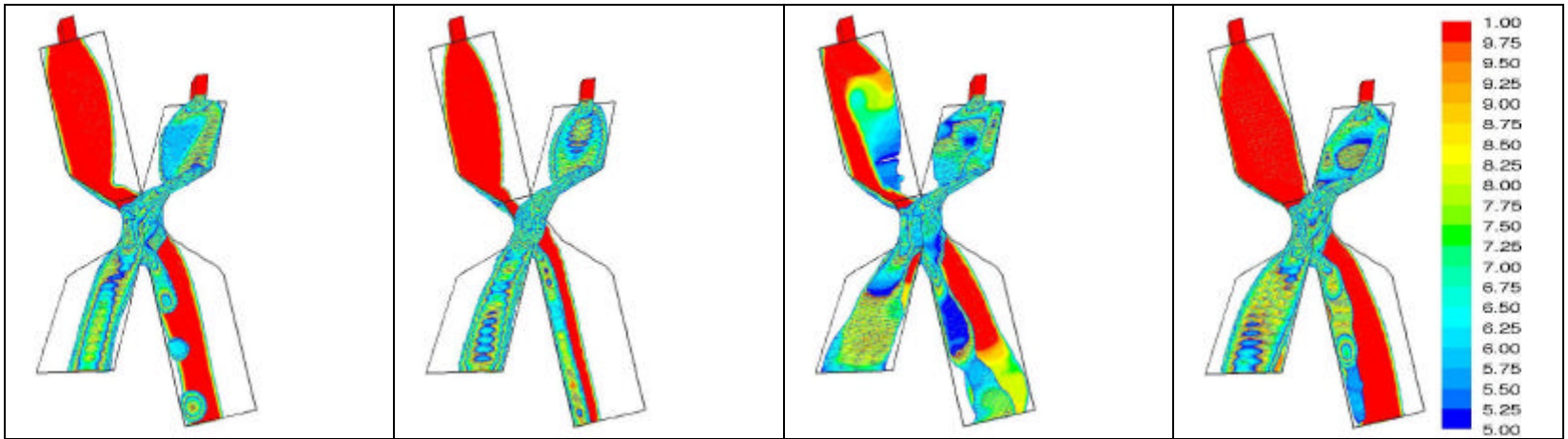

J	K	L	M
F9, grid3	F9, grid4	F10, grid3	F10, grid4

Figure (6-3) continued

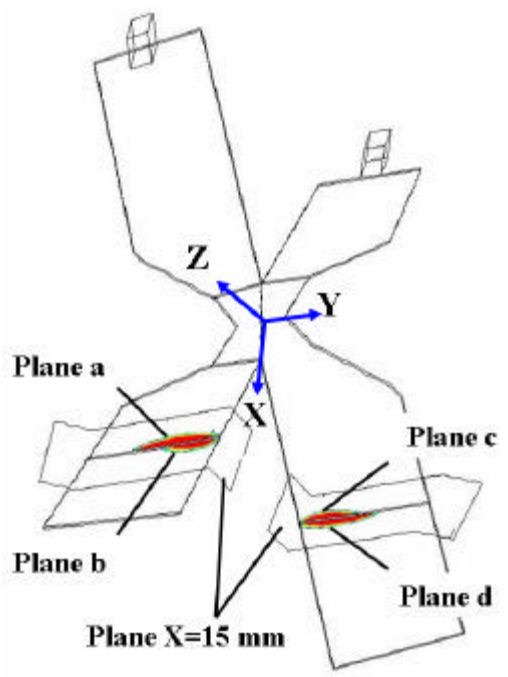

Figure (6-4): VOF contours on the planes x=15 mm

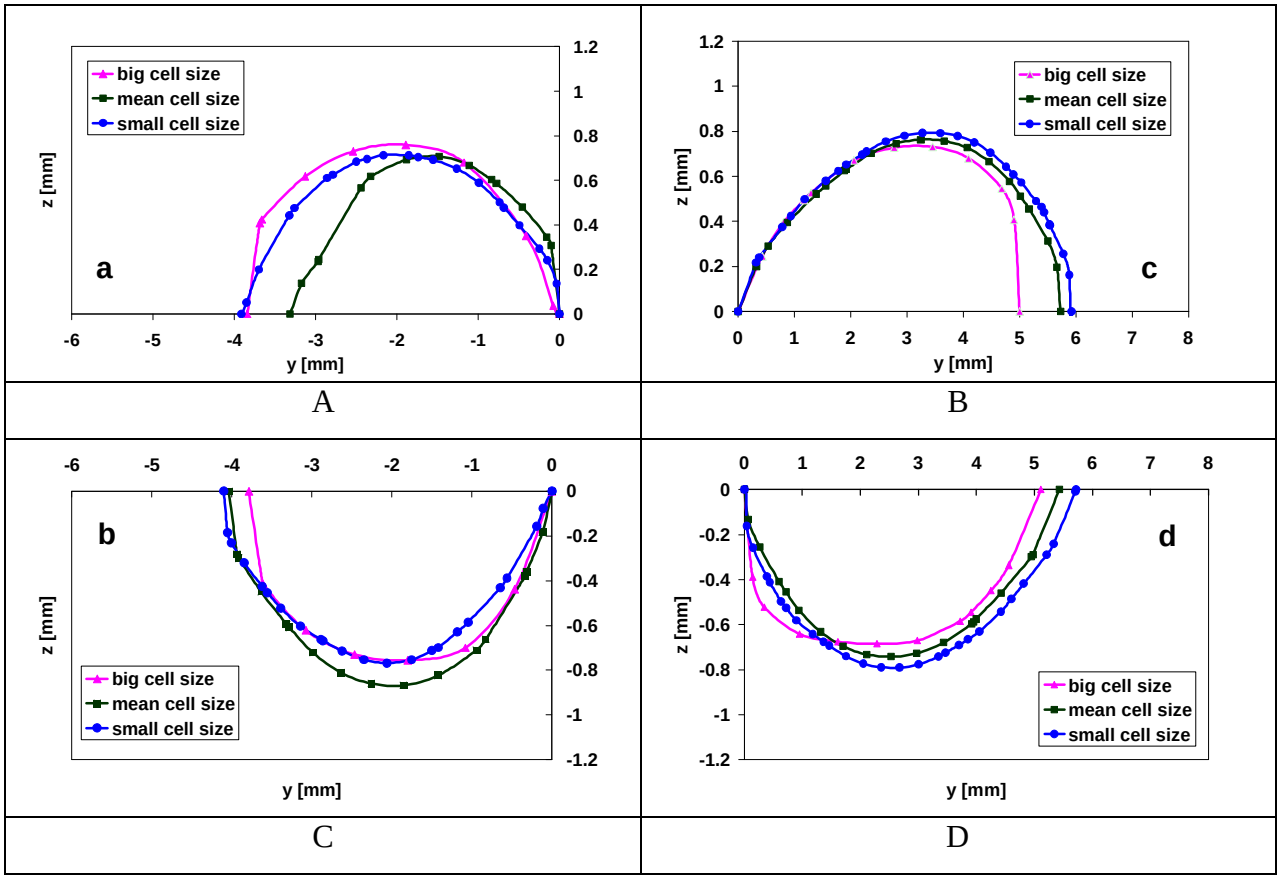

Figure (6-5): Rivulet profiles (interface at VOF=0.5) on the planes *x*=15 mm for case F4 depicted from different grid sizes, a- left front, b- left back, c- right front, d- right back, view from the observer

6.2.2 SPE: CFD-Simulations and Experiments

Fig. (6-6) shows the experimental wetting patterns at different flow rates from 13 to 84 m^3/m^2h on the top element and on the PS, which were compared to the CFD simulation results. For the liquids F1÷F3 (glycerine-water mixture 50% wt. with 1.8 mg/kg surfactant Triton X100, coloured with toluidine blue O from Merck) and F10 (chlorobenzene-ethylbenzene mixture 50%, coloured with fat red bluish from Fulka), the liquid wetted the top two plates as rivulets and liquid bridges were then created around the node. In this case, the liquid streams were mixed at the node, where the element plates are interconnected, and a self-distribution effect for the liquid on the bottom plates is observed. Not only the front plate surface but also a part of the back plate surface was wetted with a smaller rivulet. Increasing the flow rate results in increasing the wetted, interfacial area and liquid hold-up (s. Tab. (6-2). For a bad wetting liquid F6 (glycerine-water mixture 50% wt., ?=67°), the liquid flows as a single rivulet from every inlet. Wetting behaviour for a good wetting liquid F10 (chlorobenzene-ethylbenzene 50% wt., ?=16°) is similar to that observed for fluid F1. In this case the rivulet on the right hand side at the bottom end of the element is very thin, which makes the simulations very expensive and finer cell sizes were necessary. Generally, we can say that the VOF simulations and the experimental findings are very similar in the way of spreading, bifurcation and liquid bridging. In addition to that, the lower half element taken for validation of the results gives a good representation of the total packing sheet, as it is shown in Fig. (6-6). One can conclude that the CFD simulation results are in good agreement with the experimental ones and have given a detailed picture of the liquid spreading on the element. This is encouraging to further extend the CFD simulation on more complex geometries, like multi-element packing sheet, which will be discussed in the next chapter.

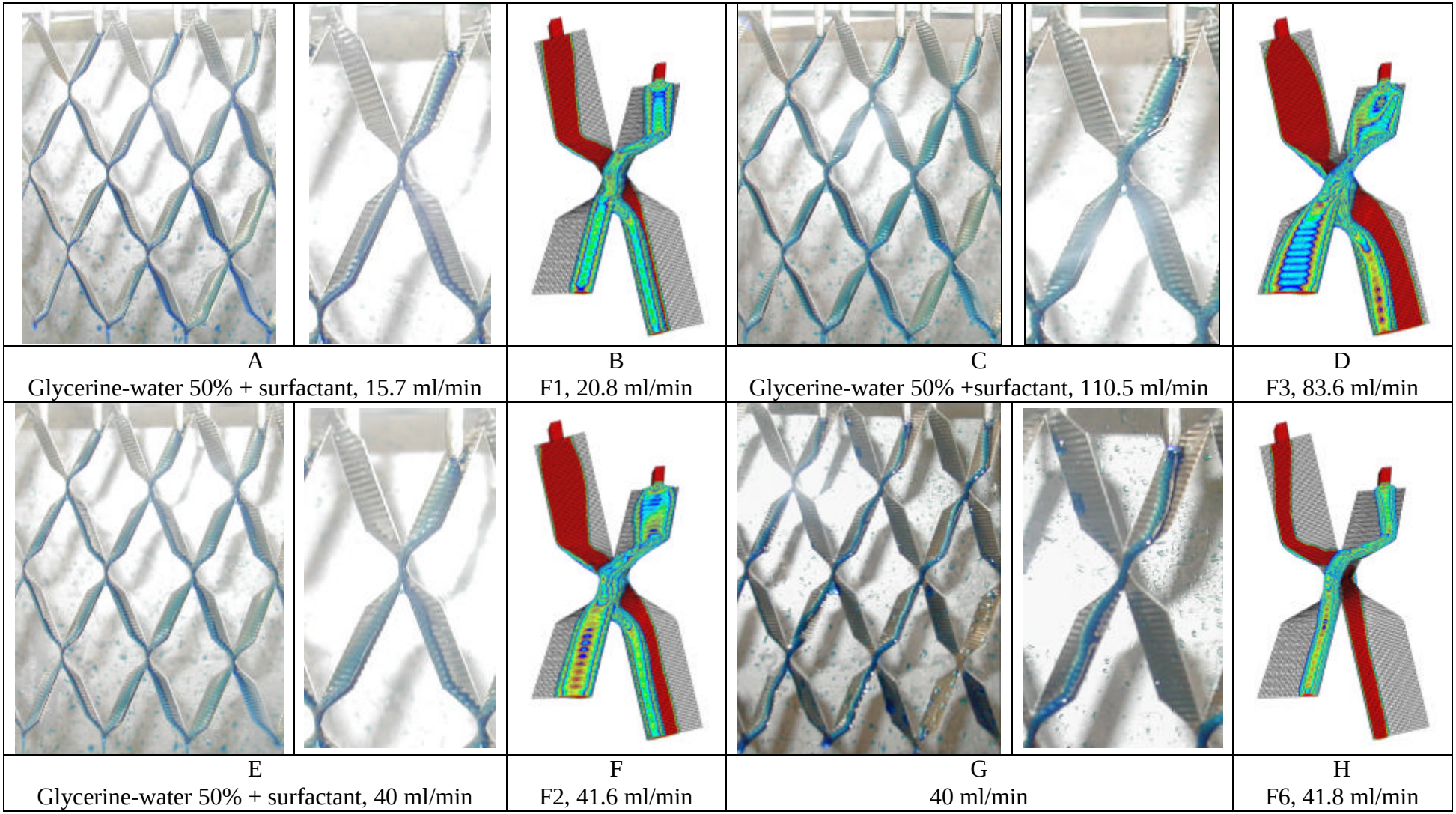

A Glycerine-water 50% + surfactant, 15.7 ml/min	B F1, 20.8 ml/min	C Glycerine-water 50% +surfactant, 110.5 ml/min	D F3, 83.6 ml/min
E Glycerine-water 50% + surfactant, 40 ml/min	F F2, 41.6 ml/min	G 40 ml/min	H F6, 41.8 ml/min

Figure (6-6): Liquid flow patterns at different flow rates and for different liquids from the experiment (PS, SPE). VOF contours of the CFD simulation for SPE

I
F10, 44.3 ml/min

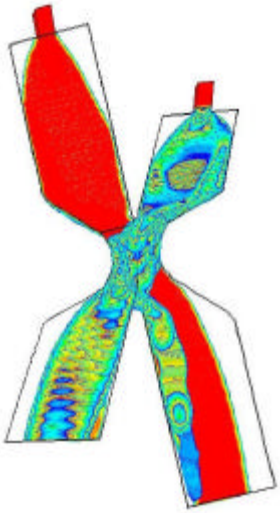

J
F10, 41.8 ml/min

Figure (6-6) continued

6.2.3 Structure vs. Unstructured Element

A detailed study on plane surfaces has been performed already and has been initially compared with 1-D models from literature [66] and discussed in chapter 5. It is anticipated that, the micro-structure should have a stability effect of the liquid film by preventing break-up and dry-batches.

Fig. (6-8) depicts the VOF flow patterns for a flat packing element using the CFD-simulation at similar conditions of cases F4 and F9 (s. Tab. (6-2)). The difference between the two liquids is the viscosity. For high liquid viscosity (F4, 10 mPas), the flow pattern on a flat element is very similar to that of the structured packing element in F4 of Fig. (6-7).

At low liquid viscosity (F9, 1 mPas), the liquid flows after the node to the two bottom sides of the element, wetting a considerable surface. For the flat plate the liquid does not flow to the element node but it drops from the top element to the bottom ones and the self-distribution effect as discussed above does not appear in this case. The reason for that are the wavy structure of the surface, which decelerate the liquid flow allowing it to spread on a larger surface, acting as a stabilizing factor.

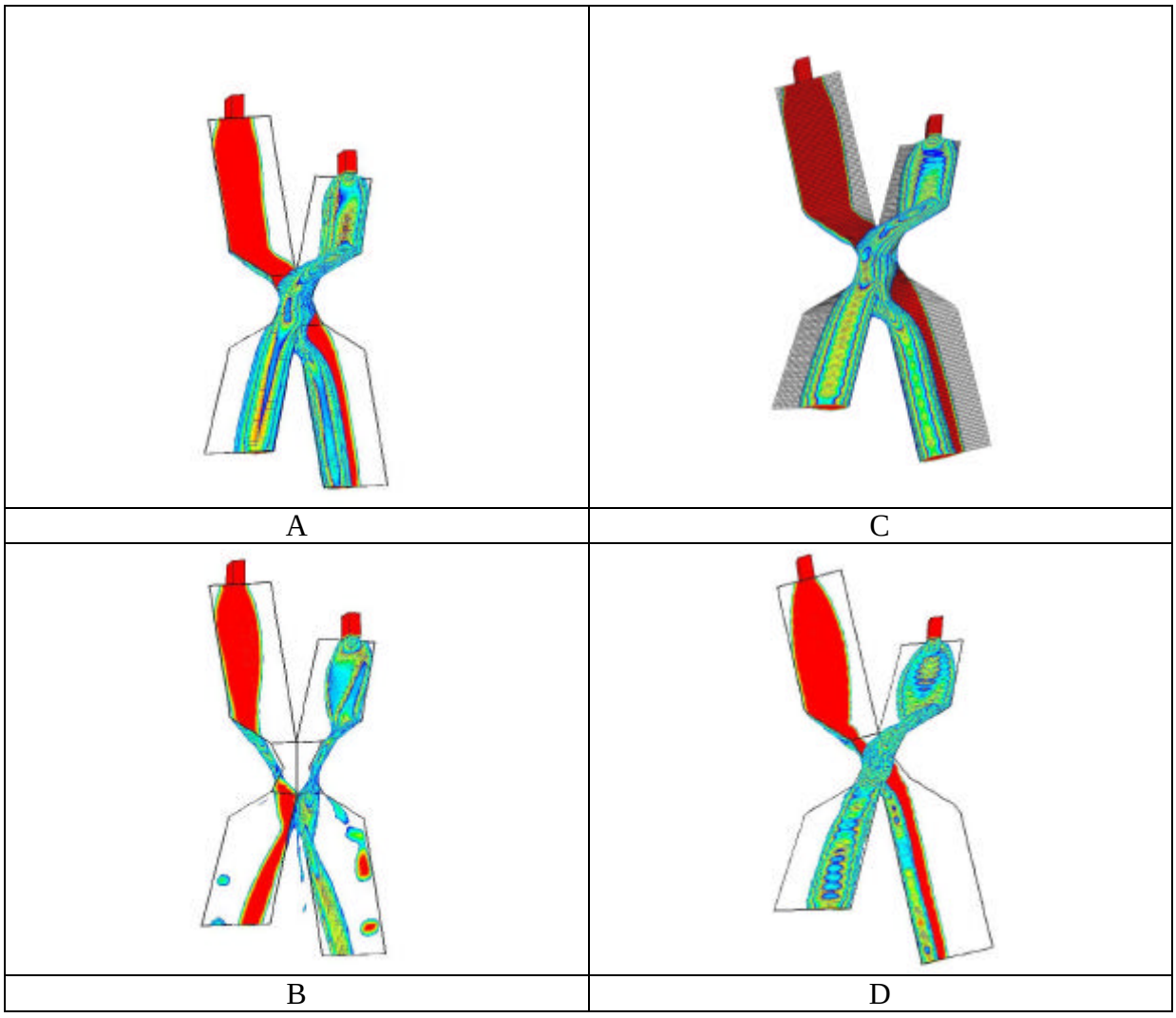

Figure (6-7): A comparison between the flow patterns between a flat packing element, A: (F4), B: (F9) and micro structured element, C: (F4), D: (F9)

6.2.4 Liquid Properties

The three liquid properties surface tension, viscosity and contact angle determine markedly the liquid spreading on a given geometry. They were varied in the CFD simulations (see Tab. (6-2)) to study their effect on the liquid spreading patterns on a lamella.

6.2.4.1 Viscosity and Density

Viscosity is a stabilization factor for the flow and it varies strongly with temperature in the distillation columns. Three different viscosities were taken in the CFD simulation 1, 4.5 and 10 mPas, with a surface tension s=29 mN/m and a contact angle of $?$=24.5° (cases F9, F2 and F4). The CFD-flow patterns are shown in Fig. (6-3). The rivulet profiles on a plane x=15 mm (compare Fig. (6-4) on one side of the lower element plates are presented in Fig. (6-8). The rivulet width and height increases with increasing of the viscosity, which means higher viscous forces act against the gravity and makes the flow more stable. As a result the wetting

degree, interfacial area and liquid hold-up increase with the viscosity (s. Tab. (6-2)). The density has a likewise effect as viscosity (compare F5 with F13).

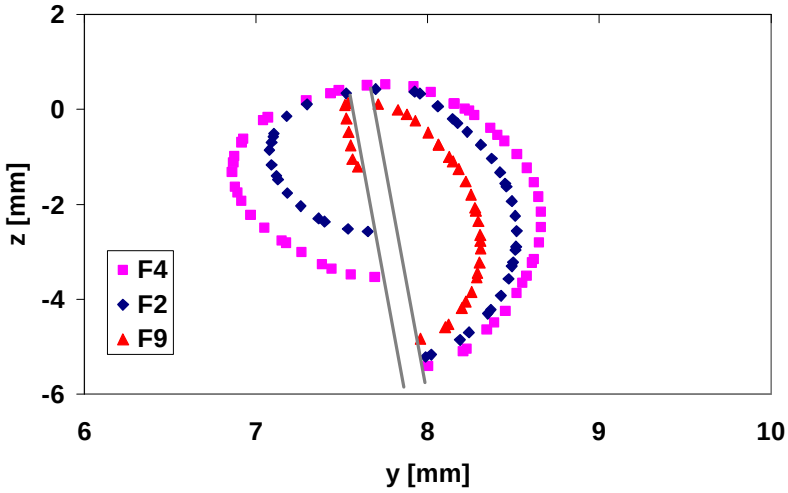

Figure (6-8): Flow profiles on one plate sides (x=15 mm) at different liquid viscosity 1 (F9), 4.5 (F2) and 10 (F4) mPas, 26.16 m^3/m^2h, ?=24.5°, s=29 mN/m

6.2.4.2 Contact Angle and Surface Tension

The contact angle was found to have a significant effect in the cases F2 and F5, which have a different contact angle of 24.5° and 10°. The wetting degree increases from 0.499 inthe case of F2 and to 0.59 in the case of F5. As a result the wetted area increases with diminishing contact angle. Wetting degree is inversely proportional to the contact angle. Surface tension has small effect on the hydraulic parameters when comparing F2 with F12 in Tab. (6-2).

6.3 Packed Column

6.3.1 Packed Column Parameter Calculation Method

The hydraulic parameters, wetted and interfacial areas, in addition to the liquid hold-up for every simulated case, were obtained in the post processing utilities of FLUENT. Dividing the grid after solution according to the iso-value 0.5 of VOF firstly, the liquid part around the element surfaces is separated as shown in Fig. (6-9A), according the x-coordinate along the element length, the lower part of the liquid is obtained (Fig. (6-9D)). Through this process, new identities are created. The interfacial and the wetted surface areas created from the lamella plates are among them. The sum of the wetted surfaces gives the wetted area as it is shown in Fig. (6-9B) for this example. Here, the liquid wetted the front and back side of every lamella is indicated with different colours (look the right lamella). The integral of the created interfacial surfaces gives the interfacial area (Fig. (6-9C)). Volumetric integration of the grid

part containing the cells, which have VOF values between 0.5 and 1, gives the liquid hold-up (Fig. (6-9D)).

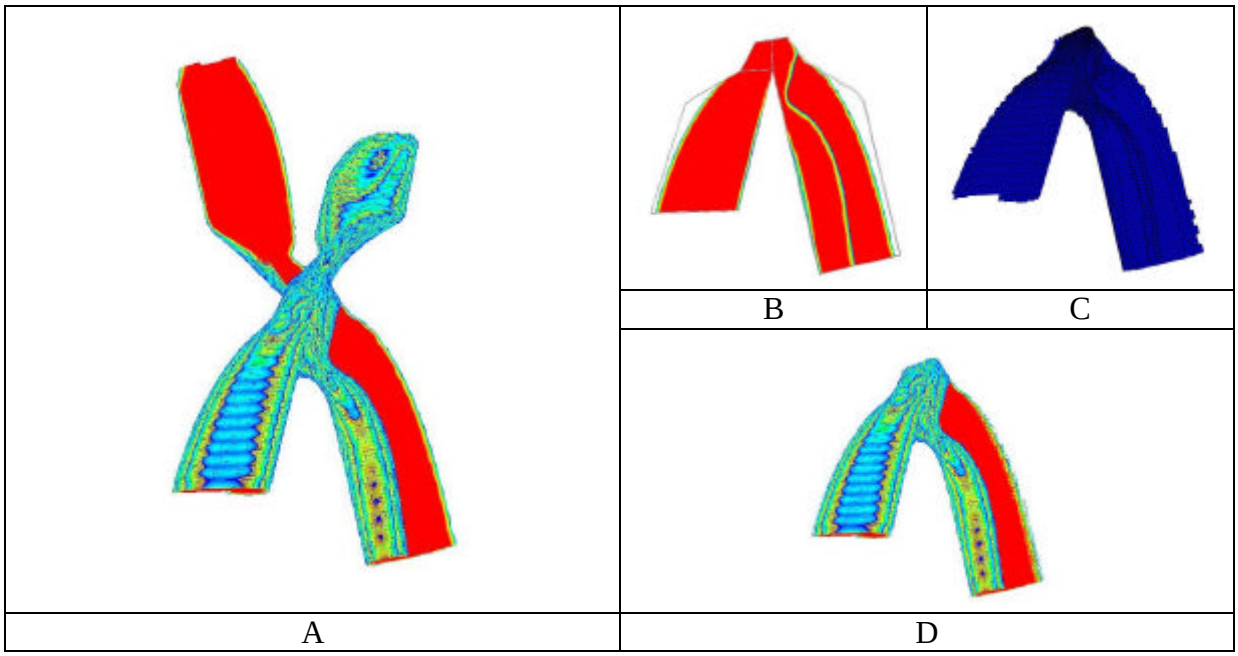

Figure (6-9): Hydrodynamic parameter of a packing via VOF contours between 0.5 and 1, A: VOF=0.5-1 for a complete SPE, B: Wetted area, C: Interfacial area, D: Liquid volume (Liquid hold-up)

For developing CFD-based correlations the following calculation method was used: the liquid superficial velocity u_L of the packing is the most important parameter in the calculation method. To calculate it, the specific packing area and the packing porosity e was obtained from the Rombopak flyer. Lamella length L_{La} was derived from the measurements of the real element. Dividing the specific packing area by the lamella area gives the number of lamellas per unit volume N_{La}. The inverse of N_{La} gives the volume occupied by a single lamella. To get the superfacial area for one lamella, its volume was divided by its length L_{La}. At last the liquid superficial velocity is obtained from the volumetric flow rate or the liquid load and the superficial area per lamella. This velocity also represents the liquid superficial velocity of the packing u_L (packed column). All other dimensionless numbers such as Reynolds and Weber numbers can then be estimated. Reference length was taken the inverse of the specific packing surface area per volume $1/a$. The analysis was based on values from the lower half element (below the element node), which was considered to be representative for the packing, avoiding inlet distribution problems.

6.3.2 Hydraulic Parameter

The correlations found in the literature for prediction of the specific interfacial area and hold-up in a packing were derived from experiments on mass transfer in the absorption or desorption processes and there are very few works about the flow structure inside the packing. CFD methods give a detailed picture about the liquid flow spreading and the interfacial area inside the packing. In this section the hydraulic parameters are discussed in scope of the CFD simulation results.

6.3.2.1 Degree of Wetting

The degree of wetting is a function of different geometrical parameters, which depends on the packing structure, such as porosity *e* and specific area *a*, liquid properties, such as surface tension *s*, contact angle *?* viscosity μ_L etc, and liquid load, represented in the superficial liquid velocity u_L as we have seen before. Fig. (6-10) summarize this dependency.

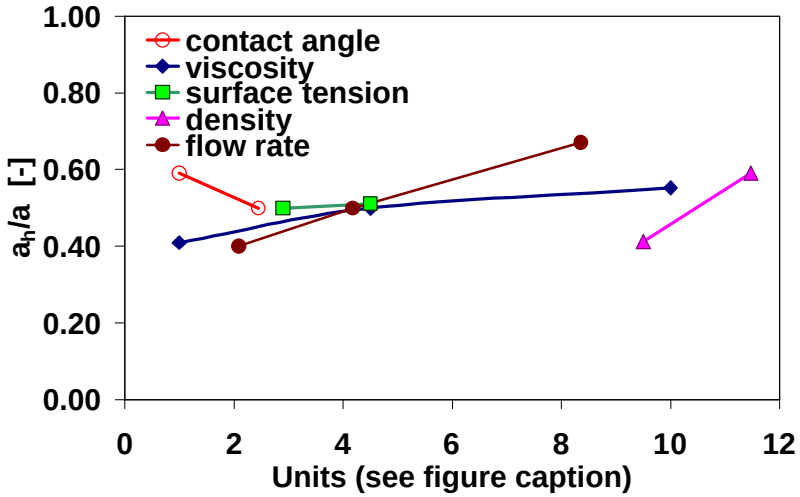

Figure (6-10): Degree of wetting as a function of different parameters. Units: contact angle (°/10), viscosity (mPasX10), surface tension (mN/m), density (kg/m^3/10), flow rate (ml/min))

To evaluate the degree of wetting of the packing element from the experimental image, every case was analyzed by dividing the wetted surface into squares and triangles. The summation of these areas gives the total wetted area. In the discussion of different correlations describing the hydrodynamics of packed columns, the results derived from the half lower element were considered. The inverse of specific packing area *1/a*, was taken as a reference length in all correlations.

The constant C_h which appears in the model of Billet & Schultes [6] in Eq. (2-38) for $Re_L<5$ depends on the packing geometry. For Rombopak 4M, its value was 0.366, with a mean

square relative error (MSRE) of 35% from the CFD results. In this correlation the dependency of the degree of wetting on the contact angle and surface tension is not included. This is obvious in the cases of F2, F5 to F7, F11 and F12, which have given the same value for the degree of wetting at different surface tension values and contact angles (s. Fig. (6-11)).

Assuming s_{Cr}=0.075 N/m [33] in the correlation given in Eq. (2-40) for the degree of wetting derived by Onda et al. [34] was found not appropriate. Too high values in comparison to the CFD-results was found. The correlation derived by Shi & Mersmann [10,18] given in Eq. (2-41) is very useful for our study, since the contact angle is represented in the correlation. Using this correlation and comparing the results to that of the CFD, it has given a relatively good prediction with a MRSE of about 19.8 %. The dominant part of this error comes from the cases F5 and F13 with low contact angle (10°), where a high wetting degree is predicted. The relative square error in these two cases is about 70 % in comparison to the CFD values.

Analyzing the correlations for wetting degree and interfacial area reveal that they are functions of the liquid properties and liquid load with different exponents as it is shown exemplarity in Tab. (6-4). As to that they are dependent on the packing type they are derived for Rombopak 4M. This derived correlation has the form given in Eq. (6-1) with a low MSRE of about 9 %, where *e* and *a* are not taken into consideration.

$$\frac{a_h}{a} = 1.279 Fr_L^{-0.044} We_L^{0.243} \mathrm{Re}_L^{-0.0266} (\cos q)^{0.927} \qquad \textbf{(6-1)}$$

Table (6-4): Exponents in correlations for wetted and interfacial area

	Re_L	Fr_L	We_L	u_L	$?_L$	μ_L	s	$?$
Wetted area, a_h	$u_L?/\mu_L a$	$u_L^2 a/g$	$u_L^2?/s\,a$	m/s	kg/m^3	mPas	mN/m	°
Billet & Shultes [6]	**0.25**	**0.1**	**0**	**0.45**	**0.25**	**-0.25**	**0**	
Shi & Mersmann [18]	**-0.2**	**0.15**	**0.15**	**0.4**	**-0.05**	**0.2**	**-0.15**	**yes**
Onda et al. [34]	**0.1**	**-0.05**	**0.2**	**0.4**	**0.3**	**-0.1**	**-0.2**	**yes**
Ataki & Bart [67] and this work	**-0.0266**	**-0.044**	**0.243**	**0.3714**	**0.2164**	**0.0266**	**-0.243**	**yes**
Interfacial area, a_{ph}								
Billet [30] (site 124)	**-0.2**	**-0.45**	**0.75**	**0.4**	**0.55**	**0.2**	**-0.75**	**no**
Rocha et al. [7]	**-0.2**	**0.15**	**0.15**	**0.4**	**-0.05**	**0.2**	**-0.15**	**yes**
Zech [68]	**0.5**	**-0.45**	**0.45**	**0.5**	**0.95**	**-0.5**	**-0.45**	**no**

Fig. (6-11) shows the results for the degree of wetting, depicted from the CFD correlation, Billet & Schultes [6,30], Shi & Mersmann [10,18] and the experimental results as a function of the CFD-results. The agreement with the experiments for glycerine-water 50% is very good, but it is less for glycerine-water (50%) with surfactant. For the chlorobenzene-

ethylbenzene (50%) system the experimental values are higher than that of the CFD predictions. Here the contact angle was very low and an error in the measurements can be the reason for this deviation. In general, the CFD simulations and Shi & Mersmann correlation [10,18] gave very similar results. See Appendix C for more diagrams on a_h/a.

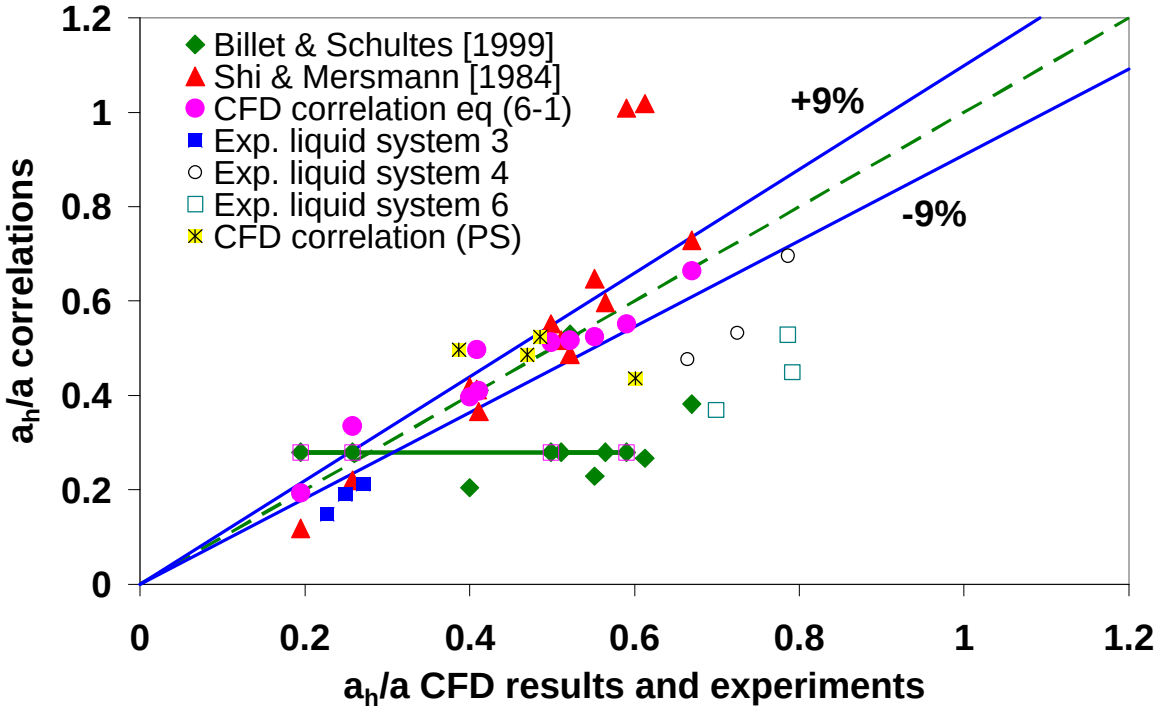

Figure (6-11): Degree of wetting as a result from the CFD based wetting model, experimental data and different correlations (see paragraph 6.4)

6.3.2.2 Specific Interfacial Area

Different correlations can be found in the literature to predict the specific interfacial area in packed columns, where most of them are for dumped packings. A literature survey about its dependency on liquid properties has been given by Nicolaiewsky et al. [69] and Last [70]. As for wetting area correlations a wide range of exponent values for the liquid properties *?*, μ and *s* was found in these correlations in spite of their applicability for the studied packings (see Tab. (6-4)). This discrepancy does not always lead to correct calculations of the specific effective area and gives rise to modifications.

The effective area was estimated from the CFD simulations (s. Tab. (6-2)) and calculated by the correlation of the SRP model [7-9] given in Eq. (2-42). The value 0.193 (for the metal sheet packing Flexipac F_{SE}=0.35 [7]) has been found the best fit for the packing specific surface enhancement factor F_{SE} with MSRE=19%, at a maximal relative error of about 60%. Changing the exponent of the parenthesis term of contact angle in this correlation from 1 to

0.392 and refitting the correlation with F_{SE}=0.604 reduces the MSRE to 6.4 % in comparison to the CFD results. The modified correlation is given in Eq. (6-2).

$$\frac{a_{ph}}{a} = 0.604 \frac{29.12(We_L Fr_L)^{0.15} S^{0.359}}{\mathrm{Re}_L^{0.2} e^{0.6} (1-0.93\cos q)^{0.392} (\sin y)^{0.3}} \qquad \textbf{(6-2)}$$

Again using the correlation of Onda et al. [34] given in Eq. (2-40), the interfacial area has too low predicted values and it was not used for this study. The Delft model [31-32] does not include the effect of different liquid properties and is not used further.

A direct correlation for the dependency of the specific interfacial area on the liquid properties and liquid load are given in Eq. (6-3). The exponent of u_L is about 0.37 and it is almost equal to the values given in the correlations of the different models listed in Tab. (6-4), which has a value of about 0.4.

$$\frac{a_{ph}}{a} = 1.939 u_L^{0.372} r^{0.217} m^{0.0266} s^{-0.243} \cos(q)^{0.927} \qquad \textbf{(6-3)}$$

Rewriting Eq. (6-3) in dimensionless form leads to Eq. (6-4), which has given good agreement to the CFD results for the interfacial area of Rombopak 4M with a MSRE of about 11.3%:

$$\frac{a_{ph}}{a} = 1.939 Fr_L^{-0.044} We_L^{0.243} \mathrm{Re}_L^{-0.0266} (\cos q)^{0.927} \qquad \textbf{(6-4)}$$

Fig. (6-12) shows the results of the interfacial area using the modified correlation (Eq. 6-2) of the SRP model [7] and the CFD correlation Eq. (6-4) as a function of the CFD-results.

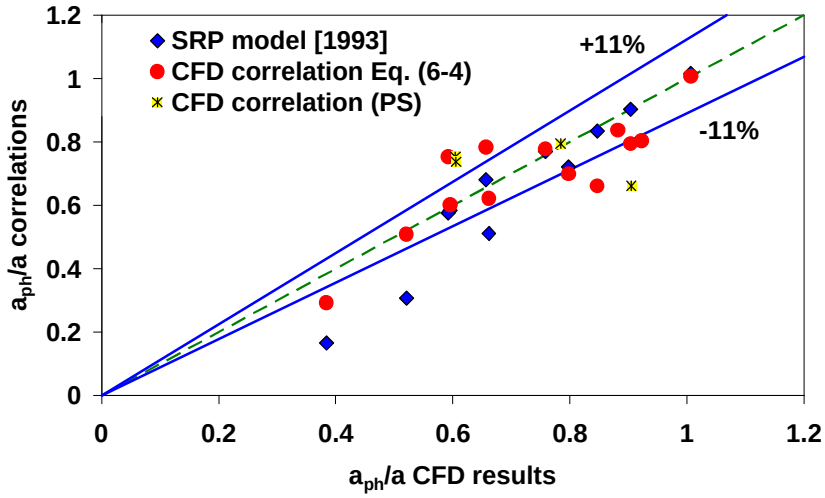

Figure (6-12): Specific effective area as a result from the CFD simulation and modified SRP-model (see paragraph 6-4)

6.3.2.3 Liquid Hold-up

The liquid hold-up correlation of Billet & Schultes [6,30] for the ordered packing given in Eq. (2-39) does not include the surface tension and contact angle. An alternative correlation discussed here is that one given in the SRP model [7] in Eq. (2-43). Both correlations have given over-predicted values for the liquid hold-up. In spite of fitting the SRP model correlation given in Eq. (2-42) by multiplying it with a constant of 0.0975 and assuming the effective gravity $g_{eff}=g$, the MSRE was about 26%. However, multiplying Eq. (2-39) with the constant 0.675 and using the CFD based correlation for a_h/a given in Eq. (6-1) has led to better agreement with the CFD results, with a MSRE of 8%. According to this the CFD based correlation has the form:

$$h_L = 0.675(12\frac{1}{g}\frac{m_L}{r_L}u_L a^2)^{1/3}(\frac{a_h}{a})^{2/3} \qquad \textbf{(6-5)}$$

where, a_h/a has to be substituted with the correlation given in Eq. (6-1). All values for the hold-up from the Billet & Schultes model [6,30], the fitted correlation of Rocha et al. [7] and the CFD based correlation are shown in Fig. (6-13) as a function of the CFD simulation results.

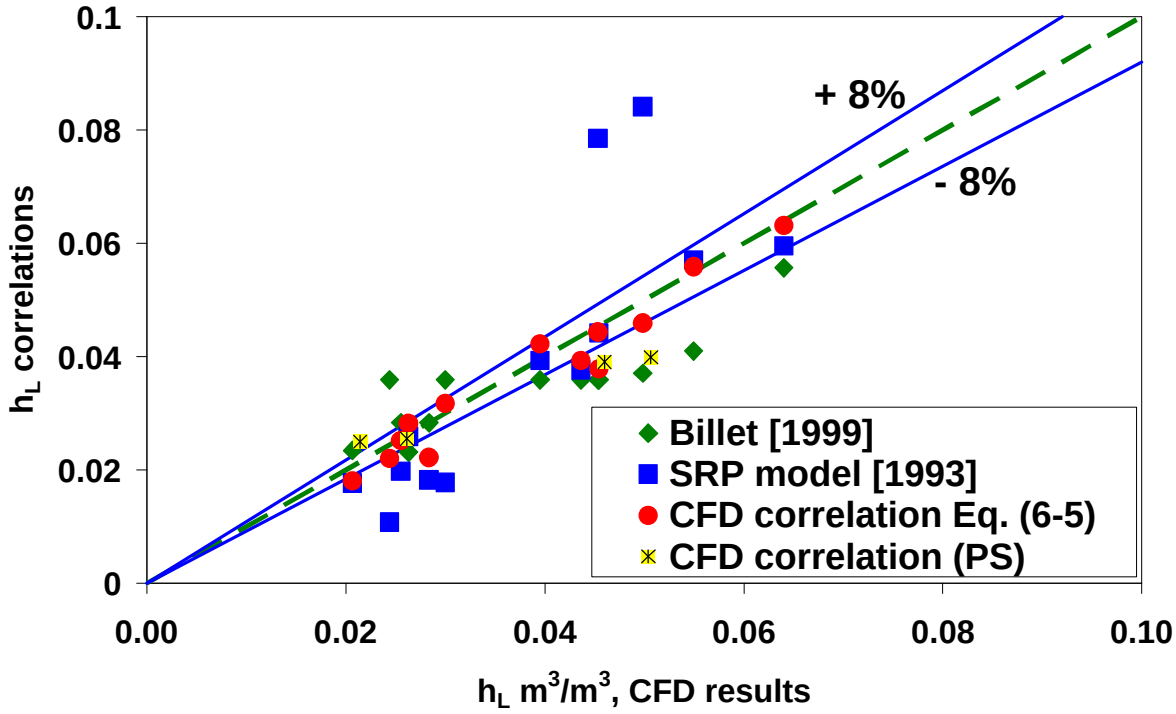

Figure (6-13): Liquid hold-up resulted from the CFD simulation versus the modified correlations of Billet and fitted SRP model and the CFD based correlation (see paragraph 6-4)

6.4 Packing Sheet vs. Structured Packing Element

Experimental liquid flow patterns on a packing sheet shown in Fig. (6-7) show that liquid flow pattern develops from the first node at the top element of the packing sheet to the second and again on the third element until it reaches a fully developed flow pattern as in the cases F3 and F10. Since the liquid is redistributed on each packing node arrangement of at least 3 packing elements (s. Fig. (6-1C)) should be used to minimize the capillary inlet flow effects and in order to obtain the fully developed flow pattern. Further, this can be used to prove the validity of the correlations derived above with help of SPE simulations to describe the hydrodynamics within a full packing element. For this purpose CFD simulations were performed for the flow on a packing sheet (PS) consists of several nodes (or elements) to numerically reveal the liquid flow developing from the first to the next node. The grid used in these CFD simulations is shown in Fig. (6-1). Examples of the VOF contours for the flow patterns on the PS are shown in Fig. (6-16) beneath to that of the SPE for comparison.

Fig. (6-16C and D) are the flow patterns of case F4 and the similarity between the flow pattern on the half bottom of the SPE and that of the top element of the PS is very clear. For the flow pattern on the bottom element of the PS, the liquid is redistributed in similar manner of the first one and qualitative comparison is needed for this case. Similar comment is valid for the case F11 in Figs. (6-16G and H). For the cases F9 and F10 the grid 6 was used in the simulations which is an extension of grid 3 and the cell was not small enough to represent the rivulet flow on the element. Because of time limitations, we stopped our research at this stage and it was better to extend grid 4 instead. However, comparison is possible for these cases with help of Fig. (6-4). The wetting pattern on the top element of the PS shown in Fig. (6-16F) and (6-16A) for cases F10 and F10 are similar to Figs (6-4L) and (6-4J).

The hydrodynamic parameters were estimated from the CFD simulations of the PS considering the part below the first node and presented in the diagrams shown in Figs (6-11, 12 and 13). The deviation from the CFD correlation are presented in Figs (6-15) and (6-16), where a SMRE of about 10 % was found. This means that the CFD correlations derived from a single element are still valid for total packing sheet.

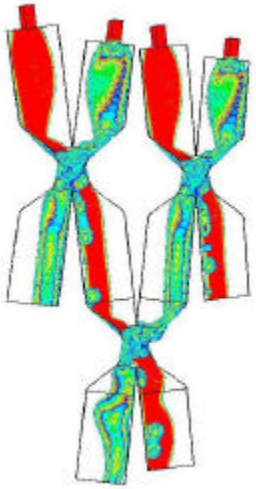	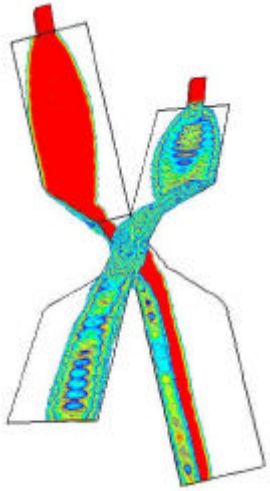	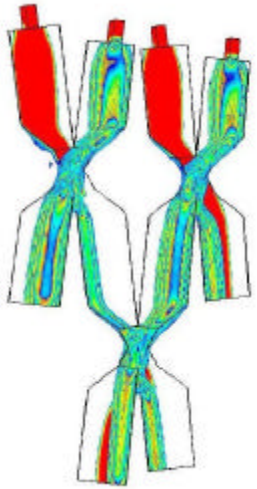	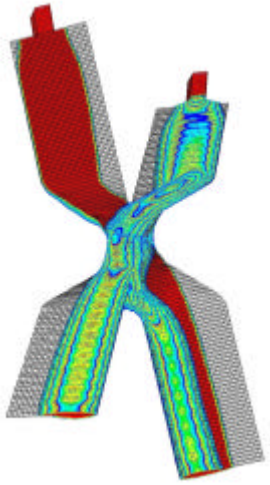
A F9	B F9	C F4	D F4
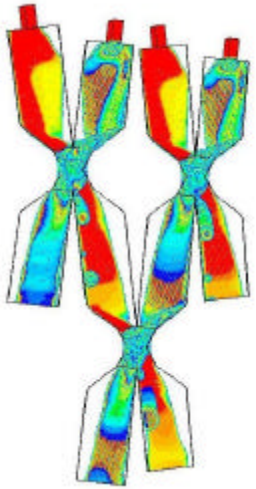	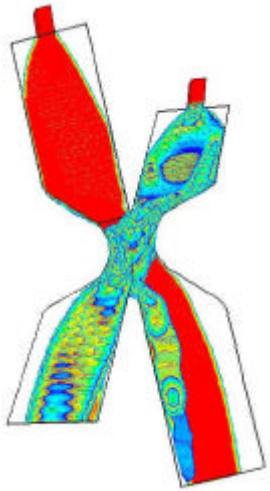		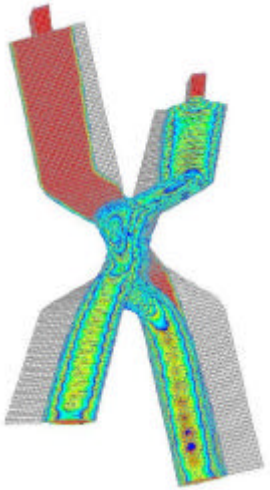
E F10	F F10	G F11	H F11

Figure (6-14): VOF-contours for PS and SPE

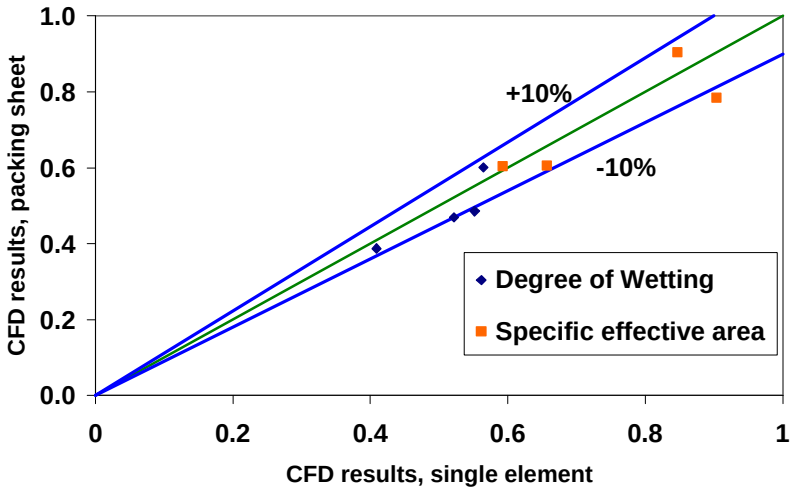

Figure (6-15): Wetting degree and specific effective area, CFD simulation results for SPE and PS

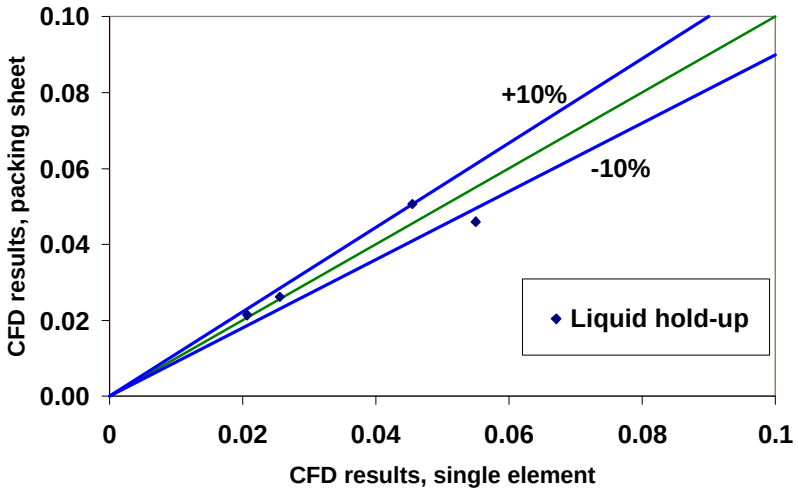

Figure (6-16): Liquid hold-up, CFD simulation results for SPE and PS

Chapter 7

Dry Pressure Drop CFD-Simulations

Pressure drop is a key factor in the design of packed distillation columns. Structured packings have a very complex geometry and the flow inside them cannot be considered as a channel or an open flow, which makes the choice of the appropriate turbulent model difficult especially in the transient region between laminar and turbulent flow. One of the main problems in turbulence modelling is also the accurate prediction of flow separation from a smooth surface. Standard two-equation turbulence models often fail to predict the onset and the amount of flow separation under adverse pressure gradient conditions. Turbulent flows are significantly affected by the presence of walls. Obviously, the mean velocity field is affected through the no-slip condition that has to be satisfied at the wall. However, the turbulence is also affected by the packing geometry.

The k-e turbulent models are primarily valid for turbulent bulk flows and care has to be taken for wall-bounded flows. In respect to this Fluent provides both the wall function and the near-wall modelling approach. Enhanced wall treatment is a near-wall modelling method that combines a two-layer turbulent model with enhanced wall functions. If the near-wall mesh is fine enough to be able to resolve the laminar sub-layer, then the enhanced wall treatment will be identical to the traditional two-layer model. This can be done through adoption the cells near the walls (see also [1]). In respect to Ansys CFX, the most prominent two-equation models in this area are the k-? based models of [71]. The k-? based Shear Stress Transport (sst) model of is recommended for high accuracy boundary layer simulations. The superior performance of this model has been demonstrated in a large number of validation studies [72].

7.1 Domain and the Turbulent Models

For the pressure drop CFD simulations with flat and corrugated plates a grid has to be selected which can represent the real packing block. The grid shown in Fig. (7-1A) for the wavy plates was chosen and a similar grid is in Fig. (7-1B) for flat plates. It is the minimal representative volume of the real packing. Every pair of parallel surfaces was defined as a periodic surface. The flow direction was set along the element with a mass flow rate equivalent to the values of the F-factor. For this complex geometry tetrahedral cells were chosen.

Different CFD simulations were performed for Rombopak 4M and 9M at different gas loads represented by F-factors (Tab. (7-1)). The rke (realizable k-e) turbulent model with ewt

(enhanced wall treatment) in Fluent was used [1]. And the k?-sst turbulent model implemented in Ansys CFX was selected for the simulated cases with this code. The grid for Ansys CFX simulations was created with Ansys ICEM 10. Additional CFD simulations were done for comparison.

The pinch, where the lamellas intersect is a critical region. Beside the gas flow the down moving liquid is redistributed between the front and back side of the lamella. This bench was embedded in different ways in the simplified 9M element with flat plates in different shapes as shown in Fig. (7-2).

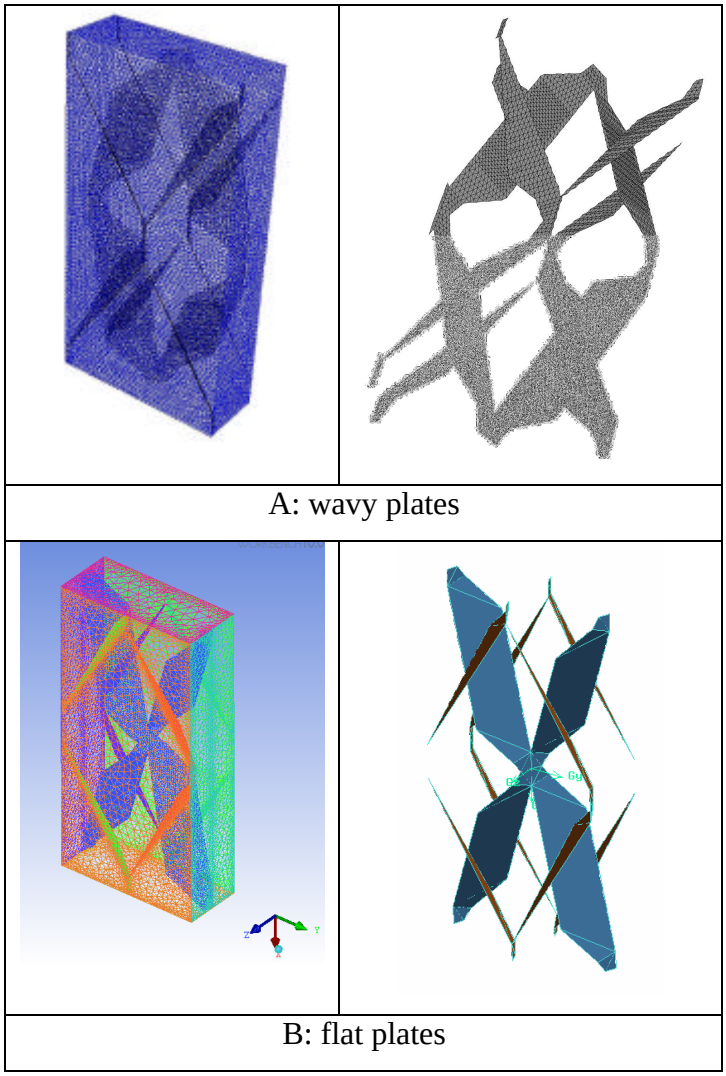

A: wavy plates

B: flat plates

Figure (7-1): Grid for pressure drop CFD simulations

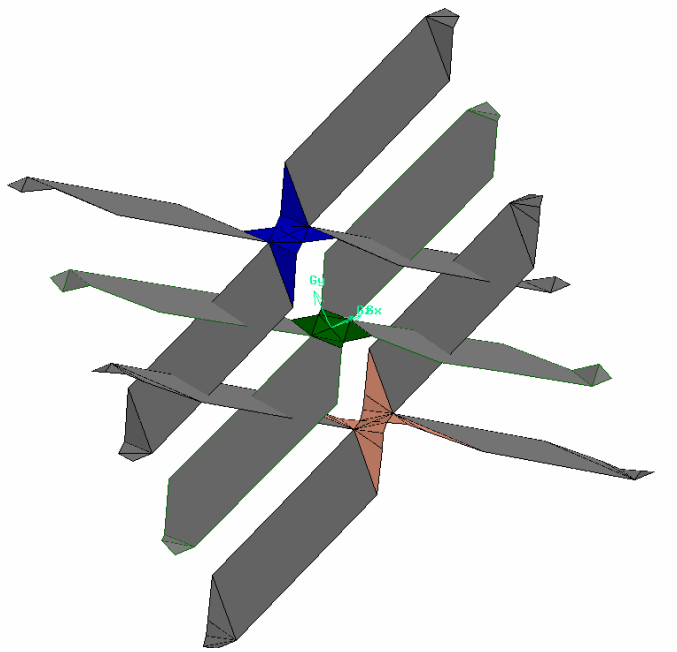

Figure (7-2): Different grid embedding of the central node, top (geometry 3), middle (geometry 5) and bottom (geometry 4),

7.2 CFD Simulations and Experiments

Fig. (7-3) shows the streamlines coloured with the velocity values for the simulated case Sim 6 (s. Table (7-1)). Fig. (7-4) shows the pressure contours on the plates for the simulation with Fluent (sim6) and Ansys CFX 10 (Sim9). The spots with high pressure values represent the positions with the highest pressure loss. This pressure mapping helps to find solutions and initialize ideas to develop or optimize packing structures. Both simulations have delivered similar static pressure distribution on the plates. The absolute values difference comes from the difference in the position of reference pressure.

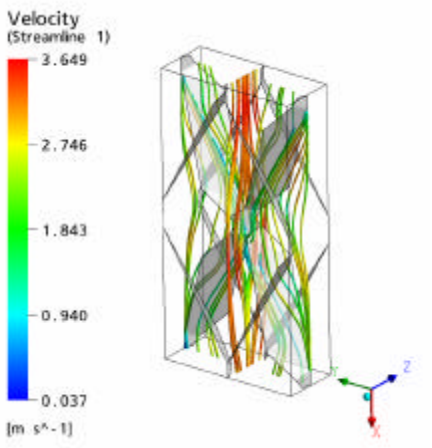

Figure (7-3): Streamlines in two central planes at the mean positions of z and y.

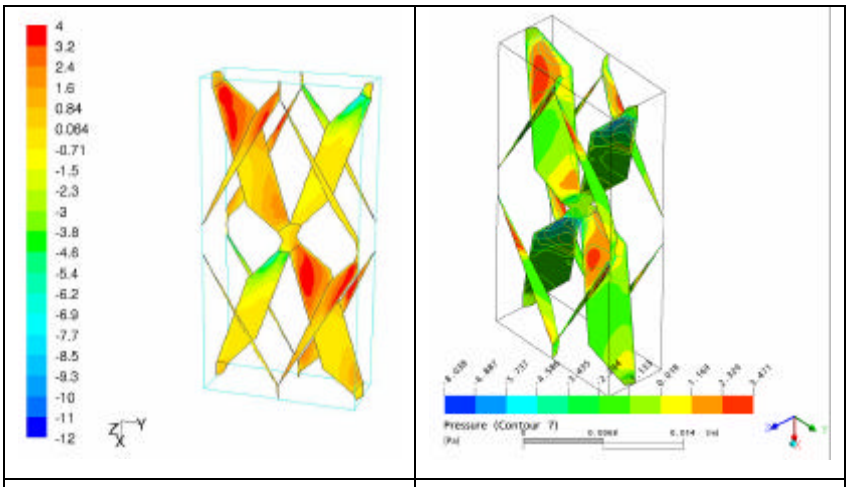

Fluent 6.2, (Sim6)	Ansys CFX 10, (Sim 9)

Figure (7-4): Static pressure drop distribution on the plates.

The pinch, where the lamellas intersect is a critical region. Beside the gas flow the down moving liquid is redistributed between the front and back side of the lamella. The fine structure for the fine 9M packing is very sensitive and small changes in embedding this region in the CFD grid (flat plates, Sim6 and 14) gave drastically changes of about 20% in the pressure drop (rke-ewt, Fluent).

For the fine packing 9M, the CFD pressure drop is about 40% to higher than the experiment and this difference increases to 40% with the gas load (Sim5 to Sim7). Performing the CFD simulation using the Ansys CFX have given values, which are about 15 to 25% (Sim8 to Sim10) less than that of Fluent (Sim5 to Sim7) and thus, they are more closer to the experimental results. The fine structure for the fine 9M packing is very sensitive and small changes in embedding this region in the CFD grid (Sim6, Sim14 and 15) gave drastically changes of about 20% in the pressure drop (Figure (7-2)). Repeating the CFD simulation for one case (Sim6) with very fine grid (about 1 million cells, Sim16) to achieve $y^+<4$ without cells adaption in the other cases including Sim6 has not changed the result. Furthermore, the last simulation was repeated with CFX setting the flow as laminar. The pressure drop value was about the same as in the turbulent case (Sim6 and Sim18). The CFD simulations with Fluent for the structured element were the nearest to the experiments (Sim 11 to Sim13). Setting the k-? based Shear Stress Transport (sst) as turbulent model did not change the result (Sim17).

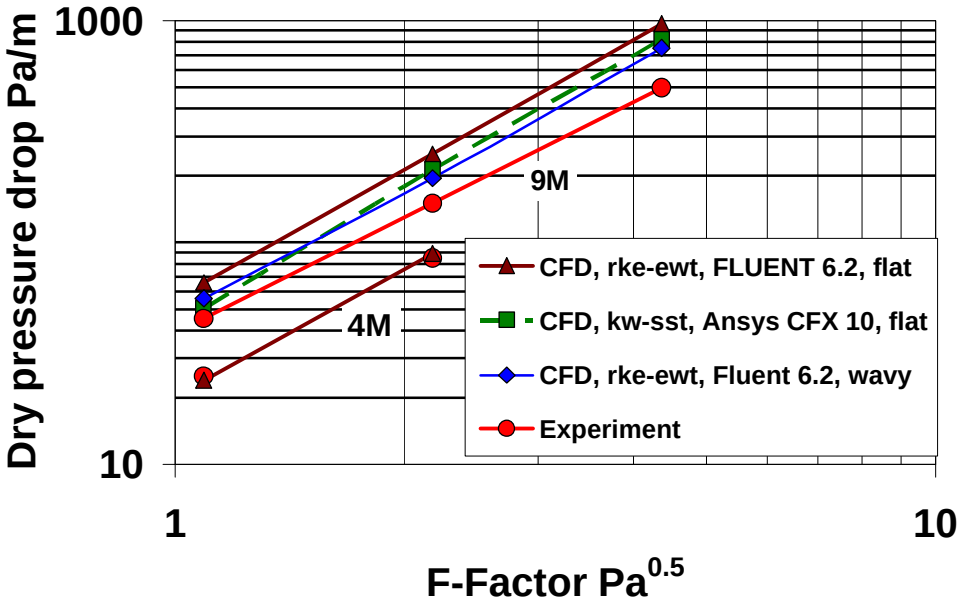

Figure (7-5): CFD simulation results for Rombopak 4M and 9M

Table (7-1): Dry pressure drop CFD-simulation results

	Rombopak	F-factor	plates	turb. Model[a]	exp. Dp	CFD Dp	remarks
		$Pa^{0.5}$			Pa/m	Pa/m	
Sim1	4M	1.09	flat	Fluent, rke-ewt	25	23.95	geometry 1
Sim2	4M	2.18	flat	Fluent, rke-ewt	85	88.9	geometry 1
Sim3	4M	1.09	wavy	Fluent, rke-ewt	25	24.97	geometry 2
Sim4	4M	2.18	wavy	Fluent, rke-ewt	85	92.86	geometry 2
Sim5	9M	1.09	flat	Fluent, rke-ewt	45.25	66	geometry 3
Sim6	9M	2.18	flat	Fluent, rke-ewt	150.16	250	geometry 3
Sim7	9M	4.36	flat	Fluent, rke-ewt	498.32	967	geometry 3
Sim8	9M	1.09	flat	CFX, kw-sst	45.25	50.2	geometry 3
Sim9	9M	2.18	flat	CFX, kw-sst	150.16	212.7	geometry 3
Sim10	9M	4.36	flat	CFX, kw-sst	498.32	820.9	geometry 3
Sim11	9M	1.09	wavy	Fluent, rke-ewt	45.25	55.96	geometry 2
Sim12	9M	2.18	wavy	Fluent, rke-ewt	150.16	194.68	geometry 2
Sim13	9M	4.36	wavy	Fluent, rke-ewt	498.32	750.49	geometry 2
Sim14	9M	2.18	flat	Fluent, rke-ewt	150.16	237.44	geometry 4
Sim15	9M	2.18	flat	Fluent, rke-ewt	150.16	208.76	geometry 5
Sim16	9M	2.18	flat	Fluent, rke-ewt	150.16	249.7	geometry 3
Sim17	9M	2.18	flat	Fluent, kw-sst	150.16	251	geometry 3
Sim18	9M	2.18	flat	CFX, laminar	150.16	212.1	geometry 3

[a] rke: Realizable k-e model, ewt: Enhanced wall treatment, kw-sst: The k-? based Shear-Stress-Transport (sst)

For the coarse 4M packing the surface structure is negligible, when comparing the cases for corrugated plates (Sim 3 and 4) with that for flat single element (Sim 1 and 2). The dry pressure drop simulations for structured 4M were found in good agreement with the experimental data with an error less than 10%. (Tab. (7-1) Sim 1 to 4). In Fig. (7-5) the experimental and CFD simulation results for dry pressure drop are presented as a function of the F-factor for Rombopak 4M and 9M.

Chapter 8

Conclusions and Outlook

The wetting of solid surfaces was evaluated in this work experimentally and with the CFD methods using the multiphase flow VOF model.

Initially rivulet flow profiles were estimated experimentally on an inclined plate by a needle fixed on a movable step motor in the three space directions assisted optically with a CCD camera and frame grabber. Liquid flow rate range between 10 and 80 ml/min was chosen. The measured rivulet profiles on an inclined flat plate were compared to that of the CFD – simulations with the VOF model of FLUENT and with different models from the literature. In this comparison the two main parameters of the rivulet, maximum thickness and width have been analyzed. The comparison has shown very good agreement between the experiments and CFD results. The analytical model of Towell & Rothfeld [3] has given profiles similar to that of the experiments. The experiments and CFD simulations using two different grids have shown that, for a constant flow rate the inlet cross sectional area at the top of the plate has no effect on the rivulet profile shape and spreading in the studied laminar case.

The rivulet profiles on the wavy plate were found similar to that of the flat plate case from the measurements and CFD results. However, there are some deviations when using the simplified model of Towell & Rothfeld [3] derived for flat plates [24]. It was also found that the rivulet on the wavy plate has no linear borderlines. At the crest, it constricts and in the dell it extends. In addition to that the interface was found to be also wavy with similar wave length of the corrugation but lower amplitude. As a result of the shrinkage and expansion, the liquid flows more slowly on the wavy plat than on a flat one and has higher interfacial area.

After this preliminary work for validating the experimental set-up and the CFD code the hydrodynamics within structured packings was investigated. Wetting of the structured packing element was compared qualitatively with experimental results from snap shoots of the flow pattern and quantitavely by measuring the wetted area optically. The flow patterns resulting from the VOF model were found very similar to that of the experiments in the way of wetting, liquid distribution at the nodes of the packing sheet and liquid bridge building under the nodes. The studied liquid flow range has shown no dropwise flow pattern on the lamella, but bridges and liquid bifurcation were observed.

It was found that the different correlations for prediction of the hydrodynamics of packed columns are not universally applicable and are dependent on the packing types. The CFD simulation results on a single packing element at different liquid properties and liquid loads

have been exploited to derive or modify correlations from the literature to describe the degree of wetting, specific interfacial area and liquid hold-up with Rombopak 4M with an error less than 20%. It could be shown that, the correlations derived are also valid for a multi-element packing sheet with a deviation of about 10%.

We have successfully used the CFD methods to simulate the flow in real packing elements, but it can be exploited for optimization and design purposes. An optimization of a geometry via the CFD tools saves money and costs of the experiments needed for such study.

CFD simulations for the turbulent gas flow inside a packing element to estimate the dry pressure drop were additionally performed. The structural effects on the dry pressure drop have been discussed. It was found that for coarse geometries (4M) the CFD simulations of dry pressure drop derived from plain lamellas were found in good agreement with the experiments. For fine textures, this is more critical and it is important to correctly embed the structure in the CFD domain.

Describing the liquid flow inside the packing is still a big challenge and simplification of the problem when analyzing basic elements of the packing have shown a big benefit to reveal partially the flow structure. Simulating the flow in a complete packed column is still the challenge for the future to the high CPU time involved. Nevertheless, CFD simulation of the flow in a small packing block is in spite of that possible and recommended.

As could be shown, CFD methods offer the potential to reveal the detailed flow structure of gas and liquid flow in complex packing geometries. This can be applied to the optimization of packing geometries after revealing the critical details to be improved.

It could be proven that the liquid inlet area does affect the profile shape but it may affect the velocity profiles inside the rivulet. Measuring the velocity profiles inside the liquid rivulets on the plate and the packing element is still difficult and more work is needed in respect to this.

Further developments are also feasible with new software releases. FLUENT 6.3 should have a new feature which enables the user to define the contact angle via user defined function (udf), when using the VOF model to simulate the stratified flow. Such a feature is vital for describing the wetting problem not only in the packing but also in many other applications.

CFD simulation on a block of the packing gives a more realistic picture but it is very CPU time expensive. Heat and mass transfer can be simulated with the VOF model and this demands more experimental and CFD work.

Implementation of the complex packing geometries and adaption of the mesh is a big challenge in the CFD simulation work. To simplify this, the development of a graphical

structured packing interface (GraSPI) and integrating it into GAMBIT was started by a team of engineers as reported in the magazine FLUENT news [73].

Symbols used

A	[m^2]	Area
A_{sec}	[m^2]	Cross section area of the column
A_r	[m^2]	Rivulet cross section area
a	[m^2/m^3]	Specific packing surface area (Rombopak 4M 165 m^2/m^3)
a_h	[m^2/m^3]	Wetted surface area per unit volume
a_{ph}	[m^2/m^3]	Hydraulic surface area per unit volume
F-factor	[$Pa^{0.5}$]	F-factor
g	[m/s^2]	Gravity
h_L	[m^3/m^3]	Liquid hold-up
L_L	[m^3/ m^2h]	Liquid load in packed column
p	[N/m^2]	Pressure
Q	[ml/min]	Flow rate per packing element
Q_r	[ml/min]	Rivulet liquid flow rate
R	[m]	Radius
S	[m]	Element maximum plate width
$u_{r,mean}$	[m/s]	Mean liquid velocity of a rivulet flow
$u_{r,max}$	[m/s]	Maximum liquid velocity of a rivulet flow
u_L	[m/sm^2]	Liquid superficial velocity
V	[m^3]	Volume
w	[m/s]	Velocity
w_r	[m]	Rivulet width
x, y, z	[m]	Space coordinates

Greek Symbols

a	[°]	Plate inclination to the vertical
ß	[°]	Plate inclination to the horizontal
d_r	[m]	Rivulet maximum thickness
e	[m^3/m^3]	Packing porosity
?	[°]	Contact angle
μ_L	[kg m/s]	Liquid dynamic viscosity
?	[m^2/s]	Kinematical viscosity
$?_g$	[kg/m^3]	Gas density
$?_L$	[kg/m^3]	Liquid density
s_L *or* s	[N/m]	Surface tension between liquid and vapour or gas
s_{Ld}	[N/m]	Liquid dispersion component of the surface tension
s_{Lp}	[N/m]	Liquid polar component of the surface tension
s_S	[N/m]	Surface tension solid and vapour
s_{Sd}	[N/m]	Solid dispersion component of the surface tension
s_{SL}	[N/m]	Surface tension between solid and liquid
s_{Sp}	[N/m]	Solid polar component of the surface tension
?	[°]	Packing plate inclination

Dimensionless numbers

Fr_L	$\frac{u_L^{\,2} a}{g}$	Packing models Froud number
Re_L	$\frac{r_L u_L}{m_L a}$	Packing models Reynolds number

Re_r	$\frac{r_L u_{r,mean} d_r}{m_L}$	Rivulet Reynolds number
$V_{r,max}$	$\frac{u_{r,\max} m_L}{r_L g d_r^{\,2}}$	Rivulet dimensionless maximum velocity
$V_{r,mean}$	$\frac{u_{r,mean} m_L}{r_L g d_r^{\,2}}$	Rivulet dimensionless mean velocity
We_L	$\frac{u_L^{\,2} r_L}{as}$	Packing models Weber number

Subscripts

Cr	Critical
eff.	Effective
h	Hydraulic (wetted)
i	Internal
L	Liquid
La	Lamella
Ld	Liquid, dispersive
Lp	Liquid, Polar
o	Outer
ph	Interfacial
S	Solid

Abbreviations

1-D	One Dimensional
3-D	Three Dimensional
CFD	Computational Fluid Dynamics
FPE	Flat Packing Element
MPIV	Micro Particle Image Velocimetry
MSRDE	Mean Square Relative Error $\sqrt{\sum_1^N \frac{1}{N}\left(\frac{X_{CFD}-X}{X_{CFD}}\right)^2}$
PS	Packing Sheet
PTV	Particle Tracer Velocimetry
SPE	Structured Packing Elment
VOF	Volume of Fluid
rke-ewt	Realizable k-e model with Enhanced wall treatment
	k is the turbulent kinetic energy, *e* is here the turbulence dissipation rate
kw-sst	The *k-?* based Shear-Stress-Transport
	? is the turbulent frequency

Literature

[1] *FLUENT 6.2 User's Guide.* **2005**, *Fluent Inc: Lebanon, NH 03766.*

[2] **Duffy, B.R., Moffatt, H.L.**,
Flow of a visous fluid on a slowly varying incline,
The Chem. Eng. J., 60, **1995**, 141-146.

[3] **Towell, G.D., Rothfeld, L.B.**,
Hydrodynamics of rivulet flow,
A.I.Ch.E Journal, 12 (5), **1966**, 972-980.

[4] **Al-Khalil, K.M., Keith JR., T.G., De Wett, K.J.**,
Hydrodynamics and thermal analysis of rivulet flow down a vertical solid surface,
Int. J. Num. Methods Heat Fluid Flow, 1, **1991**, 63-76.

[5] **Allen, R.F., Biggin, C.M.**,
Longtudinal flow of a reticular liquid filament down an inclined plane,
The Physics of Fluids, 17 (2), **1973**, 287-291.

[6] **Billet, R., Schultes, M.**,
Prediction of mass transfer columns with dumped and arranged packins: Update summery of the calculaation method of Billet and Schultes,
Trans IChemE Part A, 77 (Sep.), **1999**, 498-504.

[7] **Gualito, J.J., Cerino, J.C., Cardenas, J.C., Rocha, J.A.**,
Design method for distillation columns filled with metallic, ceramic, or plastic stuctured packings,
Ind. Eng. Chem. Res., 36 (5), **1997**, 1747-1757.

[8] **Rocha, J.A., Bravo, J.L., Fair, J.R.**,
Distillation columns containing structured packings: A comprehensive model for their performance. 1. Hydraulic models,
Ind. Eng. Chem. Res., 32, **1993**, 641-651.

[9] **Rocha, J.A., Bravo, J.L., Fair, J.R.**,
Distillation columns containing structured packings: A comprehensive model for their performance. 2. Mass transfer model,
Ind. Eng. Chem. Res., 35, **1996**, 1660-1667.

[10] **Shi, M.G., Mersmann, A.**,
Effective interfacial area in packed columns,
Ger. Chem. Eng., 8, **1985**, 87-96.

[11] **Fischer, L., Bühlmann, U., Milcher, R.**,
Charecterization of high-performance structured packing,
Trans IChemE, Part A, 81 (January), **2003**, 79-84.

[12] **Shetty, S., Cerro, R.L.**,
Fundamental liquid flow correlations for the computation of design parameters for ordered packings,
Ind. Eng. Chem Res., 36, **1997**, 771-783.

[13] **Zhao, L.**,
Liquid film flows over complex geometry,
Dissertation, Tulsa, **1991**.

[14] **Zhao, L., Cerro, R.L.**,
Experimental characterization of viscous film flows over complex surfaces,
Int. J. Multiphase Flow, 18 (4), **1992**, 495-516.

[15] **Kern, J.**,
Untersuchungen über die Hydrodynamik der Rinnsale,
Dissertation, Berlin, **1969**.

[16] **Kern, J.**,
Zur Hydrodynamik der Rinnsale,
Verfahrenstechnik, 10 (3), **1969**, 425-430.

[17] **Schmuki, P., Laso, M.**,
On the stability of rivulet flow,
J. Fluid Mech., 215, **1990**, 125-143

[18] **Shi, M.G., Mersmann, A.**,
Effektive Austauschfläche in Füllkörperkolonnen,
Chem. Ing. Tech., 5, **1984**, 404-405.

[19] **Bentwich, M., Glasser, D., Kern, J., Williams, D.**,
Analysis of rectlinear rivulet flow,
AIChE J., 22 (4), **1976**, 772-779.

[20] **Stein, W.A.**,
Benetzung überströmter Feststoffe,
VDI, Verfahrenstechnik, Nr. 752, Düsseldorf, **2002**.

[21] **Doniec, A.**,
Laminar flow of a liquid rivulet down a vertical solid surface,
The Can. J. Chem. Eng., 69, **1991**, 198-202.

[22] **Shetty, S., Cerro, R.L.**,
Spreading of a liquid point ssource over a complex surface,
Ind. Eng. Chem Res., 37, **1998**, 626-635.

[23] **Shetty, S., Cerro, R.L.**,
Flow of a thin film flow over a periodic surface,
Int. J. Multiphase Flow, 19 (6), **1993**, 1013-1027.

[24] **Bontozoglou, V., Papapolymerou, G.**,
Laminar film flow down a wavy incline,
Int. J. Multiphase Flow, 23 (1), **1997**, 69-79.

[25] **Ausner, I., Kallweit, S., Wozny, G.**,
Velocity measurements of film flow on inclined steel plates
6th International Symposium on Particle Image Velocimetry, Passadena, California, USA, **2005.**

[26] **Ausner, I., Hoffmann, A., Repke, J.-U., Wozny, G.**,
Two-liquid phase film flow over inclined plates
7th World Congress of Chemical Engineering, Glasgow, Scotland, **2005.**

[27] **Ausner, I., Hoffmann, A., Repke, J.-U., Wozny, G.**,
Experimentelle und numerische Untersuchungen mehrphasiger Filmströmungen,
Chem. Ing. Tech., 77 (6), **2005**, 735-741.

[28] **Trifonov, Y.Y.**,
Viscous liquid film flows over a periodic surface,
Int. J. Multiphase Flow, 24, **1998**, 1139-1161.

[29] **Adomeit, P.L., A., Renz, u.**,
Experimental and numerical investigations on wavy films
3rd European Thermal Sciences Conference, Piza, **2000,** Edizioni ETS, 1003-1009.

[30] **Billet, R.**,
Packed Towers in Processing and Environemental Technology,
VCH, **1995**.

[31] **Olujic, Z.**,
Effect of column diameter on pressure drop of a corrugated sheet structured packing,
Trans IChemE Part A, 77 (Sep.), **1999**, 505-510.

[32] **Olujic, Z., Kamerbeek, A.B., de Graauw de, J.**,
A currugation geometry based model for efficiency of structured distillation packing,
Chem. Eng. and Proc., 38, **1999**, 683-695.

[33] **Olujic, Z.**,
Structured Packing Performances -Experimental Evaluation of Two Predictive Models,
Ind. Eng. Chem Res., 39, **2000**, 1788-1796.

[34] **Onda, K., Takeuchi, H., Okumoto, Y.**,
Mass transfer coefficient between gas and liquid phases in packed columns,
J. Chem. Eng. Jap., 1 (1), **1968**, 56-62.

[35] **Battista, J., Böhm, U.**,
Mass transfer in trickle-bed rectors with structured packing,
Chem. Eng. Technol., 26 (10), **2003**, 1061-1067.

[36] **Hirt, C.W., Nichols, B.D.**,
Volume of fluid (VOF) method for the dynamics of free boundaries,
J. Comput. Phys., 39, **1981**, 201-225.

[37] **Ranade, V.V.**,
Computational fluid modeling for chemical reactor engineering,
Academic Press, **2002**.

[38] **Casey, M., Lang, E., Mack, R., Schengel, R., Wehrli, M.**,
Applications of computational fluid dynamics for process engineering at Sulzer,
Speedup J., 12 (1), **1998**, 43-51.

[39] **Hoffmann, A., Ausner, I., Repke, J.-U., Wozny, G.**,
Aufreißende Filmströmung auf geneigten Oberflächen,
Chem. Ing. Tech., 75 (8), **2004**, 1065-1068.

[40] **Hoffmann, A., Ausner, I., Repke, J.-U., Wozny, G.**,
Fluid dynamics in multiphase distillation processes in packed towers,
Comput. Chem. Eng., 29, **2005**, 1433-1437.

[41] **Valluri, P., Matar, O.M., Hewitt, G., Mendes, M.A.**,
Thin film over structured packings at moderate Reynolds numbers,
Chem. Eng. Sci., 60, **2005**, 1965-1975.

[42] **Raynal, L., Boyer, C., Ballaguet, J.-P.**,
Liquid holdup and pressure drop determination in structured packing with CFD simulations,
Can. J. Chem. Eng., 82 (Aug.), **2004**, 871-879.

[43] **Bühlmann, U.**,
Rombopak, ein neuer geordneter Packungskörper für Stoffaustauschkolonnen,
Chem.-Ing.-Tech., 55 (5), **1983**, 379-381.

[44] **Young, T.**,
An essay on the cohesion of fluids,
Philos. Trans. R. Soc., 95, **1805**, 65-87.

[45] **De Gennes, P.G.**,
Wetting: Statics and dynamics,
Reviews of Modern Physics, 57 (3, Part 1), **1985**, 827-863.

[46] *Ullmann's encyclopedia of industrial chemistry.* **2005**, *John Wiley & Sons, Inc Wiley-VCH & Co. KGaA, Weinheim.*

[47] **Padday, F.J.**,
Spreading, wetting, and contact angles, **1993**, 97-108.

[48] **Palzer, S., Hiebl, C., Sommer, K., Lechner, H.**,
Einfluss der Rauhigkeit einer Feststoffoberfläche auf den Kontaktwinkel,
Chem. Ing. Tech., 73, **2001**, 1032-1038.

[49] **Fox, H.W., Zisman, W.A.**,
The spreading of liquids on low-energy surfaces. I. Polytetrafluoroethylene,
J. Colloid Sci., 5, **1950**, 514-531.

[50] **Owens, D.K., Wendt, R.C.**,
Estimation of the surface free energy of polymers,
J. App. Sci., 13 (8), **1969**, 1741-1747.

[51] **Alekseenko, S.V., Aktershev, S.P., Markovich, D.M.**,
Wavy flow of liquid films and rivulets moving under the effect of gravity and gas stream,
Conference on Transport Phenomena with Moving Boundaries, Berlin, Germany, **2001,** Reihe 3, Nr.738, 107-121.

[52] **Fulford, G.D.**,
The flow of liquids in thin films,
Adv. Chem. Eng., 5, **1964**, 151-229.

[53] **Oron, A.D., S. H.; Bankoff, S. G.**,
Long-scale evaluation of thin liquid films,
Reviews of Modern Physics, 69 (3), **1997**, 931-980.

[54] **Ruyer-Quil, C., Manneville, P.**,
Modelling of film flows down inclined planes,
Eur. Phys. J. B, 6, **1998**, 277-292.

[55] **Stein, W.A.**,
Der statische Flüssigkeitsanteil in Packungskolnnen,
Springer-Verlag 2000, 66, **2000**, 129-137.

[56] **Kuhnert, J., Tiwari, S.,**
A particle method for simulation of free surface flows.
9th International Conf. on Hyperbolic Problems, Springer Verlag, **2003**, Pasadena, 889-898.

[57] **Kuhnert, J., Tiwari, S.,**
A meshfree method for incompressible fluid flows with incorporated surface tension,
"Meshfree and praticle based approaches in computational mechanics"
Revue européenne des éléments finis, **2002**, Vol.11, N° 7-8.

[58] **Brackbill, J.U., Kothe, D.B., Zemach, C.**,
A continuum method for modeling surface tension,
J. Comput. Phys., 100, **1992**, 335-354.

[59] **Johnson, M.F.G., Schluter, R.A., Bankoff, S.G.**,
Fluorescent imaging system for global measurement of liquid film flow thickness and dynamic contact angle in free surface flow,
Rev. Sei. Instrum., 68 (11), **1997**, 4097-4102.

[60] **Johnson, M.F.G., Schluter, R.A., Miksis, M.J., Bankoff, S.G.**,
Experimental study of rivulet formation on an inclined plate by fluorescent imaging,
J. Fluid Mech., 394, **1999**, 339-354.

[61] **Liu, J., Paul, J.D., Gollub, J.P.**,
Measurements of the primary instabilities of film flows,
J. Fluid Mech., 250, **1993**, 69-101.

[62] **Zhang, J.T.W., B. X.; Peng, X. F.**,
Falling film thickess measurement by optical-electronic method,
Rev. Sci. Instrum., 71 (4), **1999**, 1883-1886.

[63] **Ataki, A., Bart, H.-J.**,
Experimental study of rivulet liquid flow on an inclined plate
Int. Conf. on Adsorption and Distillation, 634th Event of the European Federation of Chemical Engineering, Baden-Baden, Germany, **2002**
VDI-GVC (ed.) 3-931384-37-3, Düsseldorf.

[64] **Ausner, *G.*, *W.***,
Analyzing the velocity field of multiphase film flow
3ed Int. Symp. on Two-phase Flow Modelling and Experimentations, Piza, Italien, **2004.**

[65] **Jiang, Y., Khadilkar, M.R., Al-Dahhan, M.H., Dudukovic, M.P.**,
CFD of multiphase flow in packed bed reactors: I. k-Fluid modeling issues,
AIChE J., 48 (4), **2002**, 701-715.

[66] **Ataki, A., Bart, H.-J.**,
The use of the VOF-model to study the wetting of solid surfaces,
Chem. Eng. and Technol., 27 (10), **2004**, 1109-1114.

[67] **Ataki, A., Bart, H.-J.**,
Experimental and CFD simulation study for the wetting of a structured packing element with liquids,
Chem. Eng. Technol., 29 (3), **2006**, 363-347.

[68] **Zech, J.B.**,
Flüssigkeitsströmung und Stoffaustausch in berieselten Füllkörperschüttungen,
Dissertation, München, **1978**.

[69] **Nicolaiewsky, A.E.M., Tavares, F.W., Rojagopal, K., Fair, J.R.**,
Liquid film flow and area in structured packed columns,
Powder Technology, 104, **1999**, 84-94.

[70] **Last, W.P.,**
Absorption mit überlagerter chemischer Reaktion in Packungskolonnen bei Drücken bis 50 bar,
Reihe 3, Verfahrenstechnik, VDI-Verlag Düsseldorf, **1999**.

[71] **Grotjans, H., Menter, F.R.**,
Wall functions for general application CFD codes
ECCOMAS 98 Proceedings of the Fourth European Computational Fluid Dynamics Conference, **1998,** John Wiley & Sons, 1112-1117.

[72] **Bardina, J.E., Huang, P.G., Coakley, T.J.,**
Turbulence modeling validation testing and development,
NASA Technical Memorandum 110446, **1997**.

[73] **De Almeida, V., Ridge, O., Khan, R., Schwalter, D.**,
Realistic distillation modeling,
Fluent News, XIII, Spring 2004 (1), **2004**, 30.

Appendixes

10.1 Appendix A

10.1.1 A1: Experimental set-up for the inclined plate

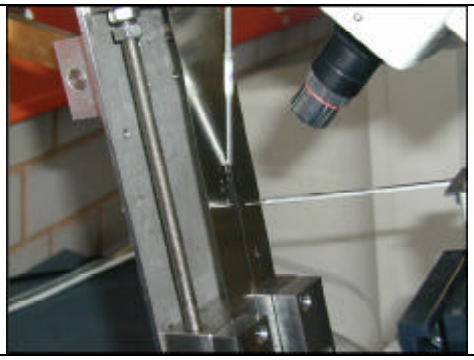

CCD camera, flat plate and the needle

Set-up

Rivulet flow on a wavy plate, needle

Pump and flow control pannel

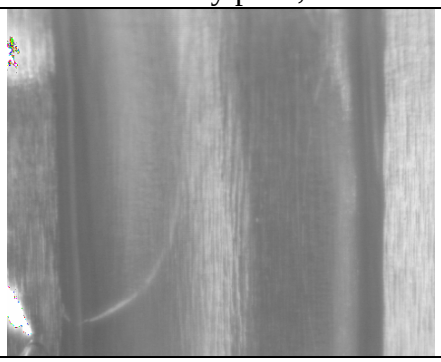

Zoomed rivulet flow on flat plate

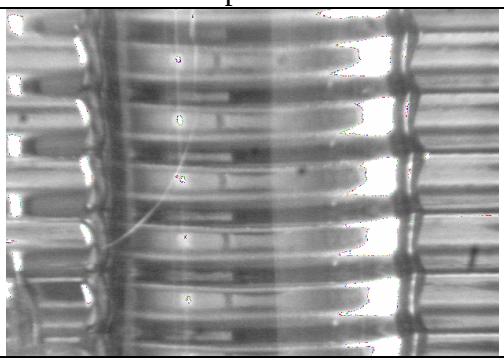

Zoomed rivulet flow on wavy plate

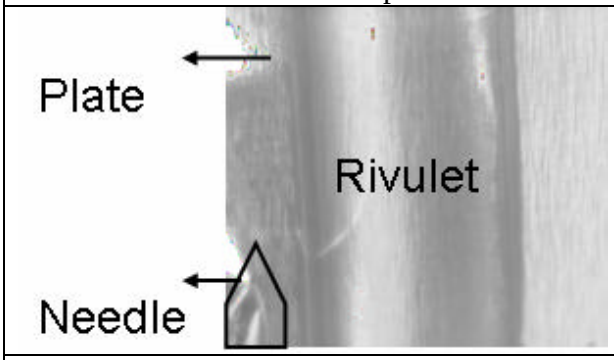

Needle position on the left hand side

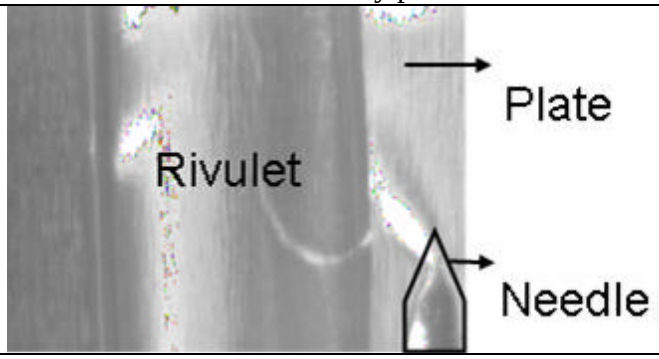

Needle position on the right hand side

10.1.2 A2: Experimental set-up for the SPE & PS

	
Liquid distributor and the packing sheet	Experimental set-up for the packing wetting
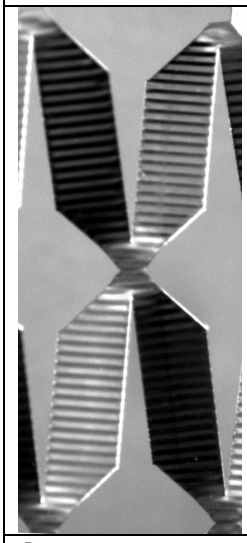	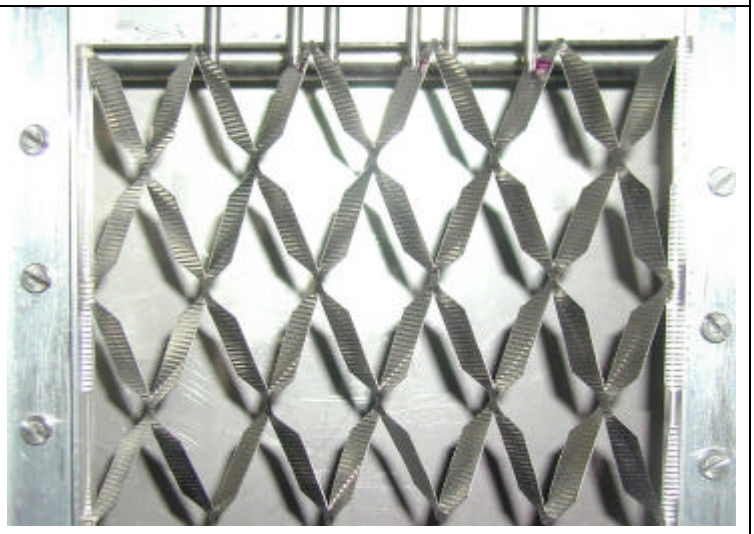
SPE	PS and fixing method

10.1.3 A3: Experimental flow patterns on SPE & PS vs. CFD

10.1.3.1 A3-1: Glycerine-water 50%

<table>
<tr><td> 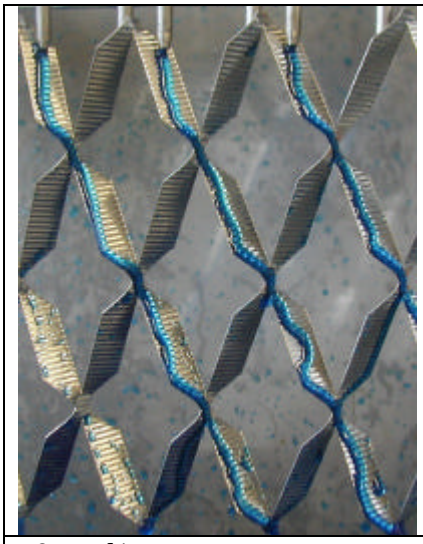 </td><td> 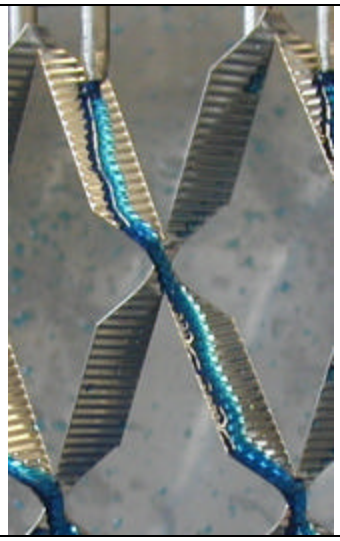 </td><td></td></tr>
<tr><td>20.5 ml/min</td><td></td><td></td></tr>
<tr><td>  </td><td> 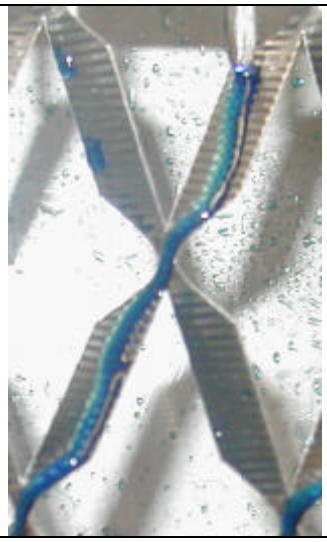 </td><td> 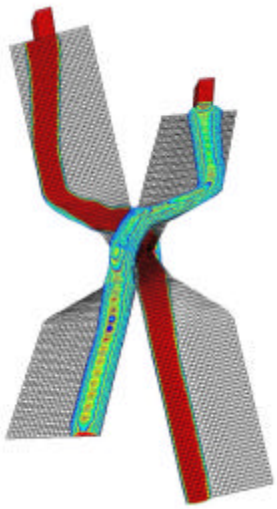 </td></tr>
<tr><td colspan="2">F6
40 ml/min</td><td>F6
41.8 ml/min</td></tr>
<tr><td> 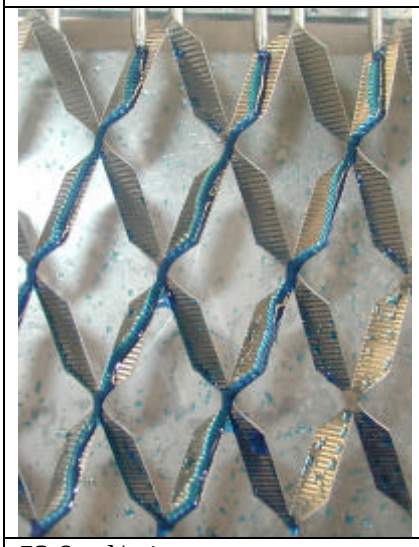 </td><td> 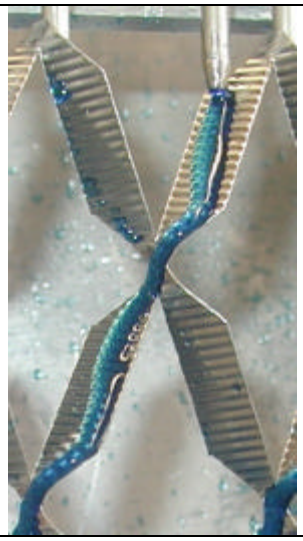 </td><td></td></tr>
<tr><td colspan="2">53.8 ml/min</td><td></td></tr>
</table>

10.1.3.2 A3-2: Glycerine-water 50% with surfactant

<table>
<tr><td colspan="2"> 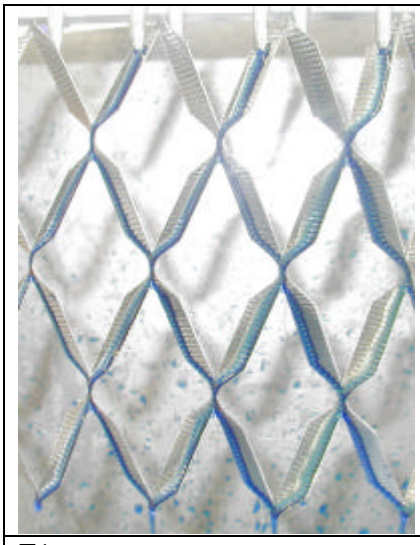  </td><td> 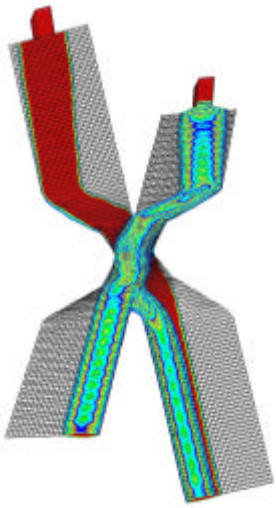 </td></tr>
<tr><td colspan="2">F1
15.7 ml/min</td><td>F1
20.9 ml/min</td></tr>
<tr><td colspan="2"> 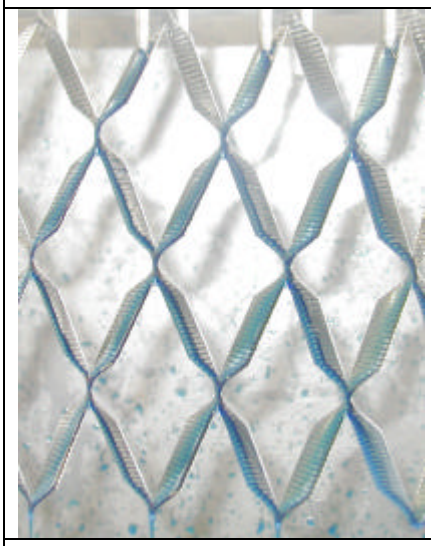 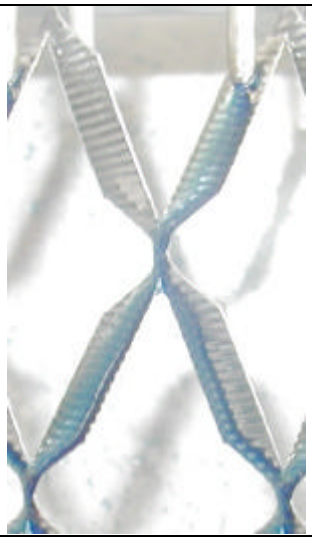 </td><td> 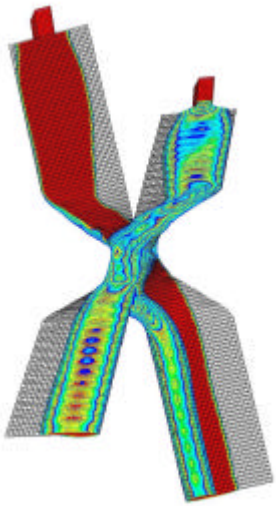 </td></tr>
<tr><td colspan="2">F2
40 ml/min</td><td>F2
41.6 ml/min</td></tr>
<tr><td colspan="2"> 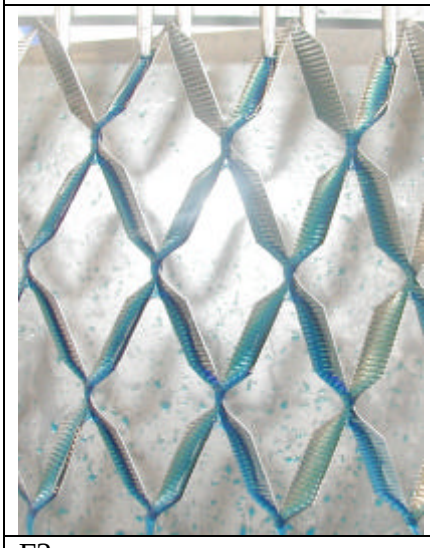 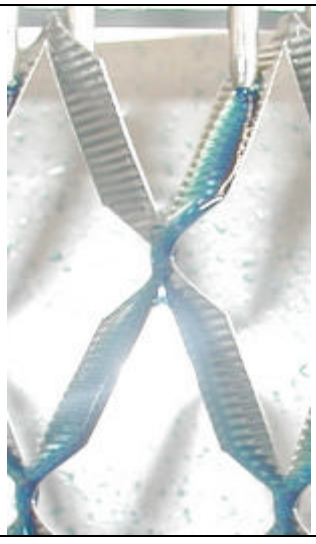 </td><td> 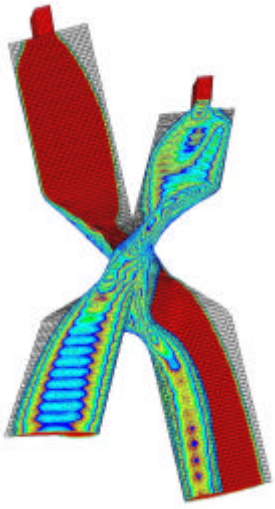 </td></tr>
<tr><td colspan="2">F3
110.5 ml/min</td><td>F3
83.6 ml/min</td></tr>
</table>

10.1.3.3 A3-3: Chlorbenzene–ethylbenzene 50% wt.%

<table>
<tr><td>  </td><td> 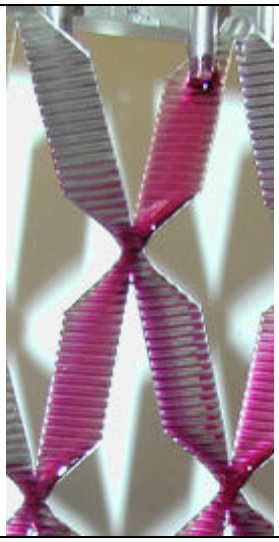 </td><td rowspan="3"></td></tr>
<tr><td colspan="2">16.9 ml/min</td></tr>
<tr><td> 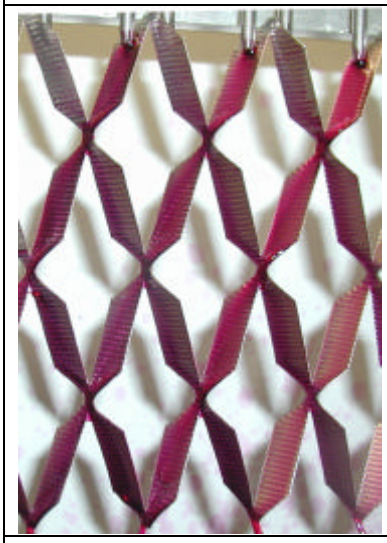 </td><td>  </td></tr>
<tr><td colspan="2">28.6 ml/min</td><td rowspan="2"></td></tr>
<tr><td> 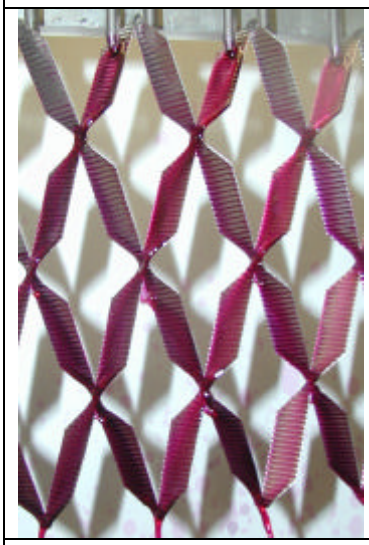 </td><td>  </td></tr>
<tr><td colspan="2">F10
44.3 ml/min</td><td>F10
41.8 ml/min</td></tr>
</table>

10.1.3.4 A3-4: Chlorbenzene – ethylbenzene 50% with 10 mm distance away from the plates surface

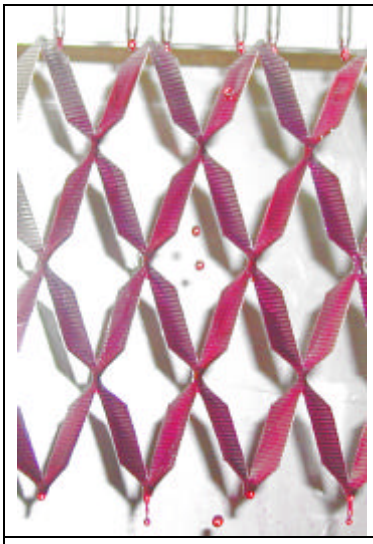	
16.9 ml/min	

10.2 Appendix B

10.2.1 B1: Rivulet profiles for dist. water (liquid system 1) on flat inclined plate (ß=68.5°)

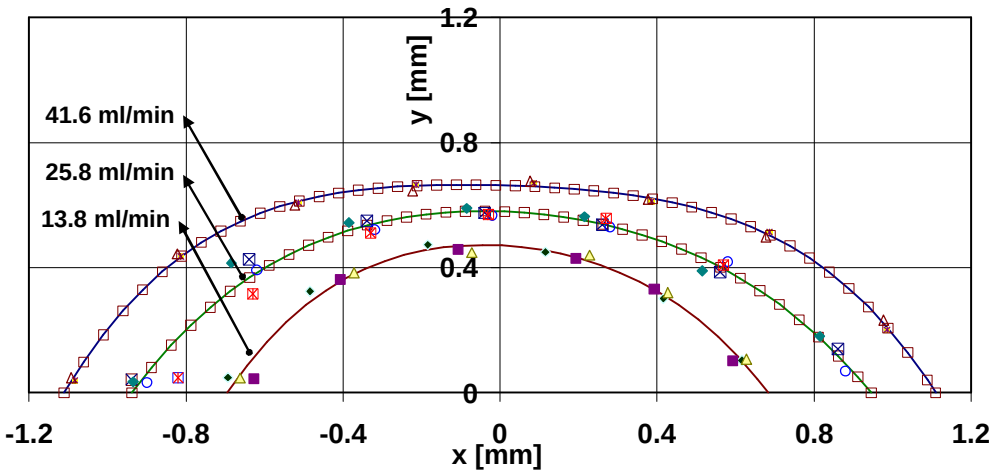

10.2.2 B2: Rivulet maximum thickness and width results on flat plate

(ß=68.5°) for liquid system 2 (glycerine-water 50% wt.) on flat plate inclined plate

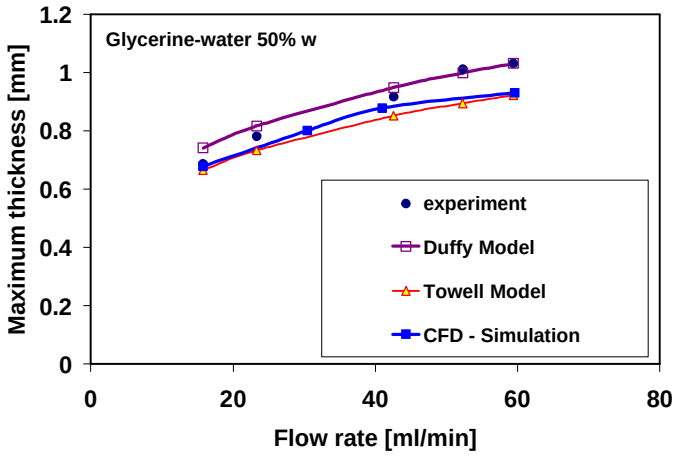

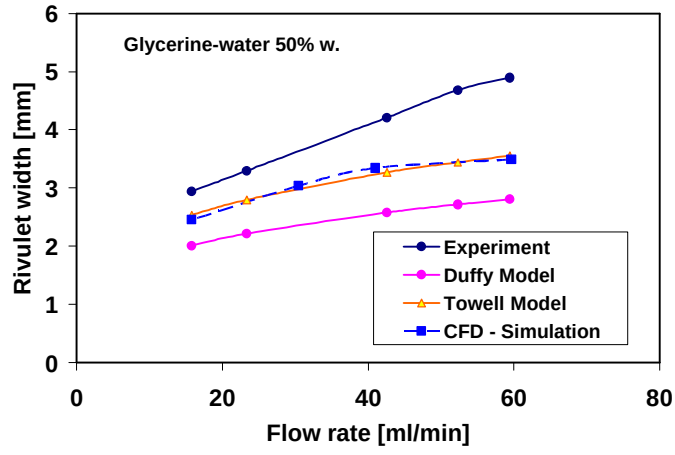

10.2.3 B3: VOF counters for the rivulet flow simulations, vertical flat plate

Parameter: Flow rate		
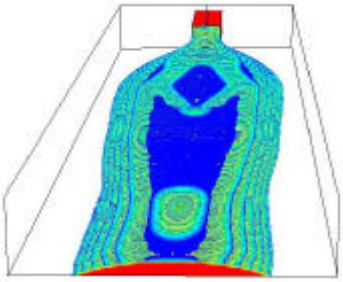	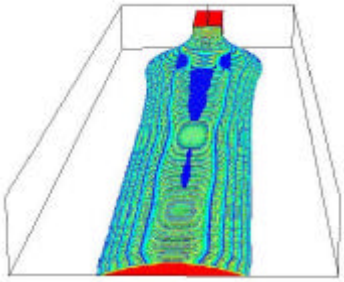	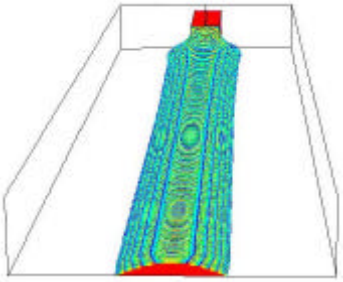
R8	R1	R7
180 ml/min	90 ml/min	45 ml/min
Parameter: Conact angle		
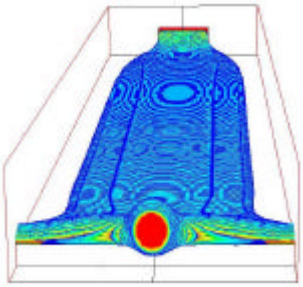	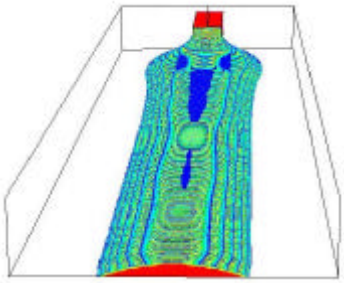	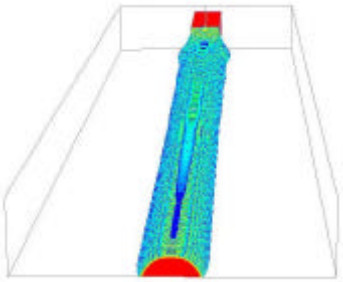
R2	R1	R3
10°	24.5°	67°
Parameter: Viscosity		
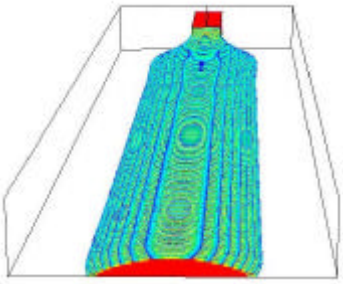	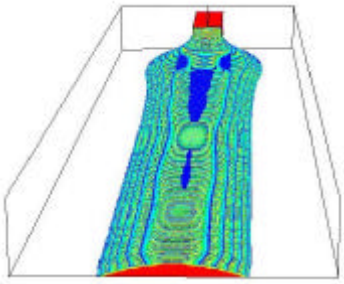	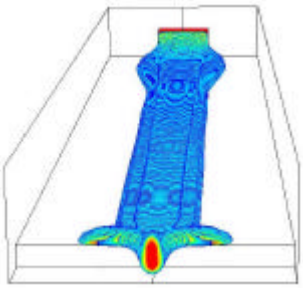
R9	R1	R6
10 mPas	4.5 mPas	1 mPas
Parameter: Surface tension		
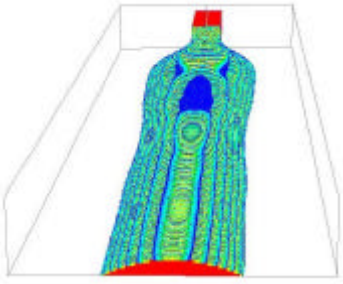	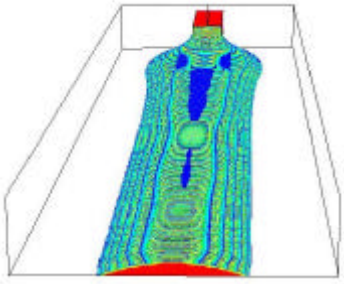	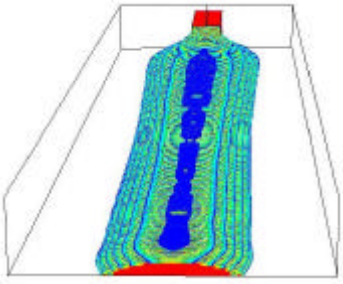
R4	R1	R5
10 mN/m	29 mN/m	64 mN/m

10.2.4 B4: VOF counters for the rivulet flow simulations, inclined flat plate

Parameter: Inclination

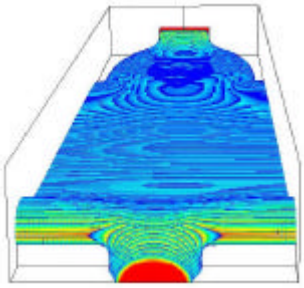	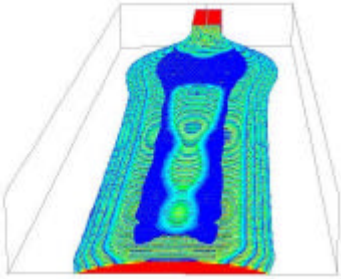
R12	R11
30°	45°
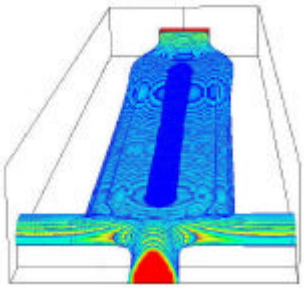	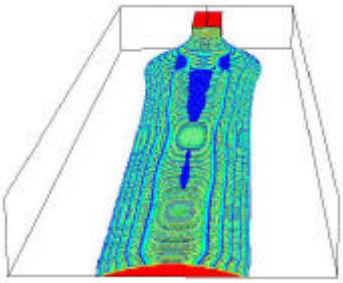
R10	R1
68.5°	90°

Parameter: Flow rate

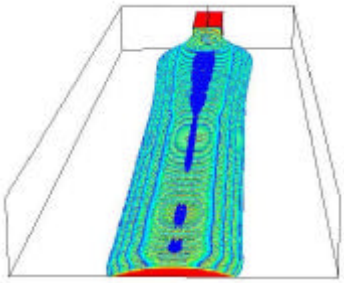	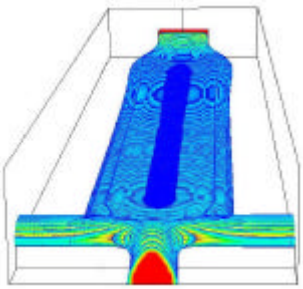
R13	R10
45 ml/min	90 ml/min

Parameter: Contact angle

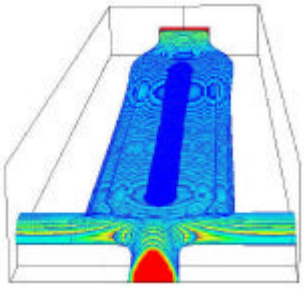	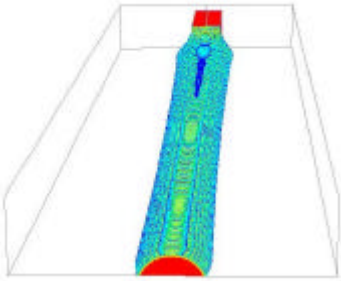
R10	R16
24.5°	67°

Parameter: Surface tension

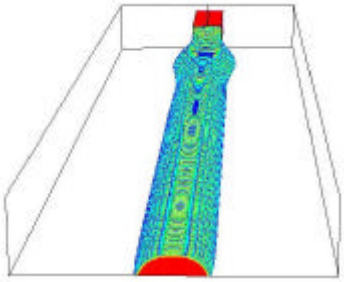	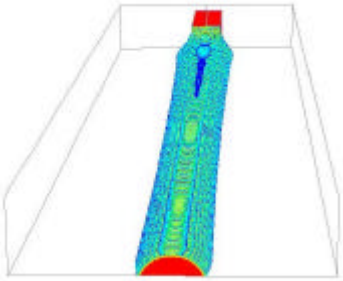
R15	R16
10 mN/m	29 mN/m

Parameter: Density

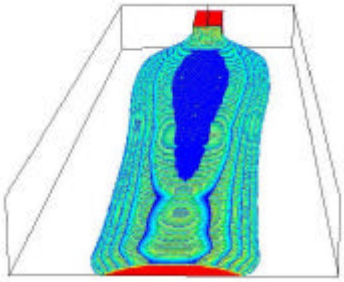	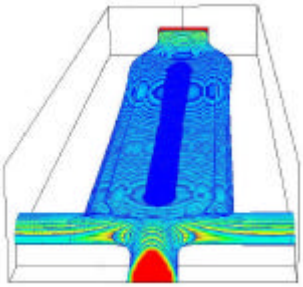
R17	R10
985 kg/m^3	1147 kg/m^3

10.2.5 B5: VOF contours of the rivulet flow on inclined flat plate for two different grids

Grid 1 Rn-nim (VOF capture with non-iterative method) (left) and grid 2 (iterative method) (right) in chapter 5

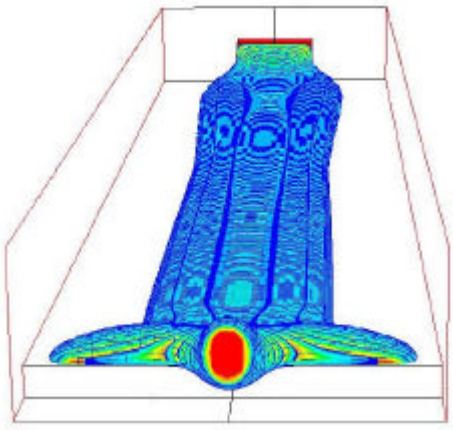	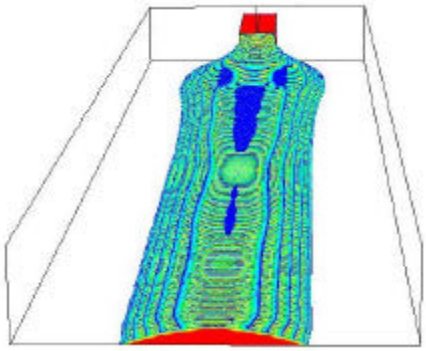
R1	R1
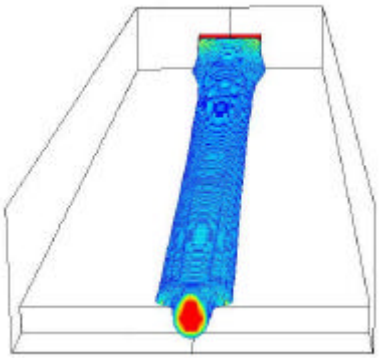	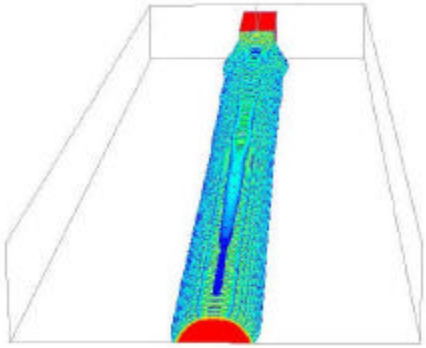
R3	R3
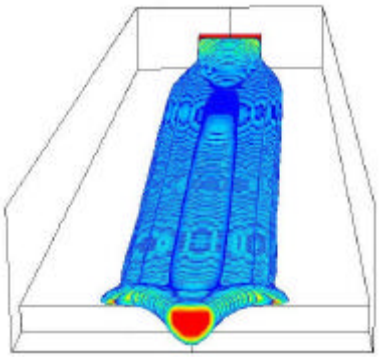	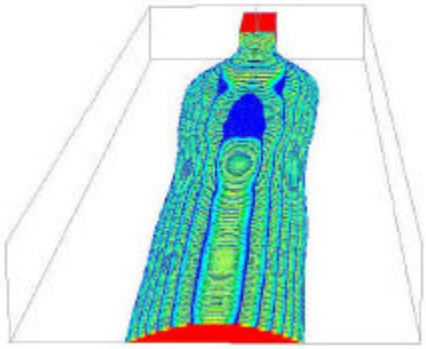
R4	R4

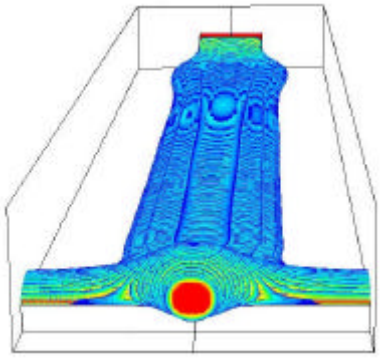	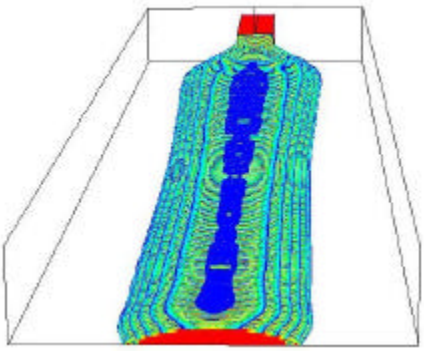
R5	R5
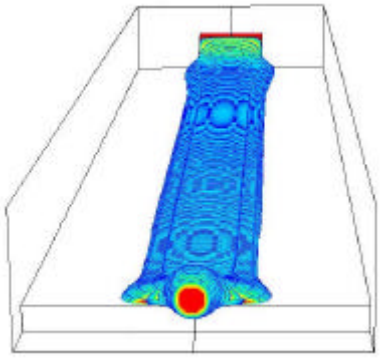	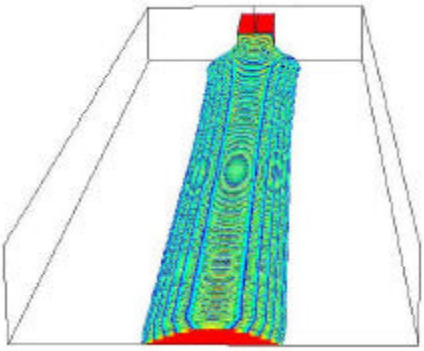
R7	R7
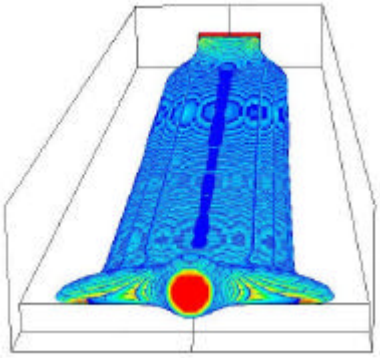	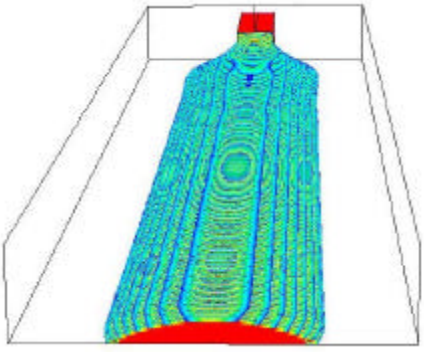
R9	R9
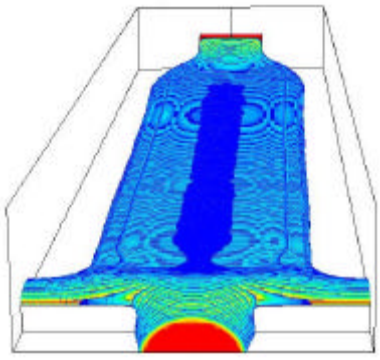	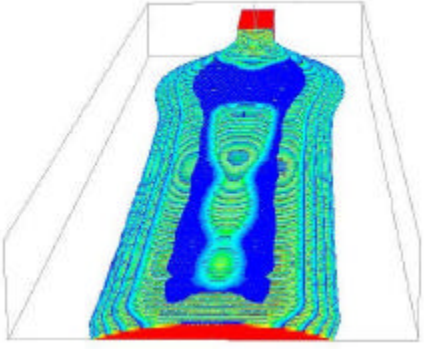
R11	R11

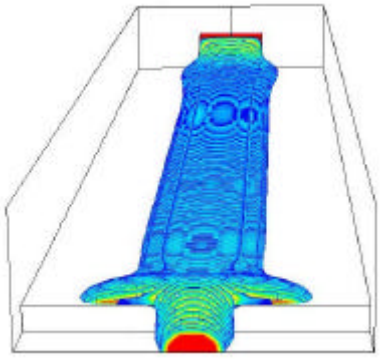	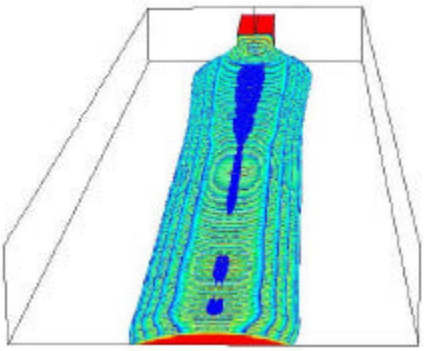
R14	R14
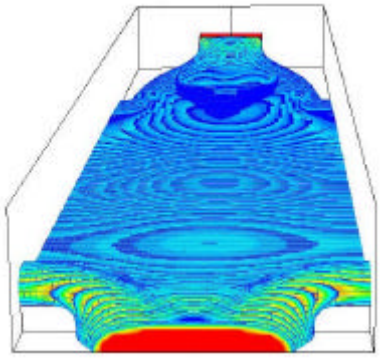	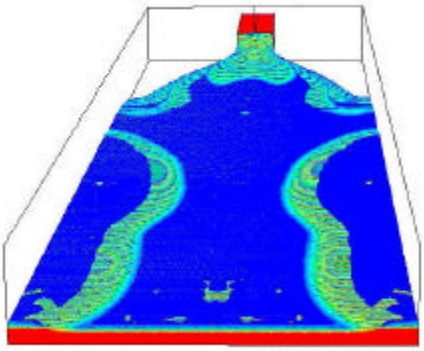
R15	R15
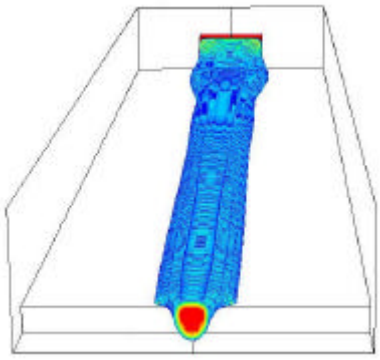	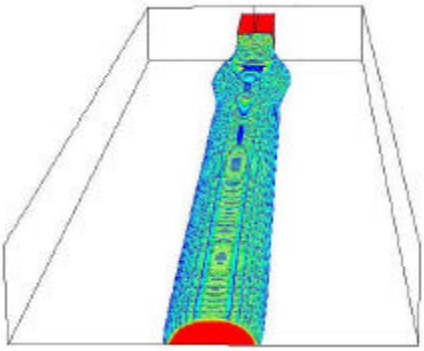
R18	R18
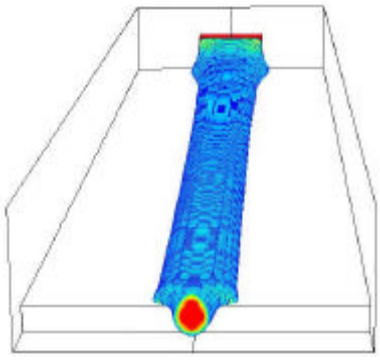	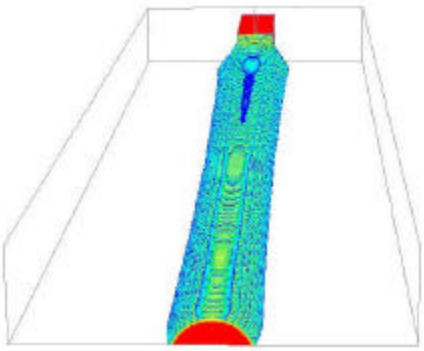
R22	R22

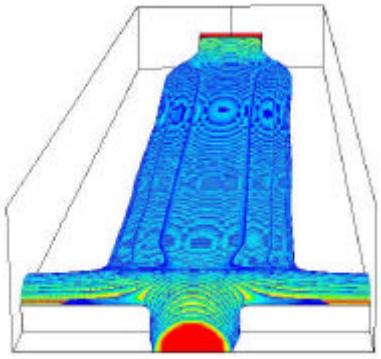	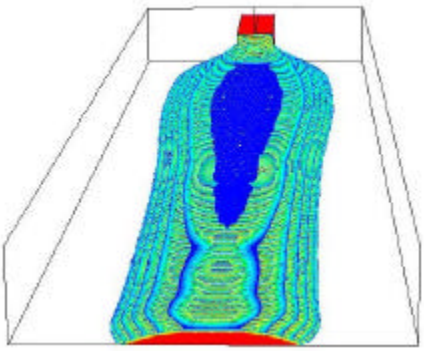
R24	R24

10.2.6 B6: VOF contours of the CFD simulation on wavy inclined plate

Parameter: Flow rate		
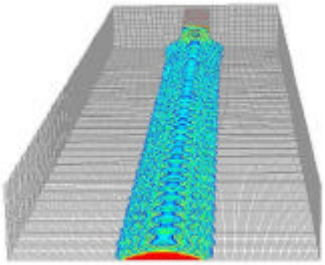	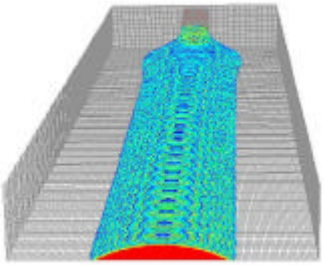	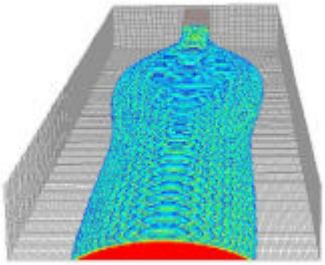
W6	W3	W4
11 ml/min	45 ml/min	90 ml/min
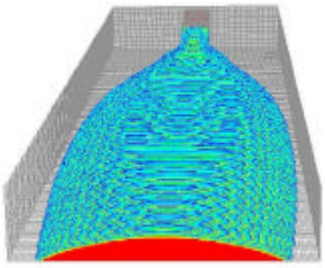		
W5		
180 ml/min		

Parameter: Viscosity	
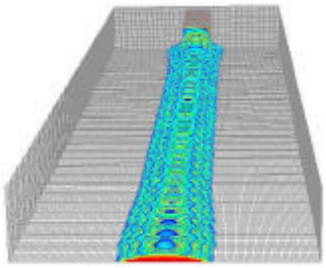	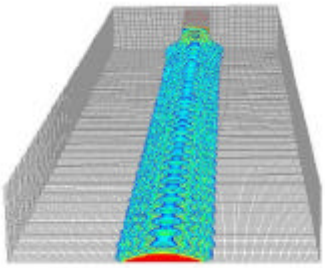
W9	W6
1 mPas	4.5 mPas

Parameter: Surface tension	
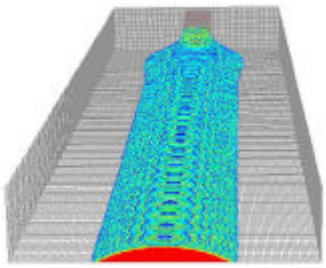	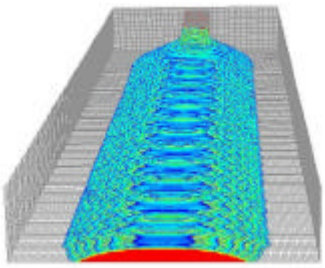
W3	W8
29 mN/m	64 mN/m

10.2.7 B7: VOF contours for the CFD simulations on a wavy plate

Glycerine-water 86.5% wt. mixture, plate inclination β=68.5°

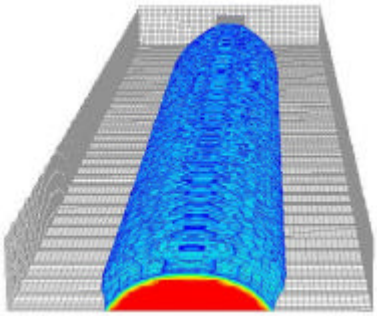	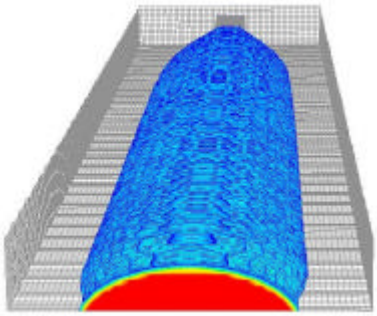	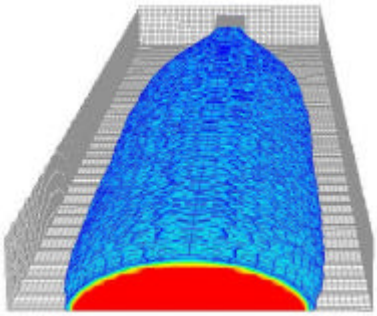
F1 32, ml/min	F2 64 ml/min	F3, 112 ml/min

10.3 Appendix C

10.3.1 C1: VOF-contours for the CFD simulations of the flow on SPE with different grids

(left) grid 3, (middle) grid 2 and (right) grid 3 in chapter 6.

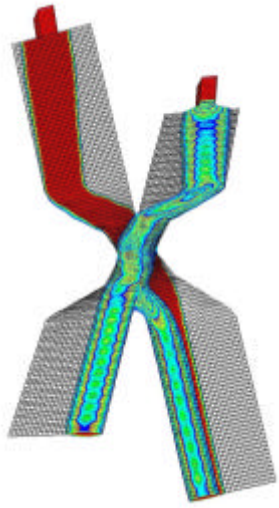	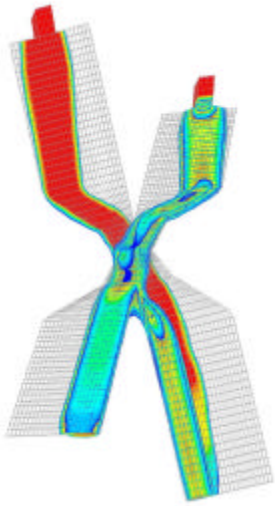	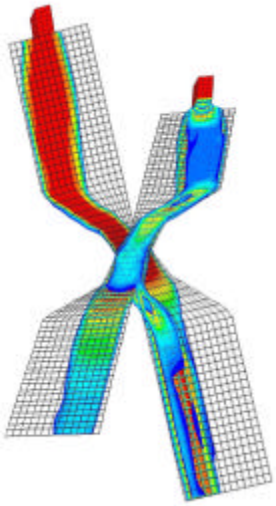
F1	F1	F1
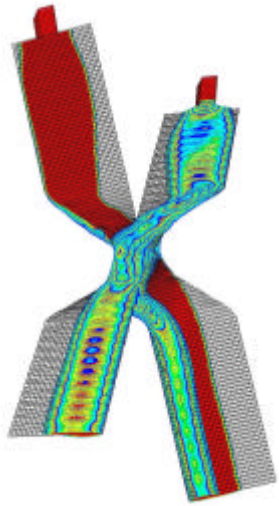	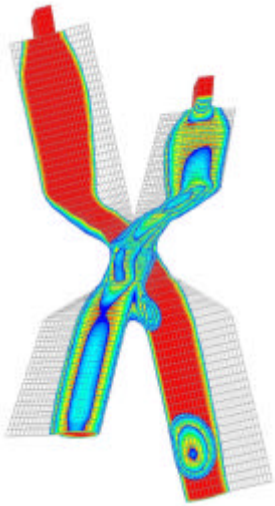	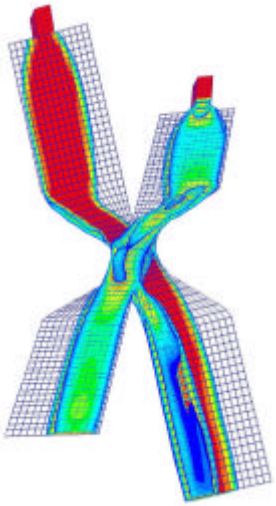
F2	F2	

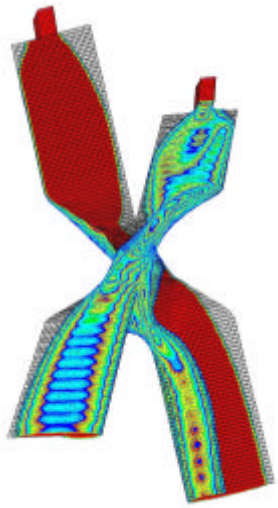	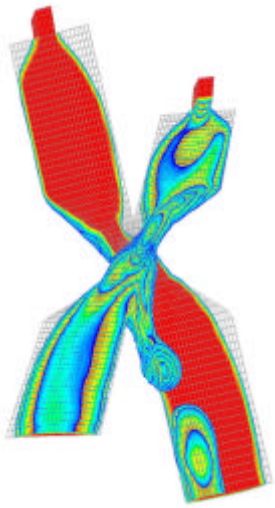	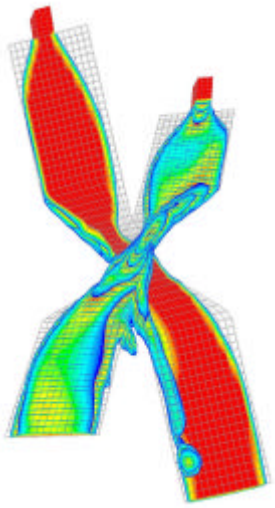
F3	F3	F3
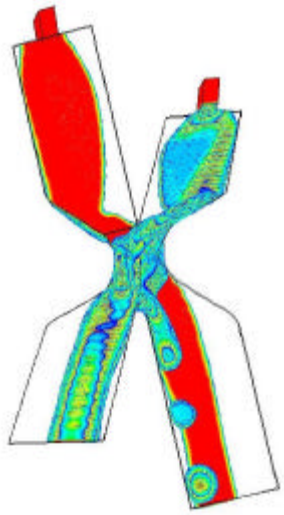	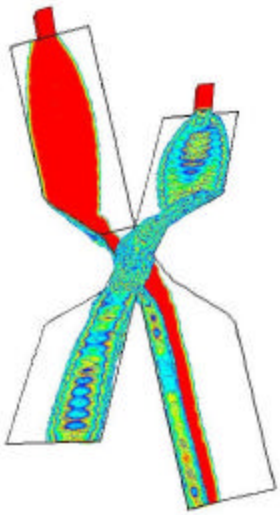	
F9	F9	
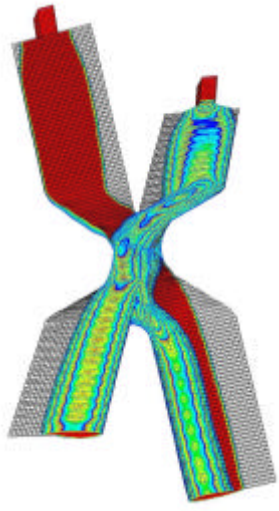	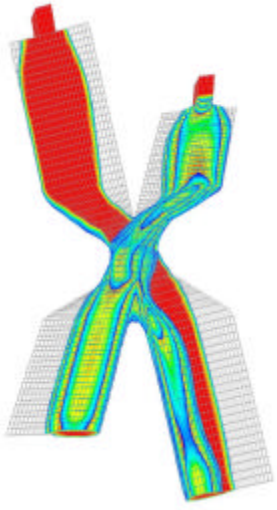	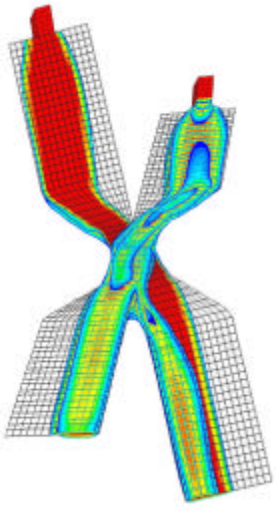
F4	F4	F4

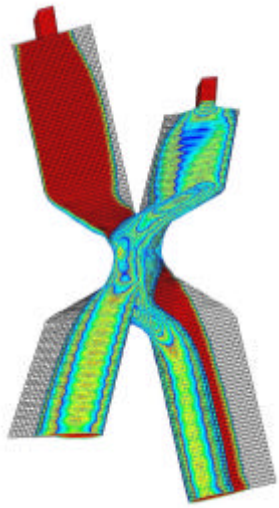	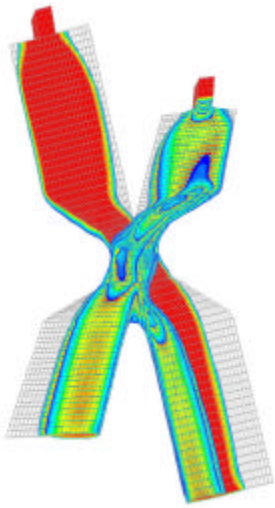	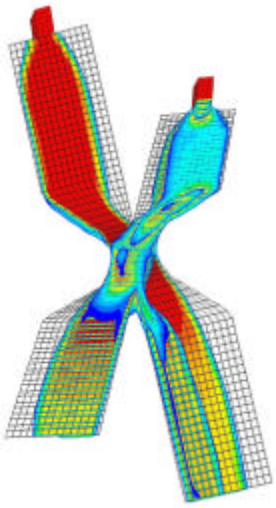
F5	F5	F5
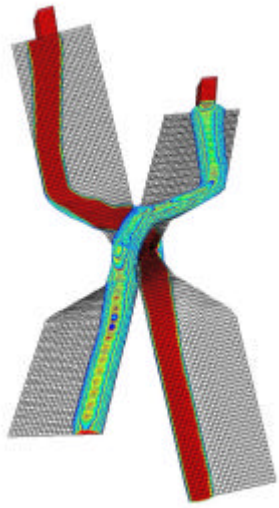	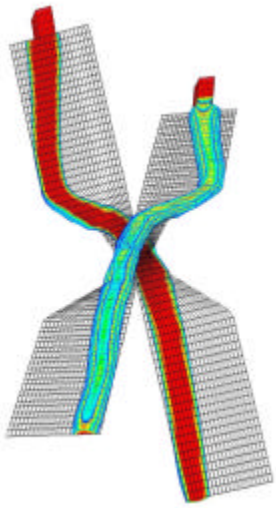	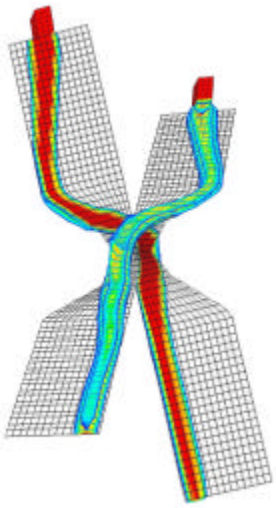
F6	F6	F6
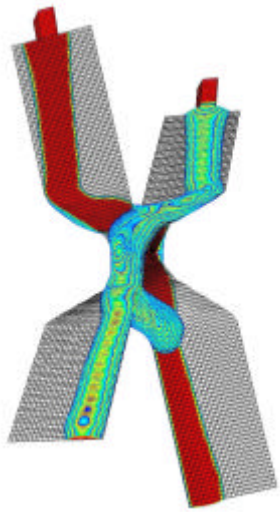	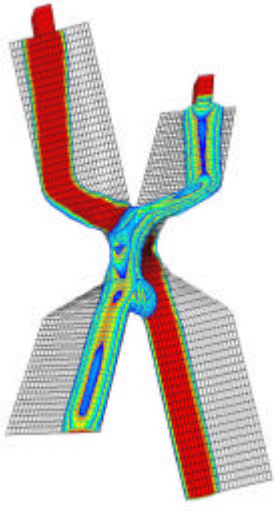	
F7	F7	

For these cases (left) grid 3 and right grid 4 in chapter 6.

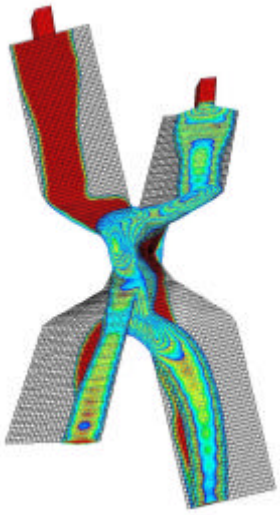	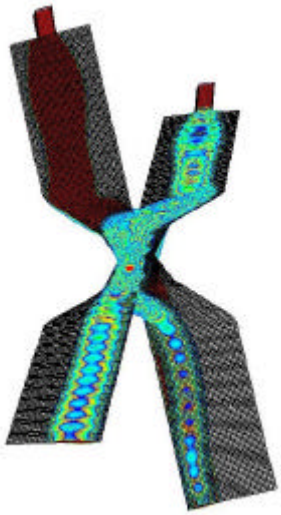
F8	F8
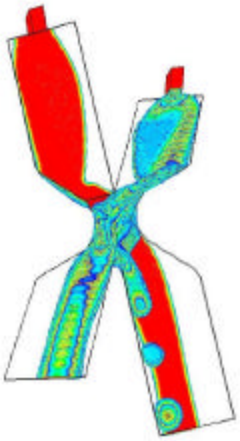	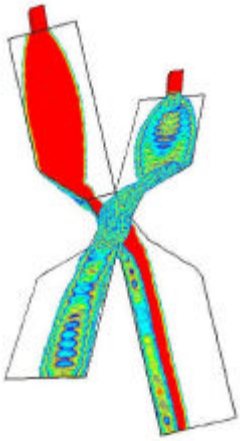
F9	F9
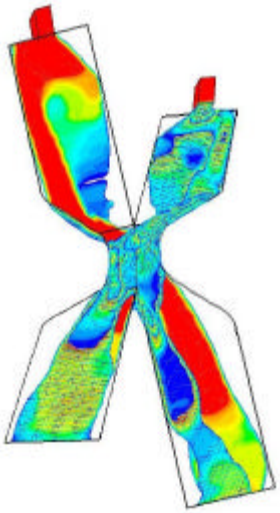	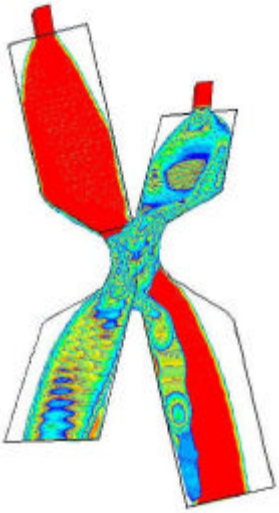
F10	F10

10.3.2 C2: Simulated hydraulic parameters for the SPE

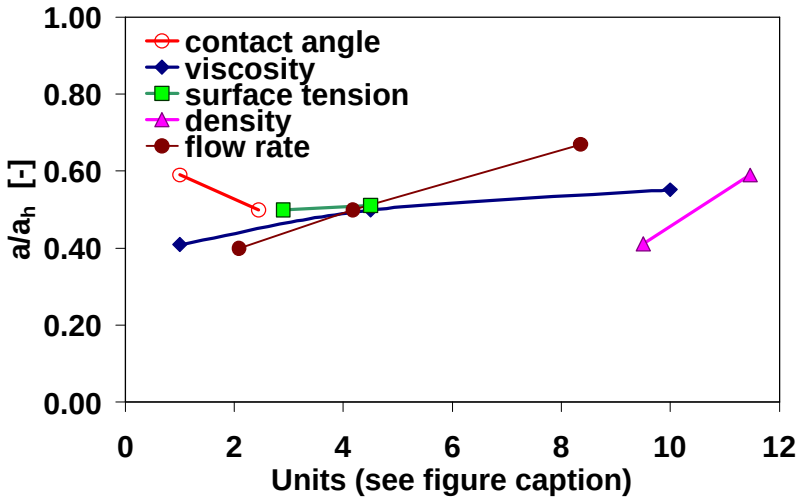

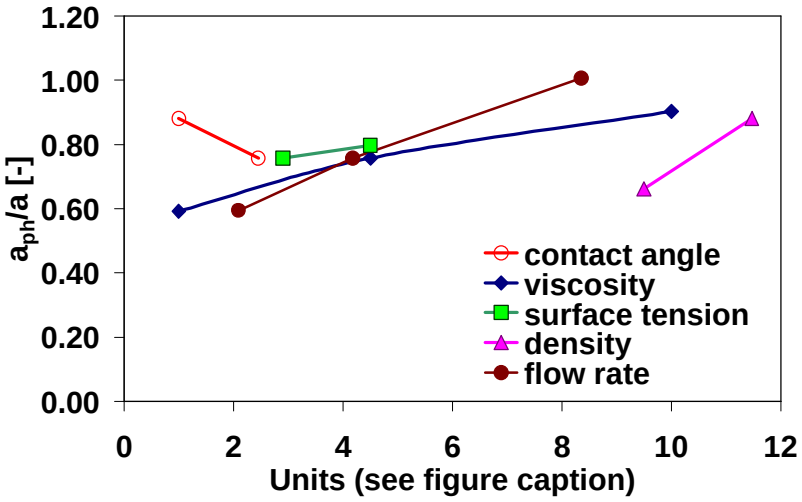

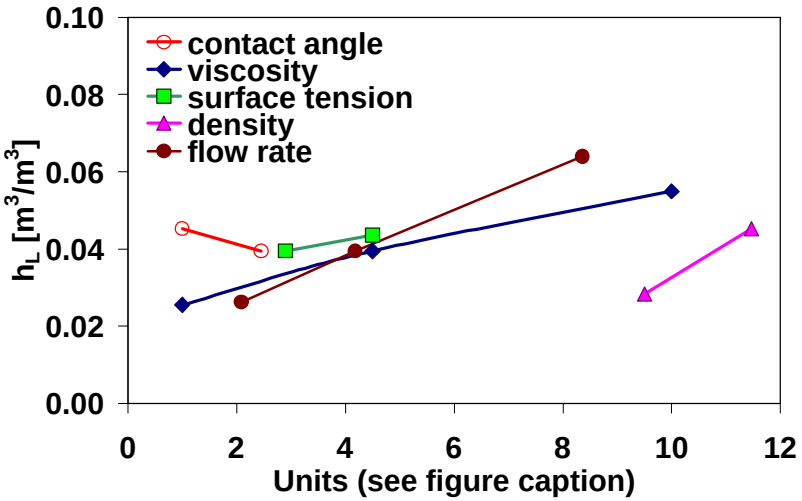

(Units: contact angle (°/10), viscosity (mPasX10), surface tension (mN/m), density (kg/m^3/10), flow rate (ml/min))

10.3.3 C3: Table for CFD simulation results on a PS in comparison to SPE

	PS				*CFD*	*CFD*	*CFD*
	Re_L	Fr_L	We_L	*cos ?*	a_h/a	a_{ph}/a	h_L
	$u_L?_L/\mu_L.a$	u_L^2a/g	$u_L^2?_L/s\,a$	-	-	-	m^3/m^3
F4	**4.94**	**0.000849**	**0.01210**	**0.910**	**0.486**	**0.784**	**0.0460**
F9	**50.52**	**0.000888**	**0.01266**	**0.910**	**0.387**	**0.604**	**0.0261**
F10	**141.47**	**0.000850**	**0.01341**	**0.961**	**0.470**	**0.606**	**0.0214**
F11	**10.98**	**0.000849**	**0.00548**	**0.940**	**0.601**	**0.905**	**0.0507**
	SPE						
F4	**4.94**	**0.00085**	**0.01210**	**0.910**	**0.552**	**0.903**	**0.0550**
F9	**50.52**	**0.00089**	**0.01266**	**0.910**	**0.409**	**0.592**	**0.0255**
F10	**141.42**	**0.00085**	**0.01340**	**0.961**	**0.521**	**0.657**	**0.0207**
F11	**10.98**	**0.00085**	**0.00548**	**0.940**	**0.565**	**0.846**	**0.0454**

10.4 Appendix E

10.4.1 MS vs. SS Correlations

The derivations of Eqs. (6-1, 6-3 and 6-5) in chapter 6 are based on the CFD virtual experiments.
However, a limited number of experimental data is also available with glycerine/water (fluid1) plus a mixture of surfactant (fluid2) respectively glycerine/water chlorobenzene/ethylbenzene (fluid 3). Fitting of the equations from above to the experimental data gives the following results:

$$\frac{a_h}{a} = 1.547 Fr_L^{0.197} We_L^{-0.136} \mathrm{Re}_L^{0.043} (\cos q)^{1.3}$$

$$\frac{a_{ph}}{a} = 1.642 Fr_L^{0.197} We_L^{-0.136} \mathrm{Re}_L^{0.043} (\cos q)^{1.3}$$

$$h_L = C_{hL} (12 \frac{1}{g} \frac{m_L}{r_L} u_L a^2)^{1/3} (\frac{a_h}{a})^{2/3}$$

where, C_{hL}=0.675

With the diagrams:

10.4.1.1 Degree of Wetting

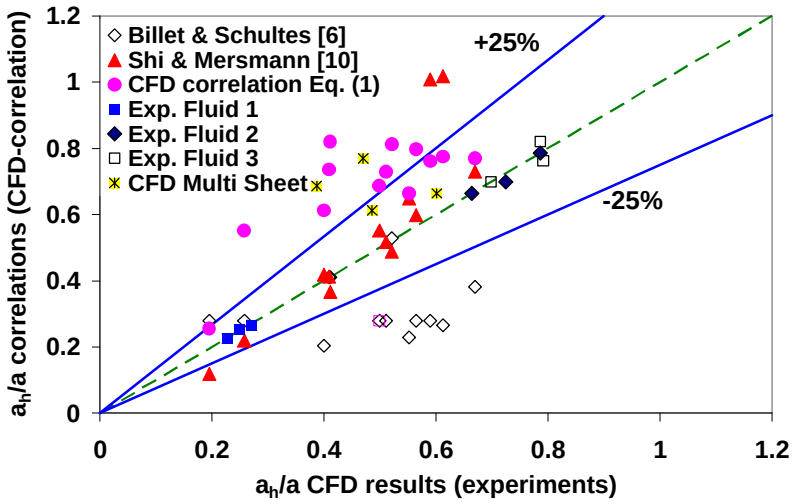

10.4.1.2 Specific Interfacial Area

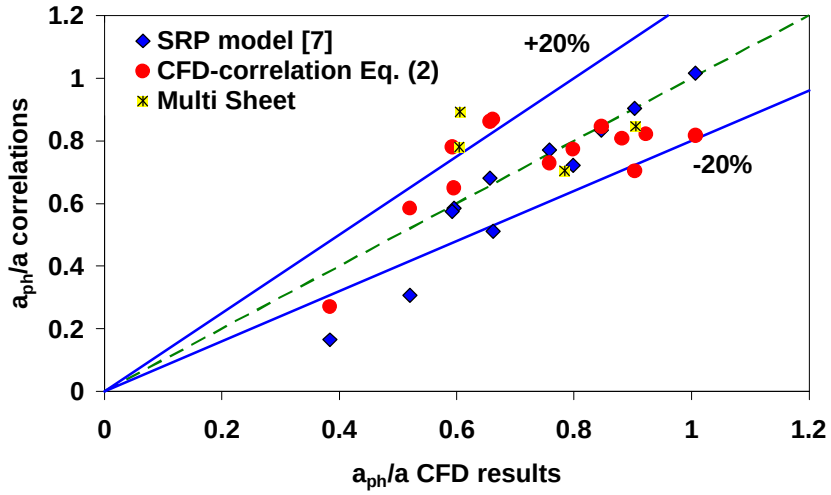

10.4.1.3 Liquid Hold-up

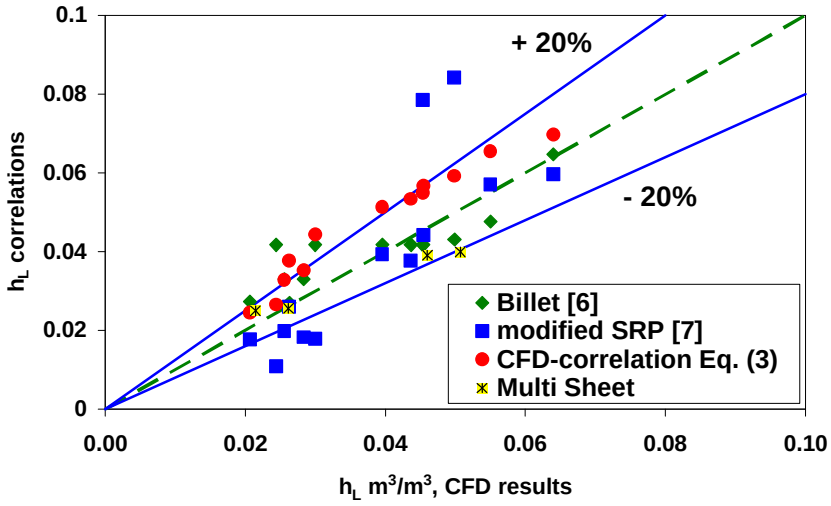

List of Publications

[1] Ataki, A. and H.-J. Bart, *Experimental study of rivulet liquid flow on an inclined plate*. Int. Conf. on Adsorption and Distillation, 634th Event of the European Federation of Chemical Engineering. 2002. Baden-Baden, Deutschland: VDI-GVC (ed.) 3-931384-37-3, Düsseldorf.

[2] Ataki, A. and H.-J. Bart, *The use of the VOF-model to study the wetting of solid surfaces.* Chem. Eng. Technol., 2004. **27**(10): p. 1109-1114.

[3] Ataki, A. and H.-J. Bart, *Wetting patterns of a structured packing element*. Fluent CFD conference. 28 bis 30 September 2004. Bingen, Deutschland.

[4] Ataki, A. and H.-J. Bart, *Experimental and CFD simulation study for the wetting of a structured packing element with liquids.* Chem. Eng. Technol., 2006. **29**(3): p. 363-347.

[5] Ataki, A., P. Kolb, U. Bühlmann, H.-J. Bart, *Wetting performance and pressure drop of structured packings: CFD and experiment*. Int. Conf. on Adsorption and Distillation, 4-6 September 2006, Imperial College, London, UK.

Lectures

1. *Benetzungsverhalten einer strukturierten Packung: CFD und Experiment.* GVC - Fachausschuss „Mehrphasenströmungen und „Computational Fluid Dynamics“, 2. bis 3. März 2006. Überlingen bei Friedrichshafen, Deutschland.
2. *Using the CFD simulation to predict the hydrodynamics of structured packed columns.* GVC-Fachausschuss „Fluidverfahrenstechnik, Adsorption und Hochdruckverfahrens-technik“, 2. bis 5. März 2005. Lübeck, Deutschland.
3. *Wetting Patterns of a Structured Packing Element*, FLUENT - Konferenz von 28 bis 30 Sep. 2004. Bingen, Deutschland.
4. *Experimental and CFD-Simulation Study for the Wetting of a Structured Packing Element with Liquids*. GVC - Fachausschüsse „ Rheologie“ und „Computational Fluid Dynamics“ von 29 bis 30 März 2004. Würzburg, Deutschland.
5. *Einsatz des VOF-Modells zur Untersuchung der Benetzung von Festkörpern mit Flüssigkeiten*, die internen Arbeitssitzung der GVC – Fachausschüsse „Mischvorgänge“ und „ Computational Fluid Dynamics“ vom 31. März bis 02. April, 2003. Berlin, Deutschland.

Posters

1. *Experimentelle Untersuchung und CFD- Simulationen zur Benetzung eines strukturierten Packungselements*, DECHEMA-GVC Jahrestagung 12 bis 14 Oktober 2004. Karlsruhe, Deutschland.
2. *Experimental study of rivulet liquid flow on an inclined plate*, International Conference on Destillation and Absorption 30 September bis 2 October, 2002, Baden-Baden, Germany: VDI-GVC (ed.) 3-931384-37-3, Düsseldorf, Deutschland.

Student Research Project

Ataki, A., 1999, , *Kinetikuntersuchungen bei Extraktionsmittel-Imprägnierten Polymeren in der Rührzelle*. TU Kaiserslautern

CV

Personal Data

Name	Ataki, Adel
Birthday / Place	14.11.1968, Aleppo-Syria
Marital Status	Single
Nationality	Syrian
Sex	Male

Education

	School, Place
1974-1979	*Elementary School, Aleppo - Syria*
1980-1983	*Preparatory School, Aleppo - Syria*
1984-1987	*Secondary School, Aleppo - Syria*
	Certificate of Secondary School

Higher Education

	University, Place/Study/Degree
1987-1990	*Faculty of Mechanical Engineering, University of Aleppo-Syria/ Pre-Degree Study*
1990-1992	*Faculty of Mechanical Engineering, University of Aleppo-Syria/ Main Study Period, Power Engineering* B.Sc. Power Engineering, 74.85 % Very good
1992-1993	*Mechanical Engineering, University of Aleppo-Syria/ Diploma of higher studies, Thermal Engineering/* Graduated Diploma, G. Dipl. in Thermal Engineering, 77.33% Very good
1999-2000	*Technical University of Kaiserslautern, Germany/ Preparation for the Promotion Admission+ Student Research Project*
Since 2000	*Technical University of Kaiserslautern- Germany/* Ph. D. Research Title: *Wetting of Structured Packing Elements - CFD and Experiment*

Experiences

1993-1995	*General Company for Consulting and Engineering/ Aleppo-Syria/ Heating and Air Conditioning Projects Studies*
1997-1998	*Assistant at the Mechanical Engineering Department/ University of Aleppo-Syria*

Languages

Arabic	*Native Language*
German	*Fluent*
English	*Fluent*

Special Experiences

MS - Office, CFD Programme: FLUENT, Gambit, Ansys-ICEM, CFX

Social Activities

Sports, Football

Military Service

1995-1997	*General Company for Medical Products/ Maintenance/ Syria*